TECHNICAL REPORT NO. 8

DESIGN CONSIDERATION FOR DEEP UNDERGROUND PROTECTIVE FACILITIES
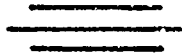
by

CARL F. BAGGE

MARCH 1972
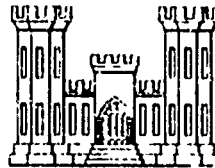
OMAHA DISTRICT, CORPS OF ENGINEERS
OMAHA, NEBRASKA 68102

DOCUMENT CONTROL DATA - R & D

(Security classification of title, body of abstract and indexing annotation must be entered when the overall report is classified)

1. ORIGINATING ACTIVITY *(Corporate author)*	2a. REPORT SECURITY CLASSIFICATION
Omaha District, Corps of Engineers Omaha, Nebraska 68102	UNCLASSIFIED
	2b. GROUP

3. REPORT TITLE

Static and Dynamic Analysis of Rock Bolt Support

4. DESCRIPTIVE NOTES *(Type of report and inclusive dates)*

Interim

5. AUTHOR(S) *(First name, middle initial, last name)*

Carl F. Bagge

6. REPORT DATE	7a. TOTAL NO. OF PAGES	7b. NO. OF REFS
March 1972	101	18

8a. CONTRACT OR GRANT NO. DACA 45-70-C-0100 b. PROJECT NO. 4DM78012A0K1 c. TASK: 09 d. WORK UNIT: 005	9a. ORIGINATOR'S REPORT NUMBER(S) Technical Report No. 8 9b. OTHER REPORT NO(S) *(Any other numbers that may be assigned this report)*

10. DISTRIBUTION STATEMENT

Approved for public release; distribution unlimited.

11. SUPPLEMENTARY NOTES	12. SPONSORING MILITARY ACTIVITY Department of the Army Office of the Chief of Engineers Washington, D. C. 20314

13. ABSTRACT

Analytical investigations of two problems of hardening a deep underground protective facility--(1) the mechanical failure of a cavity under dynamic ground shock loading and (2) the material failure of a cavity penetration under overburden loading and repeated ground shock loading--are reported.

Design requirements are derived for liner, backpacked liner, and rock bolt reinforcement, which function to prevent mechanical failure of cylindrical cavities sited in well-fractured rock and a step-by-step procedure for design is given. The results indicate that cavity survival is linearly dependent upon (1) the increment of the free-field ground shock acceleration occurring over a period of two cavity engulfment times and (2) the magnitude of the cavity radius. This dependence is not inconsistent with Pile Driver test results. The design procedure is recommended as an interim until such time as validation can be provided by laboratory and field testing or by more rigorous analytical study.

The critical nature of material failure at a cavity penetration is examined by calculation of the inelastic response of a steel-lined penetration at the horizontal axis of an unlined, horizontal, circular cylindrical cavity located at a depth of 4300 ft in a competent schistose gneiss subjected to a 25-MT surface burst. The resulting three-dimensional problem is examined by treating a two-dimensional

DD FORM 1473 REPLACES DD FORM 1473, 1 JAN 64, WHICH IS OBSOLETE FOR ARMY USE.

UNCLASSIFIED
Security Classification

problem--a transverse slice of the penetration at the cavity wall.
The response of the cavity away from the penetration is assumed
to be elastic. The analysis is accomplished with a finite element
code that allows for overburden loading, emplacement of the liner,
and repeated ground shock loading, in sequence. Ground shock
loading is applied statically. Material strength is assumed to
be unaffected by repeated loading. The analysis indicates that
(1) steel-lined penetrations can be adequately and cost-effectively
designed to withstand repeated attack with large-yield weapons pro-
vided that there is no significant deterioration of rock strength
with each attack and (2) the analysis technique used here, or an
equivalent technique, can be used effectively by today's designer,
provided material properties data are available. Recommendations
are given for further study of the penetration problem.

14 KEY WORDS	LINK A		LINK B		LINK C	
	ROLE	WT	ROLE	WT	ROLE	WT
Backpacked Liner						
Cavity Failure						
Cavity Penetration						
Dynamic Loading						
Liner Acceleration						
Material Failure						
Mechanical Failure						
Protective Facilities						
Repeated Loading						
Rock Bolting						
Rock Mechanics						
Tunnel Liners						

TECHNICAL REPORT NO. 8

DESIGN CONSIDERATIONS FOR DE P
UNDERGROUND PROTECTIVE FACILIT...S

by

CARL F. BAGGE

MARCH 1972

OMAHA DISTRICT, CORPS OF ENGINEERS
OMAHA, NEBRASKA   68102

IC

ABSTRACT

Analytical investigations of two problems of hardening a deep underground protective facility--(1) the mechanical failure of a cavity under dynamic ground shock loading and (2) the material failure of a cavity penetration under overburden loading and repeated ground shock loading--are reported.

Design requirements are derived for liner, backpacked liner, and rock bolt reinforcement, which function to prevent mechanical failure of cylindrical cavities sited in well-fractured rock and a step-by-step procedure for design is given. The results indicate that cavity survival is linearly dependent upon (1) the increment of the free-field ground shock acceleration occurring over a period of two cavity engulfment times and (2) the magnitude of the cavity radius. This dependence is not inconsistent with Pile Driver test results. The design procedure is recommended as an interim until such time as validation can be provided by laboratory and field testing or by more rigorous analytical study.

The critical nature of material failure at a cavity penetration is examined by calculation of the inelastic response of a steel-lined penetration at the horizontal axis of an unlined, horizontal, circular cylindrical cavity located at a depth of 4300 ft in a competent schistose gneiss subjected to a 25-MT surface burst. The resulting three-dimensional problem is examined by treating a two-dimensional problem--a transverse slice of the penetration at the cavity wall. The response of the cavity away from the penetration is assumed to be elastic. The analysis is accomplished with a finite element code that allows for overburden loading, emplacement of the liner, and repeated ground shock loading, in sequence. Ground shock loading is applied statically. Material strength is assumed to be unaffected by repeated loading. The analysis indicates that (1) steel-lined penetrations can be adequately and cost-effectively designed to withstand repeated attack with large-yield weapons *provided that there is no significant deterioration of rock strength with each attack* and (2) the analysis technique used here, or an equivalent technique, can be used effectively by *today's designer, provided material properties data are available*. Recommendations are given for further study of the penetration problem.

ii

PREFACE

This investigation was authorized by the Chief of Engineers (ENGMC-EM) and was performed in FY 1971 under Contract No. DACA 45-70-C-0100, between the Omaha District, Corps of Engineers and Agbabian-Jacobsen Associates, Los Angeles, California. This work is a part of a continuing effort to develop methods which can be used to design underground openings in jointed rock to survive the effects of nuclear weapons.

This report was prepared under the supervision of Mr. R. W. Anderson, Project Manager. Mr. Carl F. Bagge served as the Principal Investigator for Agbabian-Jacobsen Associates.

During the work period covered by this report, Colonel B. P. Pendergrass was District Engineer: Charles L. Hipp and R. G. Burnett were Chief, Engineering Division; C. J. Distefano was Technical Monitor for the Omaha District under the general supervision of Kendall C. Fox, Chief, Protective Structures Branch. Dr. J. D. Smart and D. G. Heitmann participated in the monitoring work.

CONTENTS

CONTENTS (CONTINUED)

ILLUSTRATIONS

LIST OF SYMBOLS

SECTION 2

$A_{180^{\circ}}$	=	Acceleration of the cavity wall at $\theta = 180^{\circ}$
A_{rb}	=	Effective cross sectional area of rock bolt
C	=	Effective propagation velocity of ground shock
DLF_{rb}	=	Dynamic load factor for rock bolt
DLF_{o}	=	Dynamic load factor for integral liner in breathing mode
DLF_{2}	=	Dynamic load factor for integral liner in ovaling mode
DLF_{o}'	=	Dynamic load factor for backpacked liner in breathing mode
DLF_{2}'	=	Dynamic load factor for backpacked liner in ovaling mode
E	=	Effective Young's modulus of liner
E_{bp}	=	Effective Young's modulus of backpacking
E_{rb}	=	Effective Young's modulus of rock bolt
g	=	Acceleration of gravity
h	=	Liner thickness
h_{bp}	=	Backpacking thickness
K	=	Ratio of stress components (normal to lateral) in ground shock wave
k_{bp}	=	Effective radial stiffness of backpacking
k_{o}	=	Radial stiffness of liner in breathing mode
k_{2}	=	Effective radial stiffness of liner in ovaling mode
L	=	Length of rock bolt
M	=	Bending moment in liner
m	=	Effective mass of liner
m_{bp}	=	Effective mass of backpacking

SECTION 2

N	$=$	Thrust in liner
$Q(t)$	$=$	$(1-0.5\frac{t}{2t_e})\frac{t}{2t_e}$
R	$=$	Cavity radius
r	$=$	Radial coordinate
S	$=$	Rock bolt spacing
T_{rb}	$=$	Vibration period of rock bolt
T_o	$=$	Vibration period of integral liner in breathing mode
T_2	$=$	Vibration period of integral liner in ovaling mode
T_o'	$=$	Vibration period of backpacked liner in breathing mode
T_2'	$=$	Vibration period of backpacked liner in ovaling mode
t	$=$	Time
t_e	$=$	$2R/C$, engulfment time of cavity
t_d	$=$	$4R/C$, duration time of transient interaction
$V_{180°}$	$=$	Velocity of the cavity wall at $\theta = 180°$
v	$=$	Particle velocity
β	$=$	Angle between direction of ground shock propagation and joint direction defined in Figure 2-2
γ	$=$	Weight density of rock
γ_{bp}	$=$	Weight density of backpacking
γ_ℓ	$=$	Weight density of liner
γ_{rb}	$=$	Weight density of rock bolt
δA	$=$	$\delta A'/J$
$\delta A'$	$=$	Increment in free field acceleration

SECTION 2

θ	=	Angular coordinate measured from head-on azimuth of cavity
μ	=	Ductility ratio
ν	=	Poisson's ratio
ρ	=	Mass density of rock
σ	=	Stress
σ_{bp}	=	Radial stress in backpacking
σ_{ff}	=	Free field ground shock stress
σ_M	=	Liner stress due to bending moment
σ_N	=	Liner stress due to thrust
σ_{NM}	=	$\sigma_N + \sigma_M$
σ_{r}	=	Radial stress in free field
$\sigma_{r\theta}$	=	Shear stress in free field
σ'_{ff}	=	Intermittent free field stress
σ'_{rr}	=	Modified radial restraining stress
$\sigma'_{r\theta}$	=	Modified shear restraining stress

SECTION 3

B	$=$	Bulk modulus
C	$=$	Propagation velocity of ground shock
C_1, C_2	$=$	Constants defined in Figure 3-7
D	$=$	Depth of facility
G	$=$	Shear modulus
E	$=$	Young's modulus of rock
f	$=$	Yield surface function
K_{gs}	$=$	Ratio of stress components behind ground shock front
K_{ob}	$=$	Ratio of vertical to horizontal overburden stress
J_1, J_1', J_2'	$=$	Stress invariants defined in Figure 3-7
N	$=$	Decay rate of ground shock stress defined in Figure 3-2
S	$=$	Slant range of burst
W	$=$	Weapon yield
α	$=$	Angular coordinate defined in Figure 3-2
α_1, α_2	$=$	Constants defined in Figure 3-7
γ	$=$	Weight density of rock
ε_{off}	$=$	Free field strain
θ	$=$	Angular coordinate defined in Figure 3-2
σ	$=$	Enhanced free field stress
σ_α	$=$	Stress defined in Figure 3-2
σ_{ob}	$=$	γD, vertical overburden stress
σ_{off}	$=$	Vertical ground shock stress for direct overhead burst

SECTION 1

INTRODUCTION

1.1 STUDY OBJECTIVES

The two objectives of this study were

a. To derive design requirements for preventing mechanical failure of deep underground cavities subjected to nuclear ground shock

b. To study mate al failure of a deep underground cavity penetration subjected to nuclear ground shock

1.2 BACKGROUND

The past decade has seen a concerted effort to develop a design methodology for reinforcing deep underground cavities subjected to nuclear-weapon-induced ground shock and in situ stresses primarily through a field testing program consisting of the Hard Hat and Pile Driver events. The principal objective of these tests was to demonstrate the viability of a cavity liner concept comprising a relatively flexible liner surrounded by soft packing and to empirically develop design parameters for this concept. The premise for this concept was that a cavity would survive much closer to a nuclear burst if the liner was separated from the cavity wall by a soft packing material, assuming the cavity wall bulks due to yielding and flow of the adjacent rock. Only incidental attention, in terms of numbers of cavity sections tested, was given to other presumably less rugged concepts, e.g., unlined, rock-bolted, integrally lined, etc., which might survive at greater ranges.

In spite of this decade of concerted effort, further studies are required to develop well-defined design procedures for the hardening of deep underground cavities against ground shock. The Hard Hat and Pile Driver events left many questions unanswered and raised still

others. Still unknown are the effect of cavity size on survivability, and the design parameters for siting conditions other than for that tested. Questions raised pertain to explaining cavity and penetration failures which were definitely not of a bulking nature, and to defining survivability under multiple-attack of the cavity sections and penetrations that were declared to have survived.

The need for and the adequacy of the backpacked liner as evolved in the Pile Driver event is questionable today (1971). With the present threat of virtually zero-CEP delivery of repeated weapons, it is highly questionable that the evolved structure concept or any contents could survive repeated pounding of an intensity which severely bulks cavity walls with just one attack. Moreover, it is apparent now after study of the Pile Driver results that another failure mode, mechanical failure, is inadequately prevented or accommodated by the evolved concept. Finally, the need for the evolved concept is in serious doubt as evidenced by preliminary study which shows that bulking resulting from material failure can be virtually eliminated by judicious selection of site location, depth of siting, and cavity design.

The Hard Hat and Pile Driver events at the Nevada Test Site, in conjunction with the Hard Rock Silo Development (HRSD) test program at Cedar City, Utah, have, however, provided information on the failure mechanisms of lined and unlined cavities in rock. What has become vividly clear after study of these tests is that two distinct types of ground-shock-induced failure of a rock cavity are possible and must be accounted for in design:

Material failure

Mechanical failure

An appreciation of the distinction between material and mechanical failure and its implications to design are, in general, lacking in the technical community. One notable exception, however, are the discussions of test results for the rock bolting experiments conducted in the Pile Driver event (Reference 1).

Material failure is characterized by yielding, flow, and swelling of the rock *within* the interaction zone to such an extent that there is a permanent reduction in cavity volume. This type of failure can occur only when the *in situ* yield strength of the *intact* rock is exceeded and when mechanical failure is precluded. Material failure was dramatically exhibited in the highly stressed close-in drifts of the Pile Driver event (Reference 2).

2

Mechanical failure, on the other hand, is characterized by relative movement along planes of weakness (joints, fractures, partings, separations, etc.) lying within the interaction zone.[*] Mechanical failure actually commences with the development of the cavity during excavation, where it is manifest as a general loosening of the rock adjacent to the cavity. During ground shock loading, the loosening effect is increased and appears as a swelling of the cavity walls under the best of conditions, and, as a worst case, as loss of structural integrity of the cavity walls. Various degrees of mechanical failure were in evidence in the more remote drifts, tunnels, and shafts of the Pile Driver event and the HRSD test program. Failures included swelling of the cavity walls without loss of structural·integrity--easily mistaken for material failure--isolated rock block expulsions, partial collapse of cavities, and complete collapse of a cavity with the formation of a new cavity in the adjacent virgin rock.

Loss of cavity-wall structural integrity can be triggered by the expulsion of unkeyed blocks of rock into the cavity resulting from (1) the enhanced (or reduced) acceleration of the cavity, relative to the free-field, on the head-on (or back) face during interaction with the free-field pulse at times of rapid change in acceleration, such as during initial engulfment, and (2) the tendency for tensile circumferential straining, i.e., unkeying action, at the head-on and back face azimuths. Depending upon the circumstances, the expulsions of rock blocks may or may not .lead to further loss of structural integrity. Evidence that this mechanism exists can be found in the Pile Driver event and the HRSD test program ROCKTEST II. In the Pile Driver event, a large rock block (roughly 2 by 4 by 8 ft) was expelled from the newly excavated extension of the main access shaft (Reference 2). The estimated free-field stress and acceleration levels at this range were 10,000 psi and 20 g, respectively. In the ROCKTFST II event, a rock block (roughly 4 by 4 by 8 ft) was expelled from the wall of a previously tested cavity located in an adjacent test bed (HANDEC II) by the ROCKTEST II generated ground shock (Reference 3). It is estimated that a free-field acceleration of 10 to 20 g existed at the range of this cavity.

These are two examples of the occurrence of the expulsion triggering mechanism without further loss of structural integrity. Whether this mechanism was responsible for the more serious mechanical failures seen in the Pile Driver and ROCKTEST II events cannot be answered. Other triggering mechanisms are, of course, possible. For

---

[*]The tightness of planes of weakness at depth, the confinement at depth, and the remoteness of a deep underground facility from the crater region preclude all block motion other than that described here, i.e., that originating within the interaction zone.

example, the simultaneous collapse of an entire forward wall under a severe acceleration is possible. Similarly, the buckling of severely compressed layers, which have been subjected to gravity stoping, is also a possible mechanism. It is not of major importance at this time to be able to identify the triggering mechanisms of mechanical failure, but rather to recognize that mechanical failure occurs, that it can occur in backpacked and integrally-lined cavities under a severe enough environment, that it is different from material failure, and that it cannot be successfully treated as material failure.

The loss of structural integrity becomes significantly more imminent with each attack because of progressive degradation of the "strength" of the planes of weakness with each attack. This fact was driven home by the report (Reference 2) that the unlined access tunnels of the Hard Hat experiment ". . . were severely damaged by the Pile Driver detonation and large quantities of rock fell into the openings." The Pile Driver acceleration environment, less severe than the previous Hard Hat environment, is estimated to be 20 to 100 g at various points along the access tunnels.

It is apparent from the above discussion that the facility designer must contend with three manifestations of cavity failure:

a.   Swelling of the cavity walls resulting from material failure of the surrounding rock

b.   Swelling of the cavity walls resulting from mechanical failure of the surrounding rock

c.   Loss of structural integrity (large scale mechanical failure) of the cavity wall

The designer can adopt either of two design philosophies, prevention of failure or accommodation of failure. The type and severity of failure determining whether the conceptual design approach should employ preventive or accommodating design philosophy (e.g., choosing between an unlined cavity, rock bolting, an integral liner, or a backpacked liner) is dependent principally upon the following factors:

a.   *In situ* strength of *intact* rock material

b.   Tectonic state of stress

c.   Overburden stress intensity

d.   Ground shock intensity

4

e. Stress distribution as determined by cavity geometry and orientation, cavity penetrations, and proximity to adjacent cavities

f. Pattern and quality of planes of weakness

g. Number of attacks

The designer, in conjunction with the agency sponsoring a deep under-ground protective facility, can control to a large degree the severity of material failure as influenced by factors a through f by judicious selection of site location, depth of burial, and cavity design. This latitude in controlling material failure, which, incidentally, is virtually absent in the design of surface or near-surface protective facilities, is an important consideration during the conceptual design of a deep underground protective facility. Material failure may be virtually eliminated for unconfined compressive rock strengths greater than 30 ksi, provided that there is no significant deterioration in rock strength with each successive attack.

In earlier studies carried out at AJA, a cavity liner concept was investigated that consisted of a protective liner and a layer of relatively stiff backpacking interposed between liner and cavity walls. The function of the backpacking in this case, however, was to buttress cavity walls against mechanical failure and, at the same time, to attenuate the more or less elastic deformation of the cavity wall to the point that the liner will survive multiple attacks. In other words, the liner and backpacking are designed to act as the structural keystone of the presumably incompetent cavity.

In these studies, it was also shown that material failure is inevitable for cavity penetrations. Unfortunately, the penetration experiments conducted in the Pile Driver event, reported in Reference 4, shed little light on the material failure of penetrations for a number of reasons. First, the tunnel sections in which the *unlined* penetrations were located experienced either mechanical or material failure. In the case of the bank of *steel-lined* penetrations located closest to the working point, severe material failure masks the response of the pene-trations. The most remote bank of lined penetrations was reported to have survived; however, no measurements of cross-section distortion were reported that would have indicated the degree of material failure for the particular loading condition, penetration-tunnel orientation, or penetration design.

This, then, is the background from which the two tasks under consideration--study of mechanical failure of cavities and study of material failure of cavity penetrations--were formulated.

5

1.3 REPORT ORGANIZATION

Design requirements for prevention of mechanical failure of a cavity are derived and presented in Section 2. In Section 3, the study of material failure of a cavity penetration is presented. Conclusions and recommendations are presented in Section 4. Appendixes A, B, and C supply additional documentation of the material failure study reported in Section 3.

SECTION 2

MECHANICAL FAILURE OF A CAVITY UNDER DYNAMIC LOADING

2.1 INTRODUCTION

Consider the two cases shown in Figure 2-1 and imagine that the planes of weakness cannot sustain tensile stresses and that the blocks of rock do not support one another through wedging action. For Case (a), the free field without the cavity, there will be little tendency for relative movement between the cavity core and either of the regions containing planes of weakness. For Case (b), however, it is easy to visualize that there will be a marked tendency for relative movement of the shadow region into the cavity during initial engulf-ment, and the illuminated region into the cavity as the free-field ground shock velocity begins to decay from its positive peak. This marked tendency for relative movement of the rock into the cavity could, if left unchecked by cavity reinforcement, lead to loss of structural integrity of the cavity.

The purpose of this section is to present *upper bound* design requirements for reinforcement that prevents loss of structural integrity of a circular cylindrical cavity under dynamic ground shock loading directed perpendicular to the cavity axis. Three types of cavity rein-forcement are considered: liner, backpacked liner, and rock bolts.

The material in this section has been organized as follows. In Section 2.2, the circumstances necessary for loss of structural inte-grity are determined. The restraining stresses which must be applied to the cavity wall to prevent loss of structural integrity are derived in Section 2.3. The required resistance of the cavity reinforcement which must supply the restraining stresses are derived in Section 2.4. A. step-by-step design procedure is given in Section 2.5. Finally, a discussion of the design requirements is presented in Section 2.6.

2.2 NECESSARY CONDITIONS FOR LOSS OF STRUCTURAL INTEGRITY

2.2.1 Nonwedging Pattern of Planes of Weakness

It is necessary to postulate that unwedged blocks of rock exist in the shadow and/or illuminated region of the cavity in order to develop a tendency for loss of structural integrity. The reasonableness of this postulation will become apparent upon examination of the three simple patterns of planes of weakness shown in Figure 2-2. A single set of planes of weakness does not present a critical condition for mechanical failure (Figure 2-2(a)). For a set of nonorthogonal planes (Figure 2-2(c)), unwedged blocks of rock are presented when the direction of ground shock propagation is parallel to the long diagonal of the formed blocks. Figure 2-2(b) shows that unwedged blocks of rock are presented wherever the direction of ground shock propagation is parallel to a diagonal of the formed blocks. A critical condition also exists for the orthogonal set of planes whenever the direction of ground shock propagation is parallel to a set of relatively compressible planes of weakness. Since multiple sets of planes of weakness are almost always encountered in practice, it is realistic to postulate that unwedged blocks of rock exist in the shadow and illuminated regions of the cavity.

The following assumption will therefore be made regarding planes of weakness:

> The entire interaction zone of the cavity is cut by several sets of planes of weakness of negligible tensile strength in such a fashion that (1) the characteristic dimensions of the blocks of rock are small compared to the cavity diameter and (2) the blocks of rock are not mutually supported by wedging action.

2.2.2 Critical Incremental steps in Free-Field Acceleration

Imagine that a cavity is engulfed by a piece-wise linear ground shock stress (velocity) disturbance. A typical interaction response is shown in Figure 2-3. Figure 2-3(c) shows that the response is quasistatic except immediately following an incremental step in the free-field acceleration, at which time the response is truly dynamic. Only during these brief periods of dynamic interaction will there exist a tendency for relative movement of the rock into the cavity, and hence, a need for cavity reinforcement.

8

The following incremental steps in free-field acceleration are critical:

a. An incremental step in the free-field acceleration, that produces a decrease in forward velocity will tend to force the rock in the illuminated region to move into the cavity.

b. An incremental step in free-field acceleration that produces an increase in the forward velocity will tend to force rock in the shadow zone into the cavity.

In effect, reinforcement is required for each increment in acceleration.

2.3 RESTRAINING STRESSES NECESSARY TO PREVENT LOSS OF STRUCTURAL INTEGRITY

The stresses which would have to be applied to the cavity wall (after complete engulfment) to *completely nullify the presence* of the cavity are (see Figure 2-4):

$$\sigma_{rr}(t) = \sigma_{ff}(t)[\cos^2 \theta + K \sin^2 \theta]$$

$$= 0.5 \sigma_{ff}(t)[1 + K + (1 - K) \cos 2\theta] \qquad (2-1)$$

$$\sigma_{r\theta}(t) = 0.5 \sigma_{ff}(t)(1 - K) \sin 2\theta$$

where

$\sigma_{rr}(t)$ = Radial restraining stress history

$\sigma_{r\theta}(t)$ = Tangential restraining stress history

$\sigma_{ff}(t)$ = Free field ground shock stress history

K = Ratio of stress components behind ground shock wave front

θ = Angular coordinate measured from head-on point of cavity

9

However, with reference to the discussion in Section 2.2.2, it is necessary only to apply a short-duration restraining stress at points of acceleration discontinuity in order to prevent loss of structural integrity of the cavity. These modified restraining stress σ'_{rr} and $\sigma'_{r\theta}$ will be assumed to have the same spatial dependence as σ_{rr} and $\sigma_{r\theta}$ i.e.,

$$\sigma'_{rr}(t) = 0.5\, \sigma'_{ff}(t)[1 + K + (1 - K)\cos 2\theta]$$

$$(2\text{-}2)$$

$$\sigma'_{r\theta}(t) = 0.5\, \sigma'_{ff}(t)(1 - K)\sin 2\theta$$

where $\sigma'_{ff}(t)$ is an intermittent free-field stress history to be defined below. It is important to realize that the application of the stresses given by Equation 2-1 to the cavity wall will completely nullify the presence of the cavity in the free field at all times; whereas, the application of the stresses given by Equation 2-2 is required to only nullify the differential motions between the cavity and free field at points of discontinuity in a linearized free field ground shock stress history.

An unduly conservative approach to the calculation of σ'_{ff} assumes that the total change in free-field stress at points of discontinuity must be supplied for a duration of $2t_e$, i.e., the presence of the cavity must be completely nullified in the sense of Equation 2-1:

$$\sigma'_{ff} = \rho C\, \delta A' t$$

$$(2\text{-}3a)$$

$$= 4 R \gamma\, \delta A\, \frac{t}{2t_e}$$

where

t = Time $0 \le t \le 2t$, reckoned from the time of discontinuity arrival

t_e = $2R/C$ = Engulfment time of cavity

C = Effective propagation velocity of ground shock

R = Cavity radius

δA = $\delta A'/g$ increment in free-field acceleration, i.e., change in slope of the velocity history at a point of discontinuity

γ = ρg, the specific weight or weight density

10

A reasonably conservative estimate of σ'_{ff} can be obtained by consideration of typical dynamic response at the shadow side of the cavity produced by an incremental increase in the free-field acceleration $\delta A'$. This response, shown in Figure 2-5*, may be thought of as occurring under an initial engulfment step or any step in the free-field acceleration (see Figure 2-3). Figure 2-5 compares both the tangential and radial components of acceleration of the cavity wall at various points with the corresponding components of the free-field acceleration. The shaded areas in Figure 2-5 are a measure of the differential motion which takes place between the free-field and the cavity wall. The requirement that the cavity reinforcement must supply the restraining stresses σ'_{rr} and $\sigma'_{r\theta}$ in such a manner that the cavity wall is accelerated with the free field is imposed. Therefore, the acceleration histories which must be supplied by σ'_{rr} and $\sigma'_{r\theta}$ are the shaded areas shown in Figure 2-5. The acceleration history which must be supplied at the extreme shadow point (see Figure 2-5(g)) can be approximated by

$$A_{180^\circ} = \delta A' \left(1 - \frac{t}{2t_e} \right)$$ (2-4)

Integration of Equation 2-4 with respect to t gives the following velocity history:

$$V_{180^\circ} = 2t_e \, \delta A' Q(t)$$ (2-5)

where

$$Q(t) = \left(1 - 0.5 \frac{t}{2t_e} \right) \frac{t}{2t_e}$$ (2-6)

Equation 2-6 is plotted in Figure 2-6.

The differential displacement at $\theta = 0^\circ$, $r = R$ can be approximated from Figure 2-5(i) by double integration of

$$A_{0^\circ} = \delta A' \, (1 - t/2t_e)$$

where t is reckoned from $t = .5t_e$. Performing the integrations gives

$$\delta D = \delta A' \, (\frac{t^2}{2} - \frac{t^3}{12t_e})$$

---

*This solution has been obtained with the GARNET Code. The code calculates the closed-form solution for elastodynamic response of a lined or unlined circular cavity located in an elastic continuum (Reference 5).

11

The maximum δD is

$$\delta D_{max} = \frac{4}{3}\delta A' t_e^2$$

for a cavity in unjointed rock. For an unlined cavity sited in critically jointed rock, the differential motion would vary roughly as the free field displacement since the rock at the cavity remains stationary (neglecting the force of gravity), as discussed in Section 2.1. The differential displacements for the other azimuths are similar.

Assuming that stress is related to velocity by

$$\sigma = \rho C v \qquad (2\text{-}7)$$

the correct relationship for one-dimensional wave propagation and a reasonable approximation for the case under consideration here, leads to the following expression for the radial restraining stress at $\theta = 180$ deg:

$$\sigma'_{rr}(t)\Big|_{180°} = 4' \gamma \, \delta A \, Q(t) \qquad (2\text{-}8)$$

where γ is the weight density of the rock and δA is the acceleration increment expressed in g's. It can be verified that Equation 2-8 is also applicable at $\theta = 0$ deg during an incremental reduction in the free-field acceleration.

Evaluating Equation 2-2a at 180 deg and using the result in Equation 2-8 leads to

$$\sigma'_{ff}(t) = 4R\gamma \, \delta A \, Q(t) \qquad (2\text{-}3b)$$

This differs from the more conservative estimate of σ'_{ff} obtained in Equation 2-3a by the factor $[1 - 0.5 \, t/(2t_e)]$.

Assuming that Equation 2-3b is a reasonable approximation for other θ leads to the following expressions for restraining stresses upon substitution in Equation 2-2:

$$\sigma'_{rr}(t) = 2R\gamma \, \delta A[1 + K + (1 - K)\cos 2\theta]Q(t) \qquad (2\text{-}9)$$

$$\sigma'_{r\theta}(t) = 2R\gamma \, \delta A(1 - K)\sin 2\theta \, Q(t)$$

These stress histories must be applied to the rock by the cavity reinforcement during each increment in the free-field acceleration. It is, of course, equivalent to think of the stresses given by Equation 2-9 as those being applied to the cavity reinforcement by the surrounding rock.

2.4 REQUIRED RESISTANCE OF CAVITY REINFORCEMENT

The effective dynamic resistance of a liner, a backpacked liner, or a rock-bolt cavity reinforcement which is required to resist the stresses given by Equation 2-9 is calculated here using the dynamic analysis procedure outlined in Chapter 9 of the ASCE Manual of Engineering Practice No. 42 (Reference 6). It is assumed that the reader is familiar with this procedure. However, as a very brief introduction to this procedure, the following paragraph is extracted from Reference 6.

"The principal method for dynamic design described here is a simplified and rapid procedure for determining the relationships among the following: The peak force applied dynamically to a structure or structural element, the effective dynamic resistance of the element, the effective duration of the applied force, the period of vibration of the element, the maximum acceptable deflection of the element, and the limiting deflection in the elastic range. The procedure described, although it may involve computational inaccuracies of the order of 20 to 25% in some cases, is sufficiently accurate for all practical purposes because the parameters entering into the problem are not accurately determinable. Even a much more precise analysis, by procedures which involve no analytical inaccuracy, could not ordinarily reduce the overall uncertainty below a value perhaps even greater than 25% because of the general physical complexity of the problem, and also because of the lack of definite knowledge in advance concerning:

1. The blast pressure at a given distance from a given energy of detonation;

2. The duration of the blast wave; or

3. The structural parameters.

The method of analysis requires:

1. A description of the loading-time curve applied to the structure.

2. A knowledge of the limiting structural resistance.

3. The shape of the resistance-deflection curve for the structure, and especially a characterization of it by a ductility parameter giving the permissible maximum deflection in relationship to the effective yield-point deflection of the structure.

4. A measure of the period of vibration in the effective "elastic range" of the structure."

The comments regarding inaccuracies and uncertainty are most applicable to the problem here.

It will be assumed that the stress histories given by Equation 2-9 are actually triangular in shape with the same peak stress and same duration $(t_d = 2t_e)$; see Figure 2-6.

2.4.1 Liner

A liner of thickness h, radius R, Young's modulus E, and weight density γ_ℓ is used to reinforce the cavity (Figure 2-7).

The following assumptions are made:

a. The liner thickness is small compared to the liner (cavity) radius $(R/h \geq 5)$.

b. The liner responds elastically.[*]

c. The liner responds in two uncoupled modes corresponding to the uniform and ovaling components of loading (see Equations 2-9).

d. The periods of vibration of the liner are taken as the breathing (T_0) and ovaling (T_2) periods of vibration of the free-standing liner under radial loading:

---

[*]This assumption is discussed in Section 2.6.

14

$$T_o = 2\pi \sqrt{\frac{\gamma_\ell R^2}{Eg}}$$

(2-10)[*]

$$T_2 = 2\pi \sqrt{\frac{\gamma_\ell R^2}{Eg}} \sqrt{\frac{5}{3}\left(\frac{R}{h}\right)^2}$$

e.   Peak response is taken as the sum of the peak response in each mode without regard to phasing.[**]

The *peak* state of stress in the liner (required effective dynamic resistance) may now be written, with the aid of Reference 8, as

Fully-welded rock-liner interface $(\sigma'_{rr}$ and $\sigma'_{r\theta})$

$$N = R^2 \gamma \, \delta A (1 + K) DLF_o$$

$$M = -0.5R^3 \gamma \, \delta A (1 - K) \cos 2\theta \, DLF_2$$

$$\sigma_N = \frac{N}{h} = R \frac{R}{h} \gamma \, \delta A (1 + K) DLF_o$$

(2-11)

$$\sigma_M = \frac{6M}{h^2} = \pm 3R\left(\frac{R}{h}\right)^2 \gamma \, \delta A (1 - K) \cos 2\theta \, DLF_2$$

$$\sigma_{NM} = \sigma_N + \sigma_M = R \frac{R}{h} \gamma \, \delta A \left[(1 + K) DLF_o \right.$$
$$\left. \pm 3 \frac{R}{h} (1 - K) \cos 2\theta \, DLF_2 \right]$$

---

[*] Reciprocals of Equations 172 and 176 of Reference 7.

[**] It should be noted that this manner of combining the two uncoupled responses is quite reasonable since the two periods of response differ by an order of magnitude.

Full-slip rock-liner interface $(\sigma'_{rr}$ only)

$$N = R^2 \gamma \, \delta A (1 + K) DLF_o$$

$$M = -\frac{1}{3} R^3 \gamma \, \delta A (1 - K) \cos 2\theta \, DLF_2$$

$$\sigma_N = R \frac{R}{h} \gamma \, \delta A (1 + K) DLF_o$$

$$\sigma_M = -2R \left(\frac{R}{h}\right)^2 \gamma \, \delta A (1 - K) \cos 2\theta \, DLF_2$$

$$\sigma_{NM} = P \frac{\ell}{h} \gamma \, \delta A \left[(1 + K) DLF_o \right.$$

$$\left. \pm 4 \frac{R}{h} (1 - K) \cos 2\theta \, DLF_2 \right]$$

(2-12)

where

$$DLF_o = \frac{\pi \, t_d/T_o}{1 + \dfrac{2.2(t_d/T_o)^2}{1 + 1.4 \, t_d/T_o}}$$

$$DLF_2 = \frac{\pi \, t_d/T_2}{1 + \dfrac{2.2(t_d/T_2)^2}{1 + 1.4 \, t_d/T_2}}$$

(2-13)

$$\frac{t_d}{T_o} = \frac{2}{\pi C} \sqrt{\frac{Eg}{\gamma_\ell}}$$

$$\frac{t_d}{T_2} = \frac{1.5}{\pi C} \frac{h}{R} \sqrt{\frac{Eg}{\gamma_\ell}}$$

(2-14)

16

The equilibrium equations for linear-elastic, thin rings (Kirchoff-Love hypotheses and truncations) given in the Appendix of Reference 8, form the basis of Equations 2-11 and 2-12. The stress resultants N and M are defined in Figure 2-7. The dynamic load factors, DLF, given by Equations 2-13 are the reciprocals of Equations 9-3.5 of Reference 6 for $\mu \equiv 1$.

2.4.2 Backpacked Liner

A layer of backpacking material--thickness h_{bp}, effective modulus of elasticity E_{bp}, and weight density γ_{bp}--is placed between the cavity wall and the liner considered in Section 2.4.1.

The following assumptions are made:

a. The liner and backpacking thicknesses are small compared to the liner (cavity) radius $(R/h \geq 5, R/h_{bp} \geq 5)$.

b. The liner and backpacking respond elastically.*

c. The rock-backpacking interface does not transmit shear stresses, i.e., the interface is a full-slip interface.

d. It is sufficient that only the radial restraining stresses (Equation 2-9(a)) are reacted by the liner and backpacking.

e. The effect of the backpacking is accounted for by treating the backpacking as a massless radial spring element of stiffness

$$k_{bp} = \frac{E_{bp}}{h_{bp}}, \qquad (2\text{-}15)$$

in series with the liner flexibility, and by adding all backpacking mass to the liner.

f. The modified liner responds in two uncoupled modes corresponding to the uniform and ovaling components of loading (see Equation 2-9(a)). **

---

*This assumption is discussed in Section 2.6.
**See footnote on p. 23.

17

g. The periods of vibration of the modified liner are taken
    as the following variations of Equations 2-10:

$$T'_o = 2\pi \sqrt{\frac{\gamma_\ell R^2}{Eg}} \quad \sqrt{\left(1 + \frac{m_{bp}}{m}\right)\left(1 + \frac{k_o}{k_{bp}}\right)}$$

$$T'_2 = 2\pi \sqrt{\frac{\gamma_\ell R^2}{Eg}} \quad \sqrt{\frac{5}{3}\left(\frac{R}{h}\right)^2}$$

$$\times \quad \sqrt{\left(1 + \frac{m_{bp}}{m}\right)\left(1 + \frac{k_2}{k_{bp}}\right)}$$

(2-16)

where

$$k_o = \frac{Eh}{R^2}$$

$$k_2 = \frac{3}{4}\frac{Eh^3}{R^4}$$

$$m = h\gamma_\ell$$

$$m_{bp} = h_{bp}\gamma_{bp}$$

(2-17)

The liner stiffnesses k_o and k_2 have been taken
as the reciprocals of the radial displacements at
$\theta = 0$ deg under unit uniform radial and ovaling
loading, respectively.

18

h. Peak response is taken as the sum of the peak response in each mode without regard to phasing.*

The peak state of radial stress in the backpacking (required effective dynamic resistance) is obtained from Equation 2-9(a):

$$\sigma_{bp} = R_Y \, \delta A [(1 + K) DLF_0' + (1 - K) \cos 2\theta \, DLF_2'] \qquad (2\text{-}18)$$

where

$$DLF_0' = \cfrac{\pi \, t_d / T_0'}{1 + \cfrac{2.2(t_d/T_0')^2}{1 + 1.4 \, t_d/T_0'}}$$

$$\qquad (2\text{-}19)$$

$$DLF_2' = \cfrac{\pi \, t_d / T_2'}{1 + \cfrac{2.2(t_d/T_2')^2}{1 + 1.4 \, t_d/T_2'}}$$

$$\frac{t_d}{T_0'} = \frac{2}{\pi C} \sqrt{\frac{Eg}{\gamma_\ell}} \sqrt{\cfrac{1}{\left(1 + \cfrac{h_{bp}}{h} \cfrac{\gamma_{bp}}{\gamma_\ell}\right)\left(1 + \cfrac{E}{E_{bp}} \cfrac{h}{R} \cfrac{h_{bp}}{R}\right)}}$$

$$\qquad (2\text{-}20)$$

$$\frac{t_d}{T_2'} = \frac{1.5}{\pi C} \frac{h}{R} \sqrt{\frac{Eg}{\gamma_\ell}} \sqrt{\cfrac{1}{\left(1 + \cfrac{h_{bp}}{h} \cfrac{\gamma_{bp}}{\gamma_\ell}\right)\left(1 + \cfrac{3}{4} \cfrac{E}{E_{bp}} \left(\cfrac{h}{R}\right)^3 \cfrac{h_{bp}}{R}\right)}}$$

---

*See second footnote on Page 15.

19

The peak state of stress in the liner (required effective dynamic resistance) is obtained by replacing the dynamic load factors in Equations 2-12 by those given by Equations 2-19:

$$N = R^2 \gamma \, \delta A (1 + K) DLF'_o$$

$$M = -\frac{1}{3} R^3 \gamma \, \delta A (1 - K) \cos 2\theta \, DLF'_2$$

$$\sigma_N = R \frac{R}{h} \gamma \, \delta A (1 + K) DLF'_o \tag{2-21}$$

$$\sigma_M = -2R \left(\frac{R}{h}\right)^2 \gamma \, \delta A (1 - K) \cos 2\theta \, DLF'_2$$

$$\sigma_{NM} = R \frac{R}{h} \gamma \, \delta A \left[(1 + K) DLF'_o \pm 4 \frac{R}{h} (1 - K) \cos 2\theta \, DLF'_2 \right]$$

2.4.3 Rock Bolts

Radially positioned rock bolts of cross-sectional area A_{rb}, weight density γ_{rb}, effective modulus of elasticity E_{rb}, and spacing S (each way) are used to reinforce the cavity wall.

The following assumptions are made:

a. It is sufficient that only the radial stress loading (Equation 2-9(a)) is reacted by the bolts

b. The bolts are anchored into the free field at a distance L from the cavity wall

c. The bolts are allowed to respond inelastically

d. The bolt material is modeled as an elastic-perfectly-plastic material

20

e.   The period of vibration of a bolt is taken as

$$T_{rb} = 2L\sqrt{\frac{\gamma_{rb}}{E_{rb}g}} \qquad (2\text{-}22)^*$$

The required pretensioning stress in the bolt is obtained from Equation 2-9(a):

$$\sigma_{rb} = R\gamma\ \delta A\ \frac{S^2}{A_{rb}}\ [1 + K + (1 - K)\cos 2\theta]\ DLF_{rb} \qquad (2\text{-}23)$$

where

$$DLF_{rb} = \frac{\pi\, t_d/T_{rb}}{\sqrt{2\mu - 1} + \dfrac{4.4\left(t_d/T_{rb}\right)^2(2\mu - 1)/2\mu}{1 \div 1.4\ t_d/T_{rb}}} \qquad (2\text{-}24)$$

$$\frac{t_d}{T_{rb}} = \frac{2\ddot{R}}{LC}\sqrt{\frac{E_{rb}g}{\gamma_{rb}}} \qquad (2\text{-}25)$$

μ = Ductility ratio, i.e., the ratio of maximum response strain in the rock bolt to the effective yield strain of the rock bolt.

---

*Fundamental period of vibration of a rod (Reference 7).

The length of the rock bolt must satisfy some minimum-length criterion. Just what this minimum length should be is not at all clear. However, judging from the load durations involved, it would appear that the rock bolt must have a length of 4R, where zero resistance is required at the outer anchor point and full resistance is required at the cavity wall. It may be tentatively assumed that it is sufficient to provide a rock bolt length of 2R, with full resistance over the entire length.

2.5 DESIGN PROCEDURE

The following inputs are assumed to be known:

a. Free-field ground shock stress, velocity, and acceleration histories

b. The stress ratio K behind the ground shock wave front

c. The effective propagation velocity C of the ground shock

d. The weight density γ of the rock

e. The cavity radius R

The following procedure can be used to determine the design parameters of the cavity reinforcement:

a. Calculate the engulfment time of the cavity: $t_e = 2R/C$.

b. Incrementalize the free-field ground shock acceleration history into a succession of constant acceleration steps of duration $2t_e$, as illustrated in Figure 2-8(a).

c. Construct an incremental free-field acceleration history as shown in Figure 2-8(c). Assume that this history is an envelope history of peak response for use in the state-of-stress equations derived for the reinforcement.

22

d. Select trial values of the reinforcement design parameters:

1. Liner: h, E, γ_ℓ

2. Backpacked liner: h, E, γ_ℓ, h_{bp}, E_{bp}, γ_{bp}

3. Rockbolts: A_{rb}, S, L, E_{rb}, γ_{rb}, μ

e. Calculate the state of stress in the reinforcement using the applicable set of equations given in Section 2.4 with the envelope δA history constructed in Step c.

f. Calculate the quasistatic stress history of the reinforcement that arises from the normal interaction of the reinforcement with the free-field ground shock and overburden loadings.

g. Add the stress histories calculated in Steps e and f.

h. Compare the peak stresses found in Step g to the allowable dynamic resistances of the reinforcement.*

i. Reiterate Steps d through h until an acceptable state of stress is obtained.

---

*If the stresses arising from the rigid-body acceleration of the reinforcement itself are not negligible compared to those in Steps f and g, then they must also be taken under consideration. Also, the buckling resistance of liners must be considered.

2.6 DISCUSSION

The following assumption was made at the outset of this investigation:

The entire interaction zone of the cavity is cut by several sets of planes of weakness of negligible tensile strength in such a fashion that (1) the characteristic dimensions of the blocks of rock are small compared to the cavity radius and (2) the blocks of rock are not wedged to one another.

Although this assumption was made so that the required restraining stress would be a function of only uniform and ovaling components--a familiar loading condition to the designer--it is very likely to be applicable to a real-life design situation. However, in cases where the assumption is not valid and the failure tendency is more irregular, e.g., where a single column of unwedged rock exists at the 0-deg azimuth, the same general solution technique can be followed after the more or less discontinuous restraining stresses are expanded in a Fourier series with respect to θ.

It was necessary to restrict the liner and backpacked liner to elastic response since it was not obvious during the course of this investigation just how inelastic deformation could be rationally handled. Further study of this problem may prove fruitful and should be undertaken. It should be noted, however, that the requirement for elastic behavior may not be an unrealistic design goal, considering the likelihood of an imposed multiple-attack threat (see Section 1.2).

The derived design requirements can also be used for cylindrical cavities with noncircular cross sections--provided the deviation from circularity is not severe--by use of an equivalent circular cavity. In the case where the direction of ground shock propagation is not perpendicular to the cavity axis, the component of the free-field ground shock acceleration that is perpendicular to the cavity axis should be used. It is suggested that this component not be less than K times the resultant acceleration.

Probably the most interesting aspect of the results is the fact that the required stress resistance of the cavity reinforcement (e.g., Equation 2-11(e)) is a function of the magnitude of the cavity radius. Such a relationship has been postulated to exist and has been the subject of much discussion since the Pile Driver shot. The relationship obtained here is a simple linear dependence upon the magnitude of the radius. This simple dependence is not inconsistent with the Pile Driver data presented in Reference 2.

Another interesting aspect of the investigation is that loss of structural integrity of a cavity under dynamic ground shock loading was found to be dependent upon the rate of change of the free-field acceleration, a highly nebulous quantity today (1971). This dependence is a fact of life and must be accepted.

The investigation presented here represents a first attempt at establishing design requirements for reinforcement which functions to prevent mechanical failure of a cavity under dynamic loading. Validation and assessment of the reliability of the design requirements will come from both laboratory and field testing and from more rigorous analytical investigations. Although a number of the assumptions made during the course of this investigation require more careful assessment, it is felt that there is sufficient validity underlying the investigation to warrant interim adoption of the derived design requirements.

GROUND SHOCK

(a)

ASSUMED REGION OF
PLANES OF WEAKNESS

ILLUMINATED
REGION

SHADOW
REGION

GROUND SHOCK

(b)
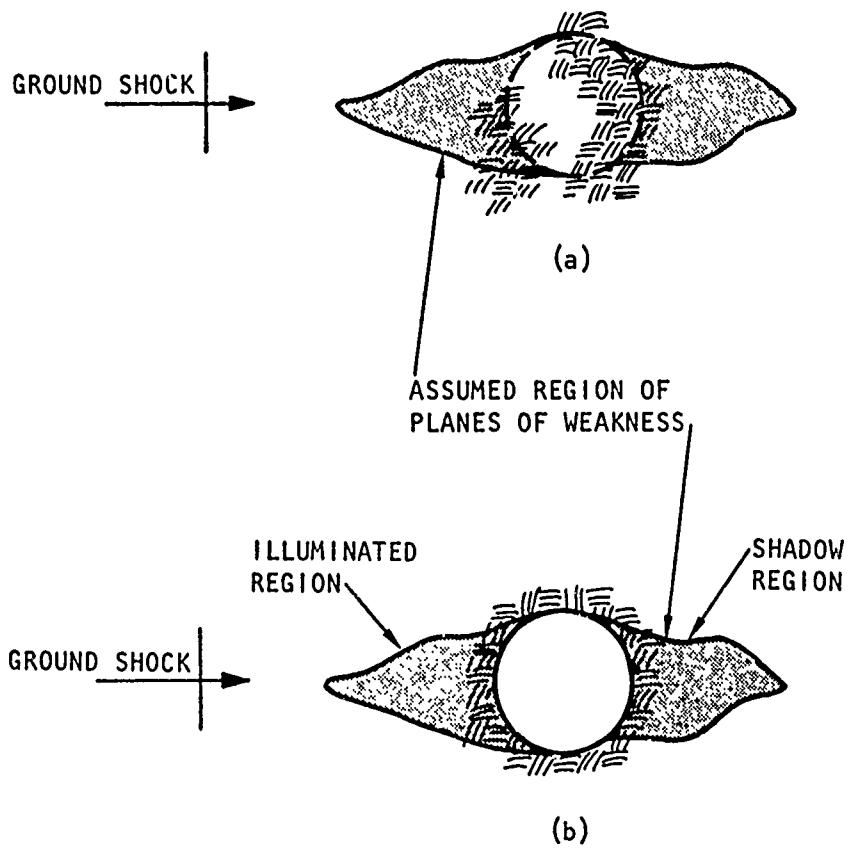
FIGURE 2-1. MECHANICAL FAILURE OF CAVITY
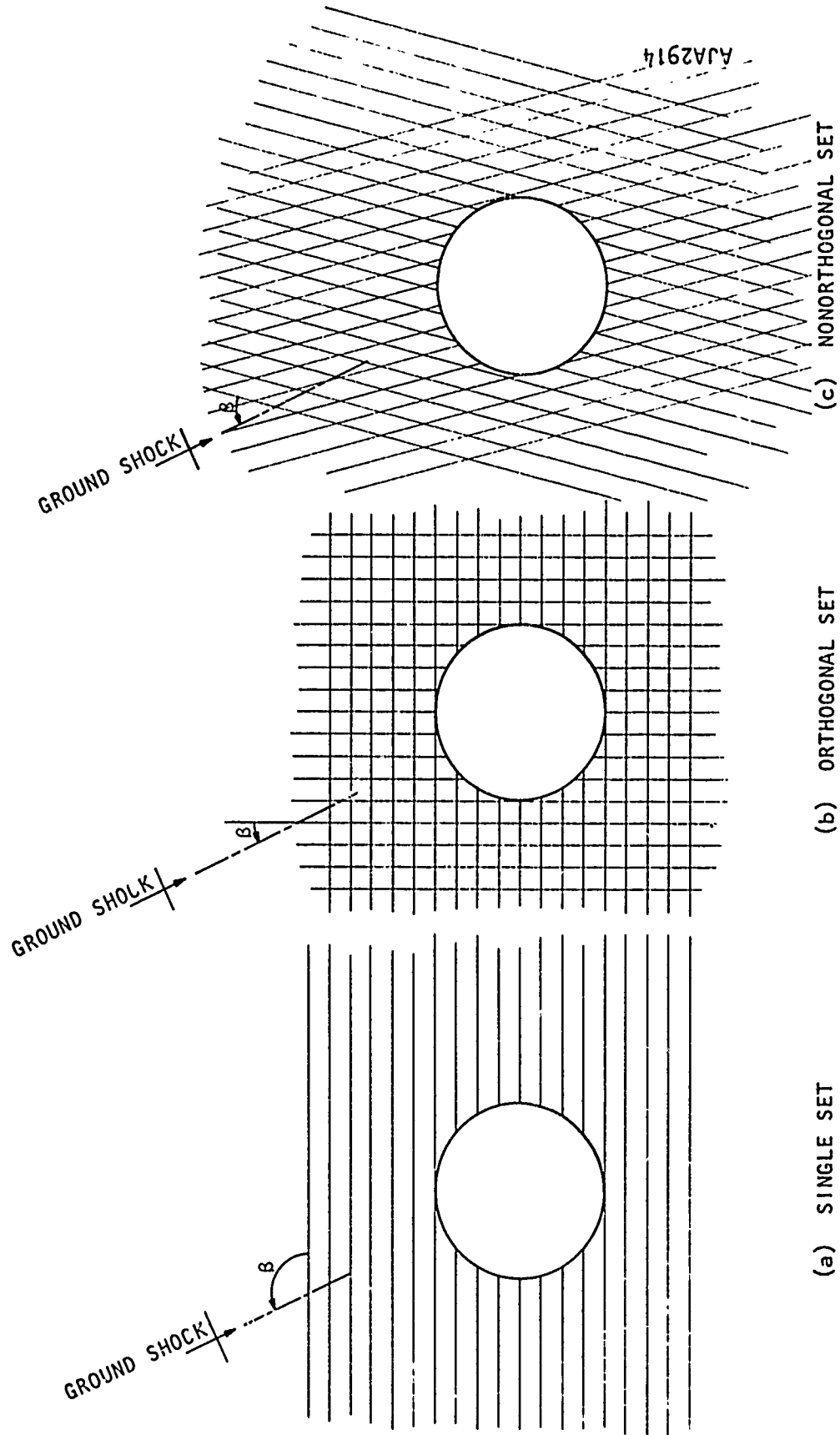
(a) SINGLE SET

(b) ORTHOGONAL SET

(c) NONORTHOGONAL SET

AJA2914

FIGURE 2-2. THREE PATTERNS OF PLANES OF WEAKNESS

27
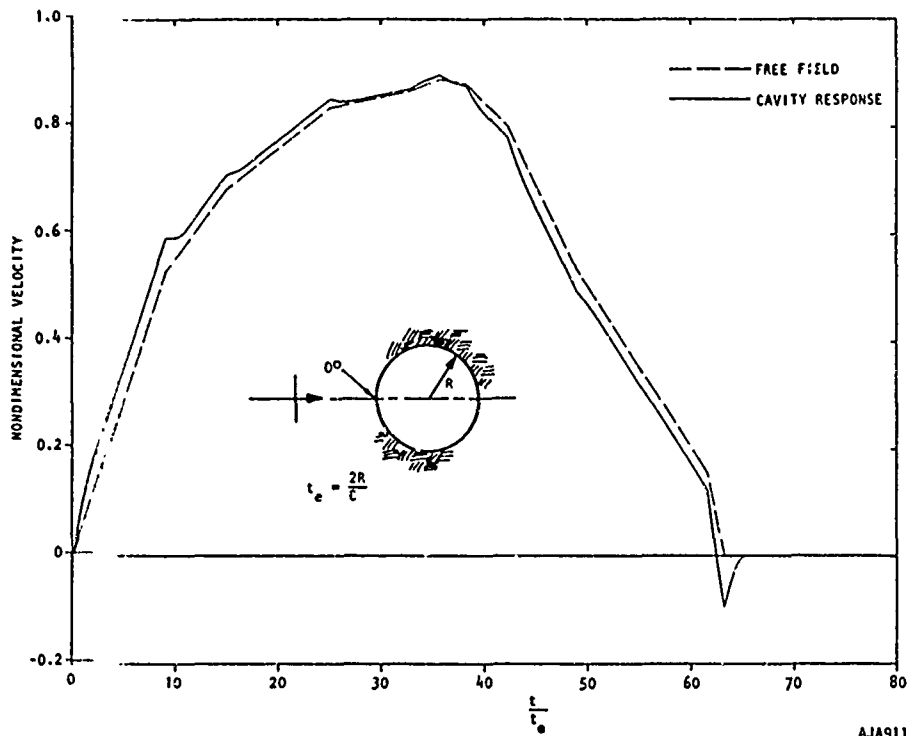
(a) FREE-SURFACE RADIAL VELOCITY AT 0°

AJA911
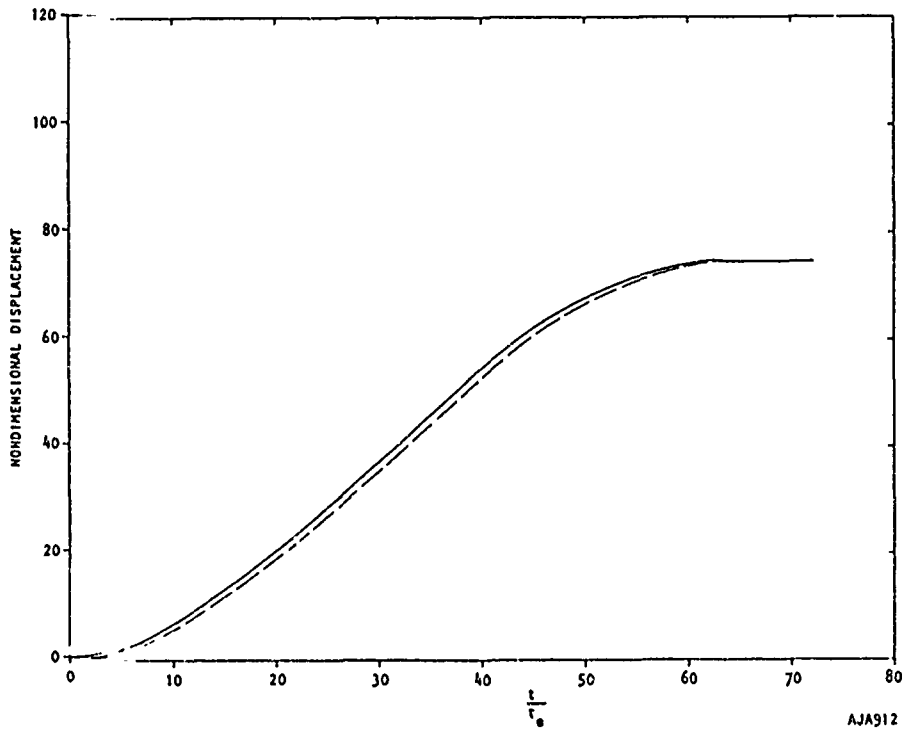
(b) FREE-SURFACE RADIAL DISPLACEMENT AT 0°

AJA912

FIGURE 2-3.   TRANSIENT RESPONSE OF CIRCULAR CYLINDRICAL CAVITY TO PIECEWISE
LINEAR PULSE (REFERENCE 5)

28
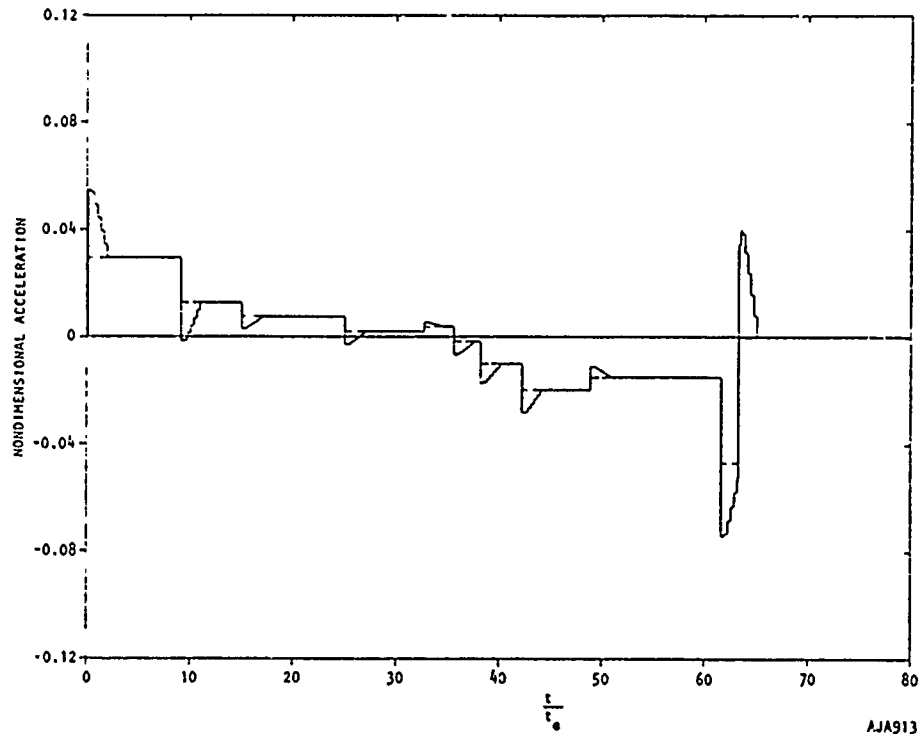
(c) FREE-SURFACE RADIAL ACCELERATION AT 0°

AJA913

FIGURE 2-3. (CONTINUED)

29
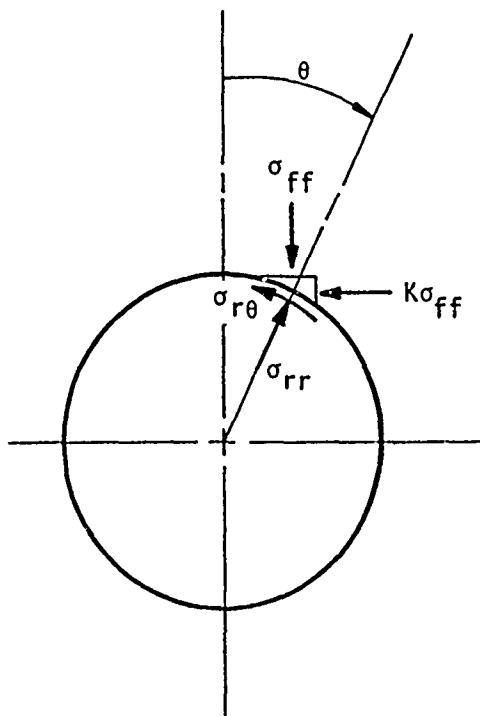
FIGURE 2-4. STRESSES AT POINTS ON CIRCLE

$$t_e = 2R/$$
$$\nu = 0.25$$

(a) $\theta = 90^{\circ}$, $r = R$

(b) $\theta = 90^{\circ}$, $r = R$

FREE FIELD
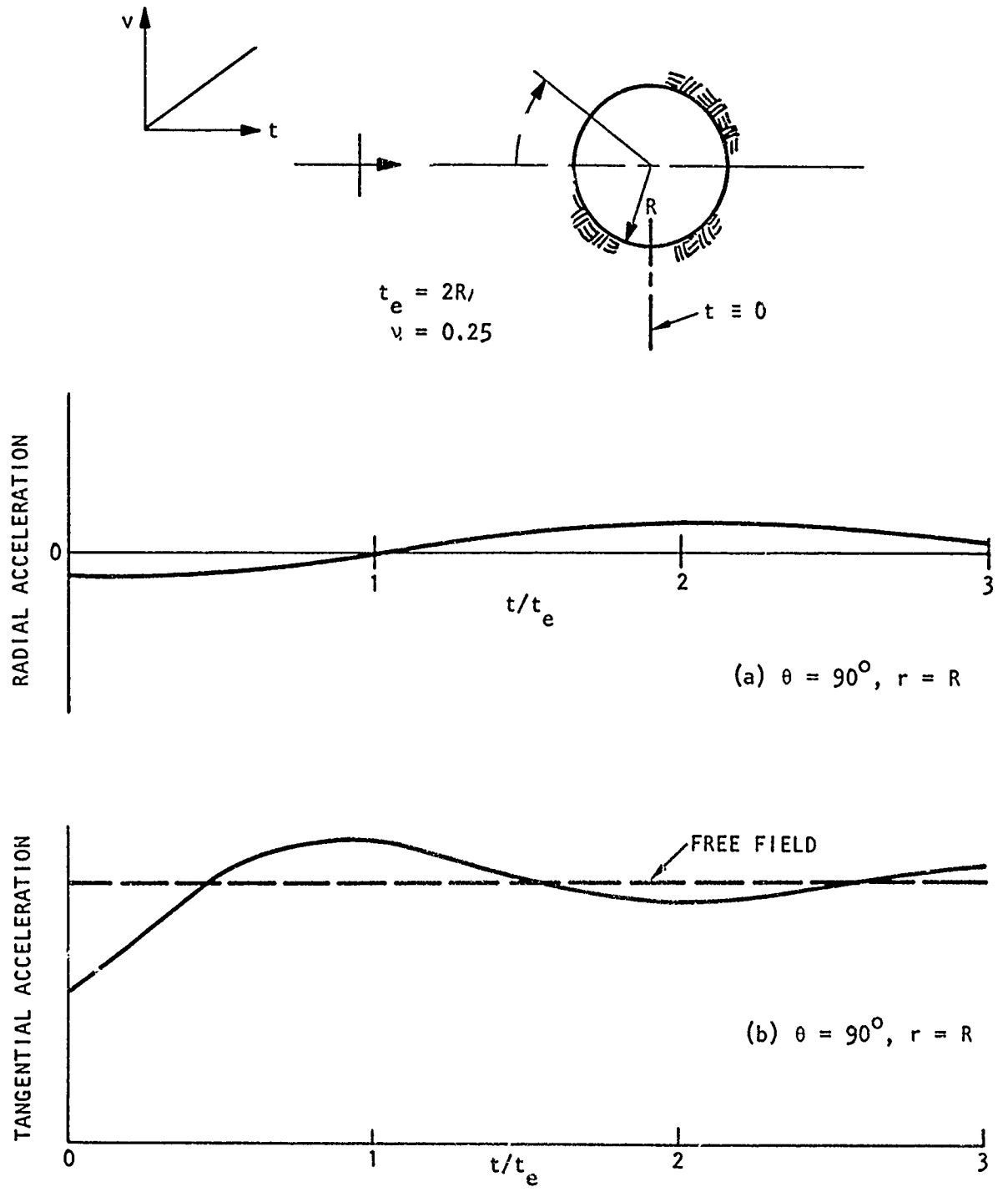
FIGURE 2-5.   TRANSIENT ACCELERATION RESPONSE ON SHADOW SIDE OF
UNLINED CAVITY

31

RADIAL ACCELERATION

(c) $\theta = 120^{\circ}$, $r = R$

t/t_e

TANGENTIAL ACCELERATION

(d) $\theta = 120^{\circ}$, $r = R$

t/t_e

FIGURE 2-5. (CONTINUED)

(e) $\theta = 150°$, $r = R$

(f) $\dot{\theta} = 150°$, $r = R$

FIGURE 2-5. (CONTINUED)

33

(g) $\theta = 180°$, $r = R$

$A_{180°} = \delta A' (1 - t/2t_e)$

FREE FIELD

RADIAL ACCELERATION

$\delta A'$

t/t_e

(h) $\theta = 180°$, $r = R$
$\dot{\theta} = 0°$, $r = R$

TANGENTIAL ACCELERATION

t/t_e

(i) $\theta = 0°$, $r = R$

FREE FIELD

$\delta A'$

$\delta A'$

RADIAL ACCELERATION

t/t_e

34
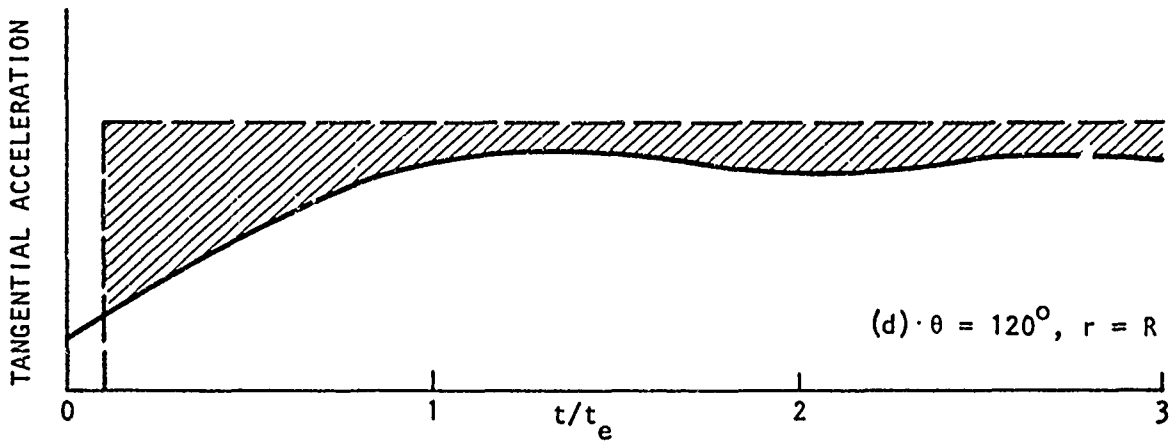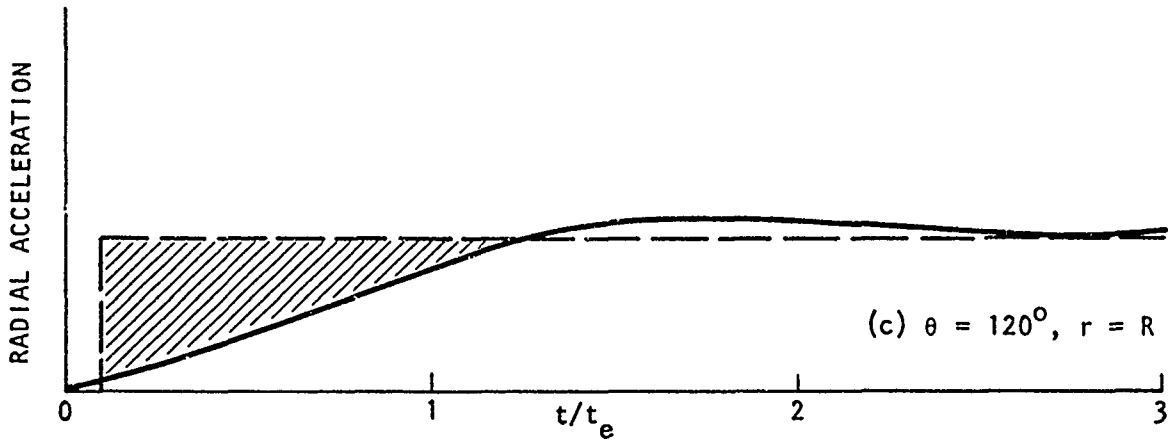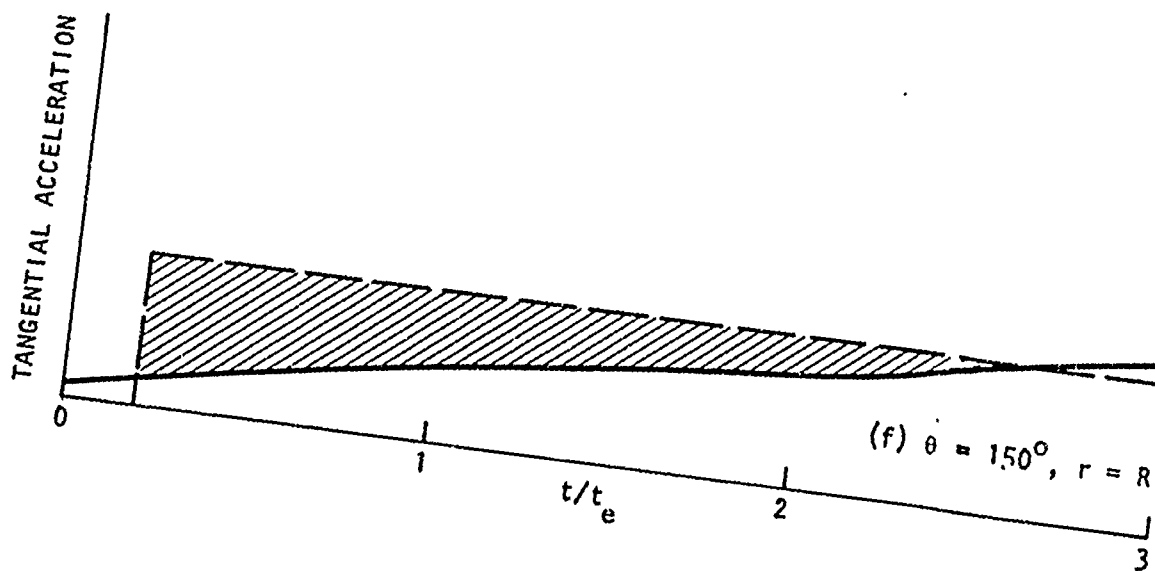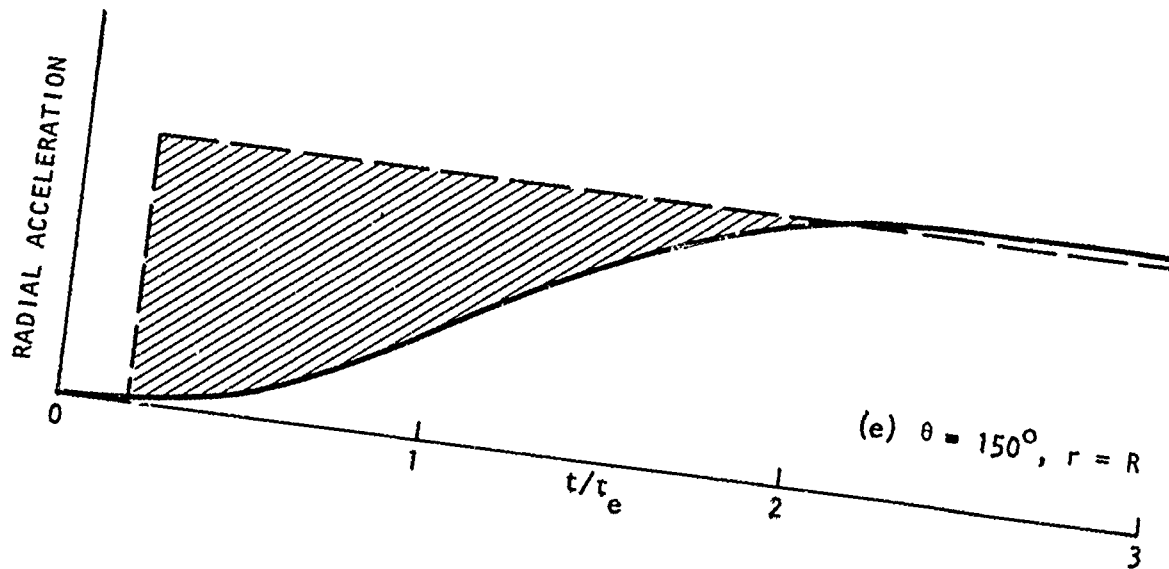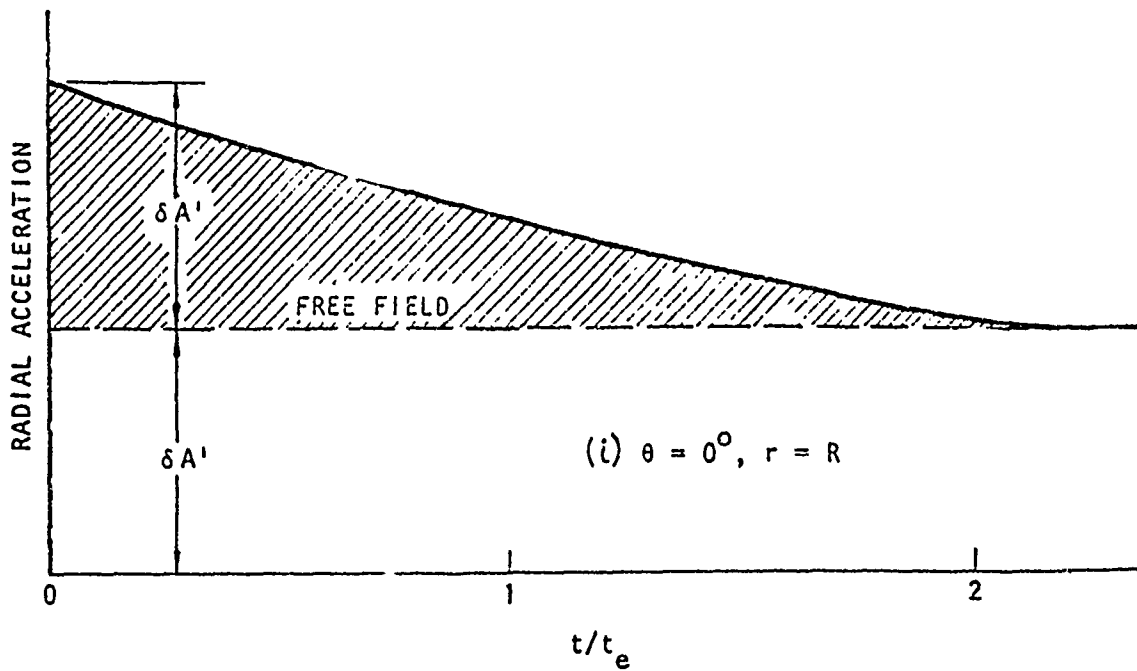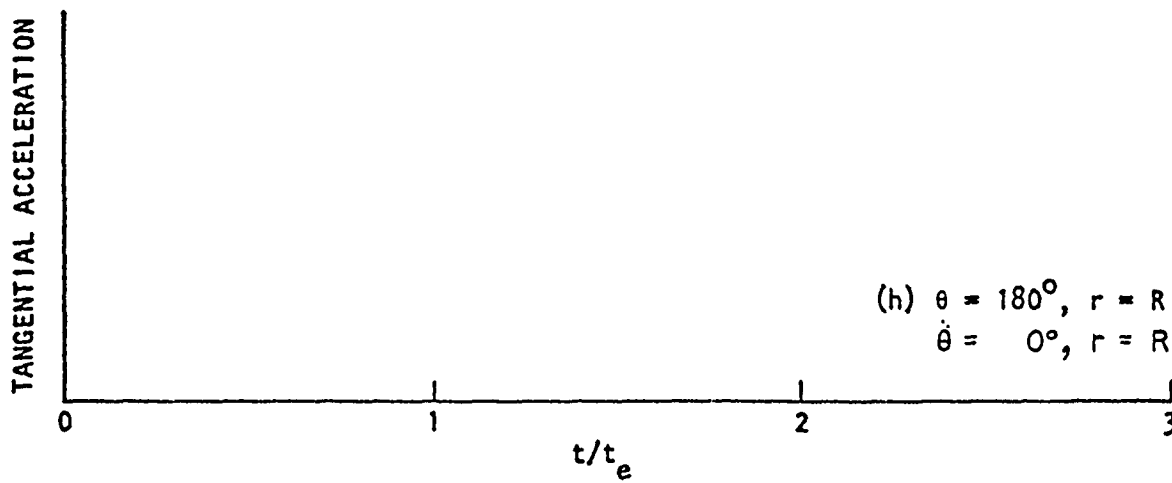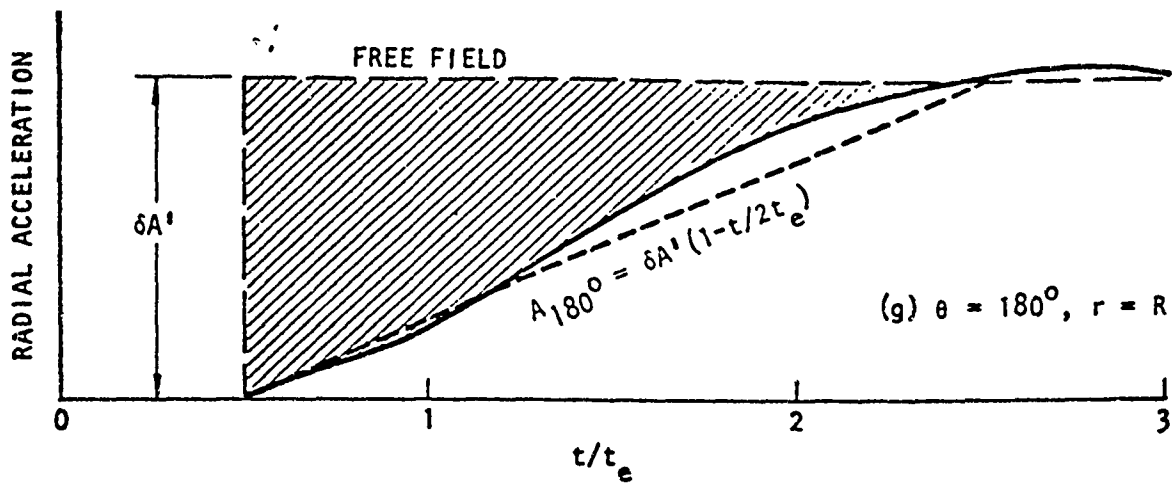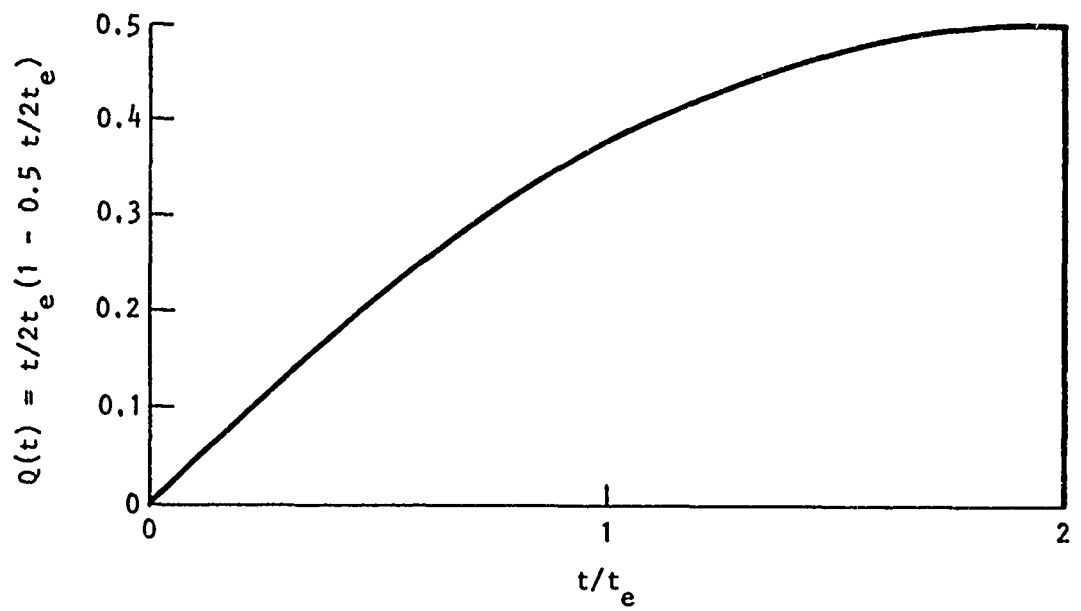
FIGURE 2-6. PLOT OF TIME FUNCTION Q(t) (EQUATION 2-6)

35
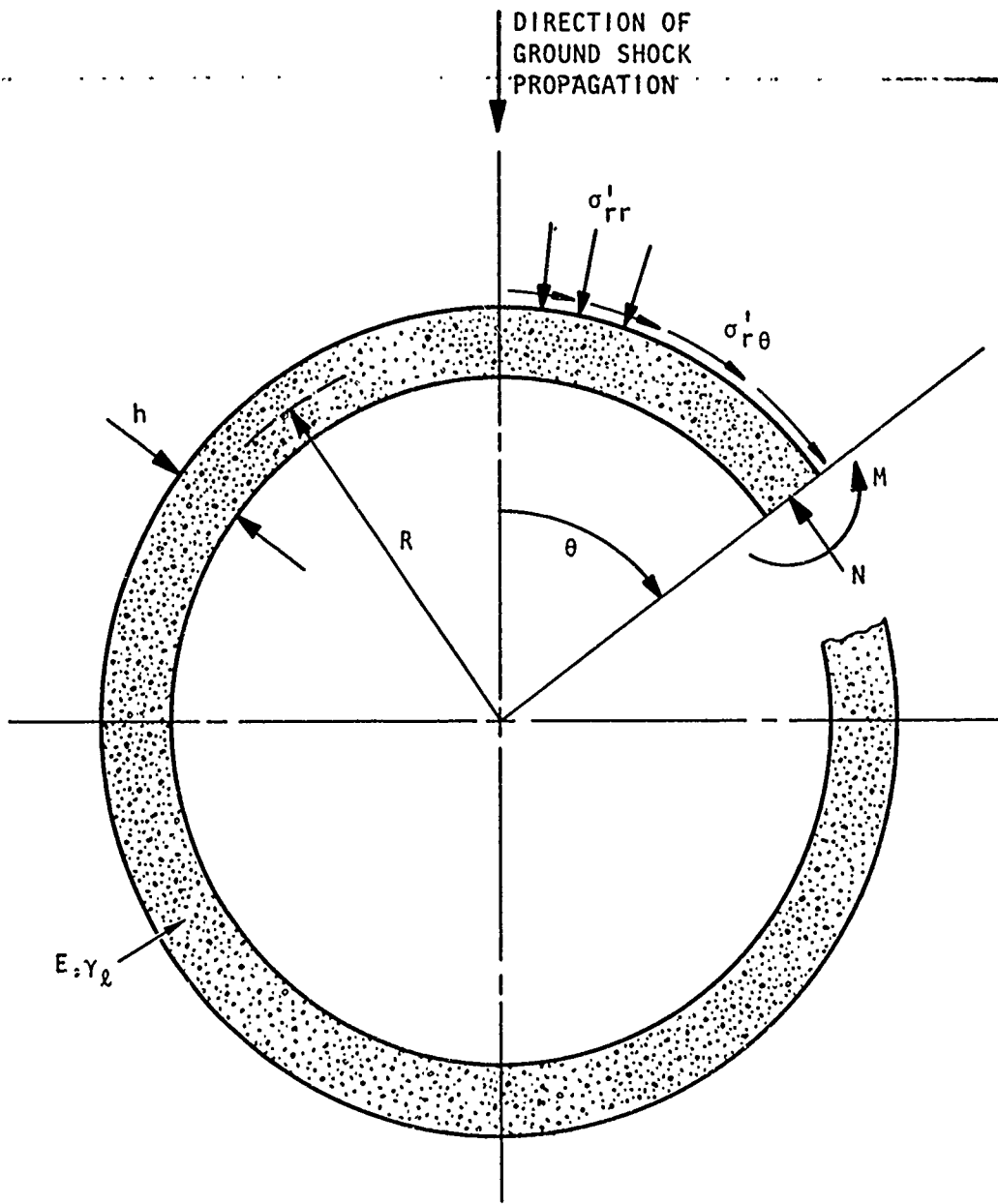
FIGURE 2-7.   LINER REINFORCEMENT

(a) FREE-FIELD ACCELERATION HISTORY

(b) CRITICAL INCREMENTS IN FREE FIELD ACCELERATION

(c) INCREMENTAL FREE-FIELD ACCELERATION HISTORY
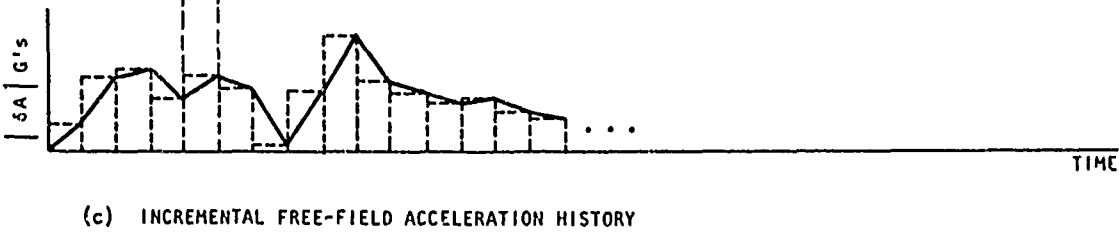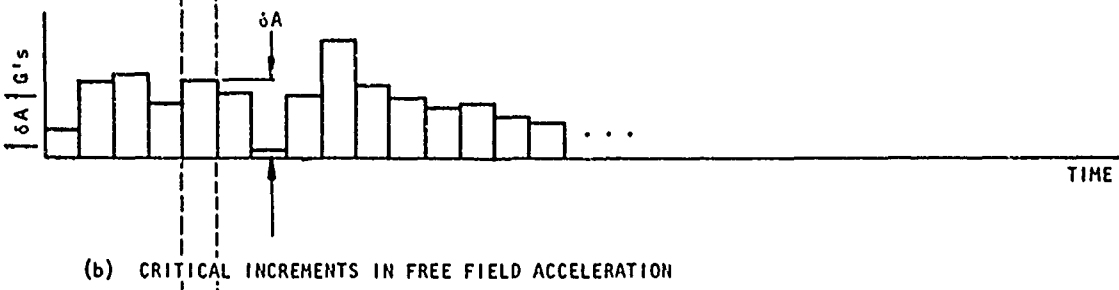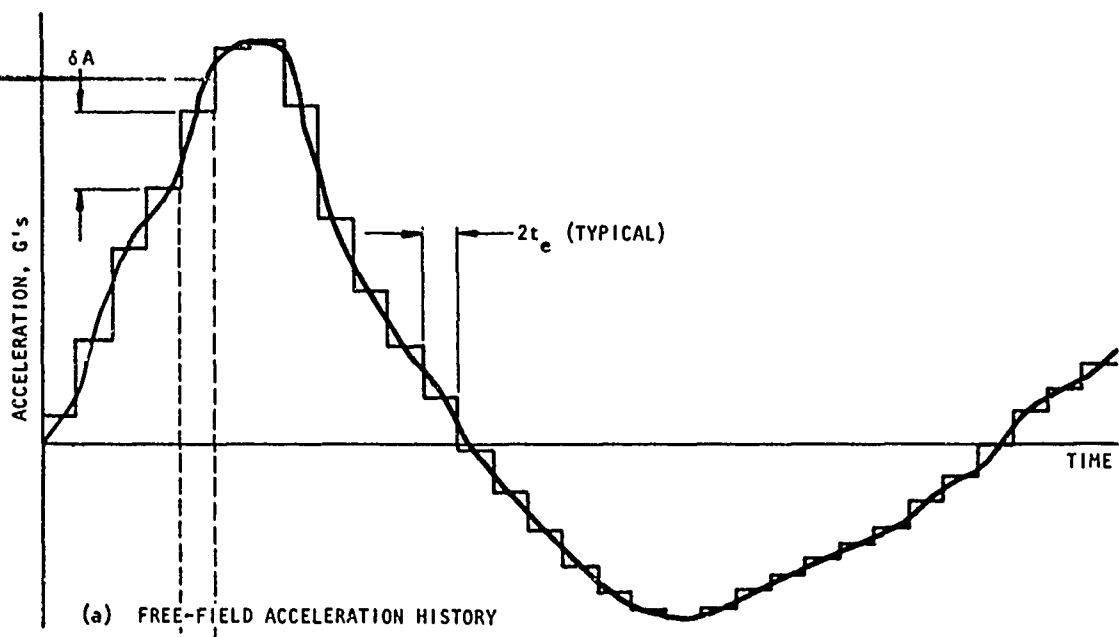
FIGURE 2-8. CONSTRUCTION OF INCREMENTAL FREE FIELD ACCELERATION HISTORY

SECTION 3

MATERIAL FAILURE OF CAVITY PENETRATIONS

3.1 INTRODUCTION

Hardened underground cavities must be penetrated at various points to provide personnel and equipment access and utility connections (air, electrical, water, fuel, etc.) with adjacent cavities and with the ground surface. The hardening of these penetrations to withstand material failure of the rock is complicated by the fact that the penetrating bore hole passes through the interaction field of the cavity, a region much more severely stressed than the free-field region in which the cavity and remote points of the penetration lie. In effect, the penetrating bore hole is subjected to an enhanced free-field stress.

The criticality of the penetration problem is examined here by calculating the inelastic response of a circular, cylindrical bore hole which penetrates a horizontal, circular, cylindrical cavity. The penetrating bore hole is assumed to be radially directed. Although this configuration of penetration and cavity may not be the most critical one possible, it is the configuration that would be expected most frequently in practice. The three-dimensional penetration problem is represented by the two-dimensional configuration as shown in Figure 3-1. This idealization is a reasonable simplification when the diameter of the penetating bore hole is small compared to the cavity diameter and when the response of the cavity without penetration is essentially elastic.

Before turning to the calculation of the inelastic response at the penetration, it is of interest to calculate the enhanced free field stress state for the penetration and the elastostatic response at the penetration. These stress states are shown in Figure 3-2 in terms of elastostatic stress concentration factors (SCF). The cavity is assumed to be in a state of plane strain; hence, the loading of the penetration in the direction of the axis of the cavity is 0.33 $\sigma_\alpha/\sigma_{off}$. Note that (1) the attenuation of ground shock stress is assumed to be proportional to $S^{-2.5}$, according to Reference 9, where S is the slant distance between the cavity and the point of burst, and (2) the depth of burial is such that the vertical overburden stress σ_{ob} is equal to the ground shock stress for a direct overhead burst σ_{off}. The SCF's in Figure 3-2 are dimensionalized, as shown in Figure 3-3, using the overburden and ground shock stresses (Figure 3-4) for a schistose gneiss rock (Reference 10).

The results shown in Figure 3-3 clearly indicate the relative severity of the penetration stresses with regard to material failure. Similar relative severities would also be obtained for other cavity

shapes, rock materials, definitions of ground shock stress, and other values of σ_{ob}/σ_{off} and K). Since the unconfined compressive strength of rock at candidate sites ranges between, say, 20 and 35 ksi, one might hastily conclude from these results that the solution to the penetration problem is simply to avoid penetration of a horizontal cylindrical cavity near the horizontal axis, say, between ±60 deg from the horizontal. This would indeed be a goal of the designer, but, unfortunately, this goal cannot always be met.

Hence, the penetration problem remains real and requires investigation to determine its severity. The penetration problem has been addressed here by way of an inelastic static analysis of a single penetration configuration subjected to repeated ground shock loading. The modeling shown in Figure 3-1 has been employed. Problem definition and the method of solution are summarized in Section 3.2. The results and a discussion of the results are presented in Sections 3.3 and 3.4, respectively.

3.2 PROBLEM DEFINITION AND METHOD OF SOLUTION

The configuration studied is shown in Figure 3-5 and consists of a steel-lined penetration at the springline of an unlined horizontal, circular, cylindrical cavity located at a depth of 4300 ft in a schistose gneiss rock mass subjected to a 25-MT surface burst. The penetration liner, fabricated from 50,000-psi yield strength steel, is 6 in. thick and has a 72-in. internal diameter.

The vertical free field overburden and ground shock stresses applicable for the cavity, each 5,000 psi, are taken from Figure 3-4. The response of the cavity is assumed to be elastic. The critical SCF's for the cavity at the point of penetration result from a direct overhead burst and are taken to be 2.5 and 0.43 in the circumferential and axial directions, respectively. Under these conditions, the enhanced free field environment for a transverse slice of the penetration at the cavity wall becomes 2.5 x 5000 = 12,500 psi overburden plus 2.5 x 5000 psi = 12,500 psi ground shock in the vertical direction, and 0.43 x 5000 psi = 2,100 psi overburden plus 0.43 x 5000 psi = 2100 psi ground shock in the axial direction of the cavity. The penetration slice examined in the analysis is assumed to be in a state of plane stress.

The response of the penetration slice to this enhanced free-field environment was calculated using a static, two-dimensional non-linear finite element computer program called INSTEP. Static application of the ground shock loading is quite reasonable for most combinations of rock material, cavity size, and ground shock pulse shape encountered in practice (Reference 5). Features of the code as applied to the penetration problem include the following:

    a.   Use of constrained quadrilateral finite element specialized for plane stress

39

b. Use of a midpoint rule of integration for the incremental overburden and ground shock loading

c. Acceptance of nonlinear material property representations incorporating yield criterion, flow rule, and bulk and shear moduli

d. Allowance for the addition or elimination of elements and variations of the material properties of designated elements during execution

Each of these features is discussed briefly in Appendix C.

The finite element mesh used in the computations is shown in Figure 3-6.

Material property data for the schistose gneiss were derived from Reference 10 (see Appendix A). The following bulk and shear moduli were obtained for both loading and unloading:

$$\text{Bulk Modulus} \quad B = 5.5 \times 10^6 \text{ psi}$$

$$\text{Shear Modulus} \quad G = 2.5 \times 10^6 \text{ psi}$$

The yield criterion adopted, shown in Figure 3-7, is consistent with the data presented for the dry intact specimens of rock. The above properties were assumed to be unaffected by the first or subsequent attack.

The bulk modulus, shear modulus, and yield criterion for the steel liner were taken as:

$$B = 1.97 \times 10^7 \text{ psi}$$

$$G = 1.185 \times 10^7 \text{ psi}$$

$$f = \sqrt{J_2'} - 29,000 \text{ psi} \leq 0$$

The loading sequence was as follows:

Step (a)--In the absence of the steel liner, the enhanced free field overburden stress was applied in 12 incremental steps.

Step (b)--The steel liner was emplaced.

Step (c)--The enhanced free field ground shock stress was applied in 16 incremental steps.

Step (d)--The ground shock stress was removed in 16 incremental steps.

Step (c) and (d) were then repeated four times.

3.3 RESULTS

The results of the analysis are summarized in Figures 3-8 to 3-12 and in Appendix B.

3.4 PHYSICAL INTERPRETATION OF RESULTS

The radial displacement at the penetration crown and springline (Figures 3-8 and 3-9) illustrate well the effects of liner reinforcement and repeated attack on material failure of penetrations. Considering the crown displacement shown in Figure 3-8, the rock undergoes inelastic response under the overburden alone. The extent of the inelastic incremental response under the last increment of overburden loading is shown in Figure 3-12(a). After the steel liner is emplaced, the response to ground shock becomes essentially elastic due to the confirement provided by the liner. It should be noted that the confinement increases the hydrostatic state of stress in the rock, and thus increases the effective yield strength of the rock. Hence, some inelastic rock elements revert to elastic behavior upon further loading after confinement. Comparison of Figures 3-12(a) and 3-12(b) illustrates the effect of liner confinement as seen by the reduction in the number of elements undergoing inelastic incremental strain between the last increment of overburden loading and the first increment of ground shock loading. At roughly 20-ksi loading, the liner begins to yield as seen by the deviation of the displacement curve from the elastic solution. At roughly 22-ksi loading, the liner is yielded across its thickness at the springline and thereafter offers a reduced restraint to the opening. The extent of inelastic incremental response at the last loading increment of the first attack is shown in Figure 3-12(c). The growth of inelastic incremental response for each loading increment from first application of overburden to the last increment of the first attack ground shock can be traced in the figures contained in Appendix B.

Unloading of the first attack ground shock occurs virtually parallel to the loading branch, where the liner response was elastic (see Figure 3-8). Examination of the solution printout shows that the liner immediately unloaded, and continued to unload, elastically, while the rock unloaded inelastically. The extent of the inelastic incremental response for the last increment of unloading is shown in Figure 3-12(d)*. The rock which experiences inelastic response during this last unloading increment can be thought of as a region of locked-in "plastic stress." In the absence of the liner, it is believed that the rock would have unloaded elastically and, thus, would not have exhibited this region of "locked-in" stress.

---

*The islands of incremental elastic response shown in Figure 3-12(d) are believed to result from the inherent inaccuracy in determining whether the yield criterion is satisfied. Execution of the problem with smaller load increments would reveal if this is indeed the source of these islands.

Repeated attack produces additional permanent displacement (Figures 3-8 through 3-11). The extent of the inelastic incremental response for the last load increment of the second, third, and fourth attacks is shown in Figure 3-12(e) to (g). The additional permanent displacements appear to be real judging from their large magnitudes. It would appear unlikely that these large increments in displacement would be due to solution accuracies and/or the encroachment of the yielded rock boundary on the mesh boundary. The seemingly erratic growth increments could be due to solution inaccuracies, as noted earlier. Unfortunately, the problem had to be terminated before it could be determined if the growth was in the process of stabilizing, or would continue its erratic growth, or was dying out.

3.5 IMPLICATION OF RESULTS IN DESIGN

The results presented above have two unmistakable implications in design, namely:

a. Steel-lined penetrations can be adequately and cost-effectively designed to withstand repeated attack with large-yield weapons, *provided that there is no significant deterioration in rock strength with each attack*

b. The analysis technique used here, the INSTEP Code, or an equivalent technique, can be effectively used today by the designer, *provided material property parameters are available*

Although a single penetration configuration has been examined, it is concluded that adequate penetration designs can be provided for threats and sites of current interest, except for the effects of a deterioration in rock strength. Assuming as a worst case for the configuration examined that each attack after the first produces a 0.1-in. reduction in the penetration radius, an 8-percent reduction in the cross-sectional area of the penetration results after ten 25-MT bursts. Even allowing for considerable error or change in the configuration parameters would still result in a closure that could be tolerated or compensated for. Since the rock material considered has an uncommonly low unconfined compressive strength compared to what would normally be sought for candidate sites, the generalization of this example would tend to be on the conservative side. Thus, the feasibility of penetration design, in general, hinges upon the favorable performance of the rock under repeated loading. This aspect of the problem can be easily incorporated in the analysis technique simply by changing material parameters after each attack, once material property parameters have been defined for repeated loading.

In order that a sophisticated analysis tool have utility in complex design, it is necessary that the tool yield useful design information that is easily given physical interpretation. The INSTEP Code used here, or an equivalent code, provides this utility as evidenced by the useful and easily interpreted results obtained in this study. It is of interest to note that the execution time for this problem through the completion of four "dynamic" load cycles was 1-1/2 hr on a UNIVAC 1108 computer.
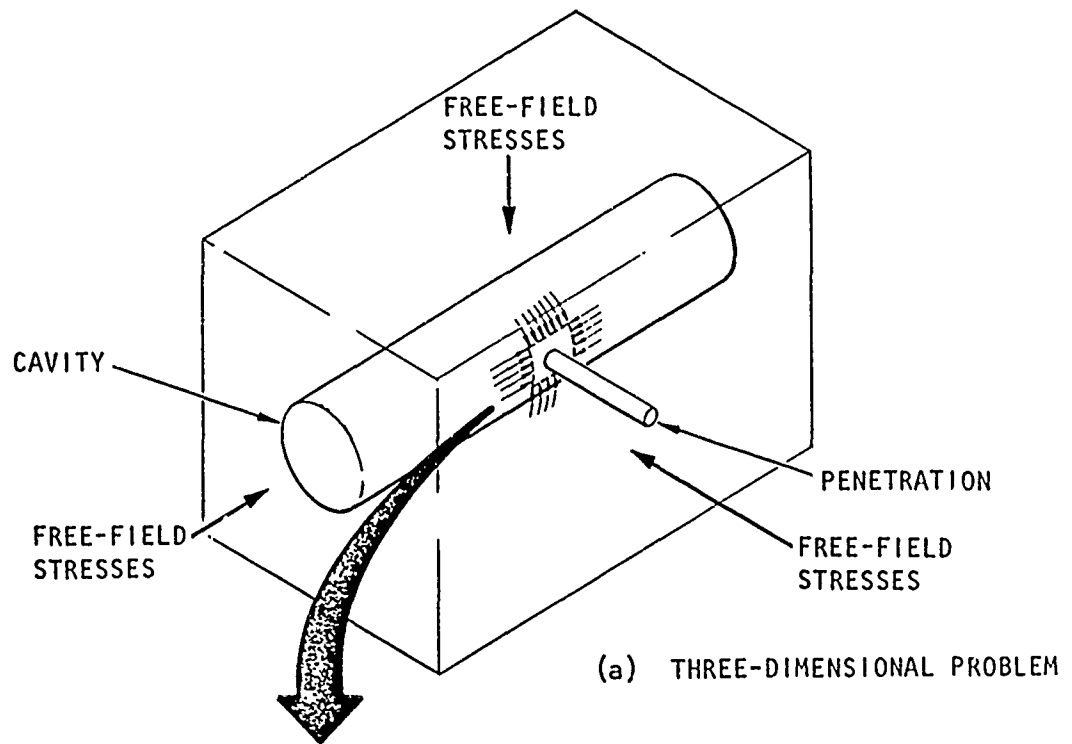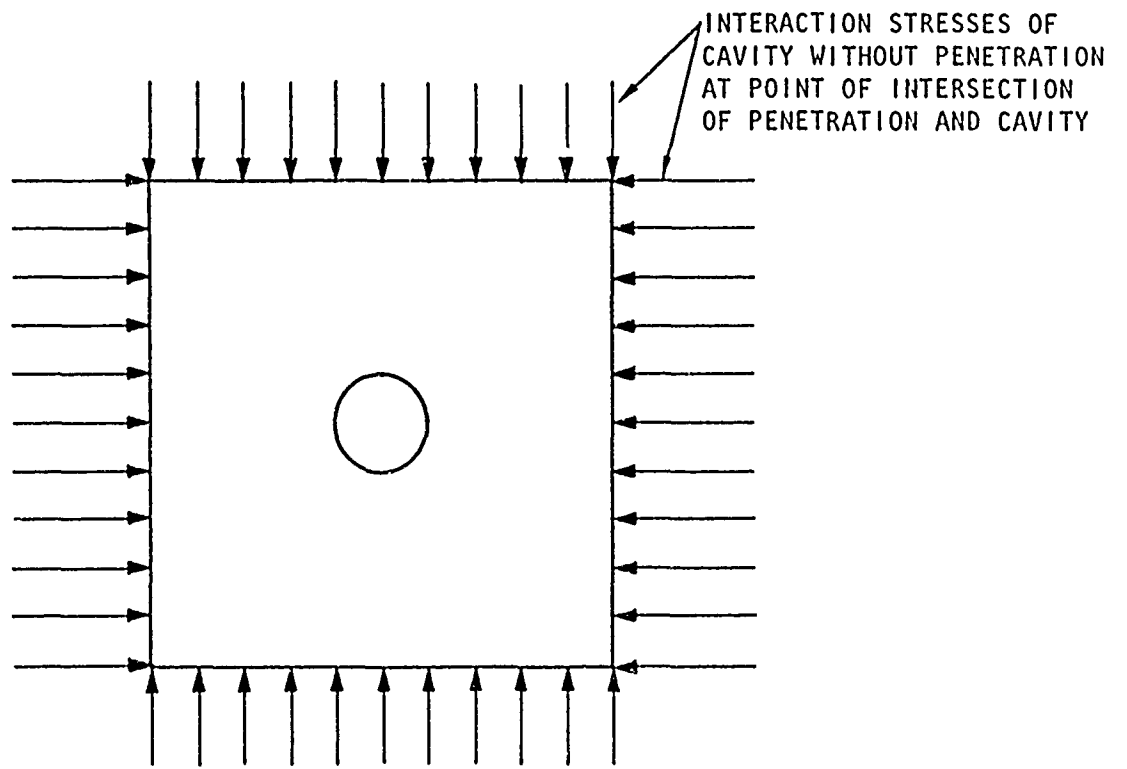
FIGURE 3-1.   IDEALIZATION OF PENETRATION PROBLEM

44

$$\frac{\sigma_\alpha}{\sigma_{off}} = \cos^N \theta \left\{ 1 + K_{gs} - 2(1 - K_{gs}) \cos(2\alpha + 2\theta) \right\}$$

$$+ \frac{\sigma_{ob}}{\sigma_{off}} \left\{ 1 + K_{ob} - 2(1 - K_{ob}) \cos 2\alpha \right\}$$
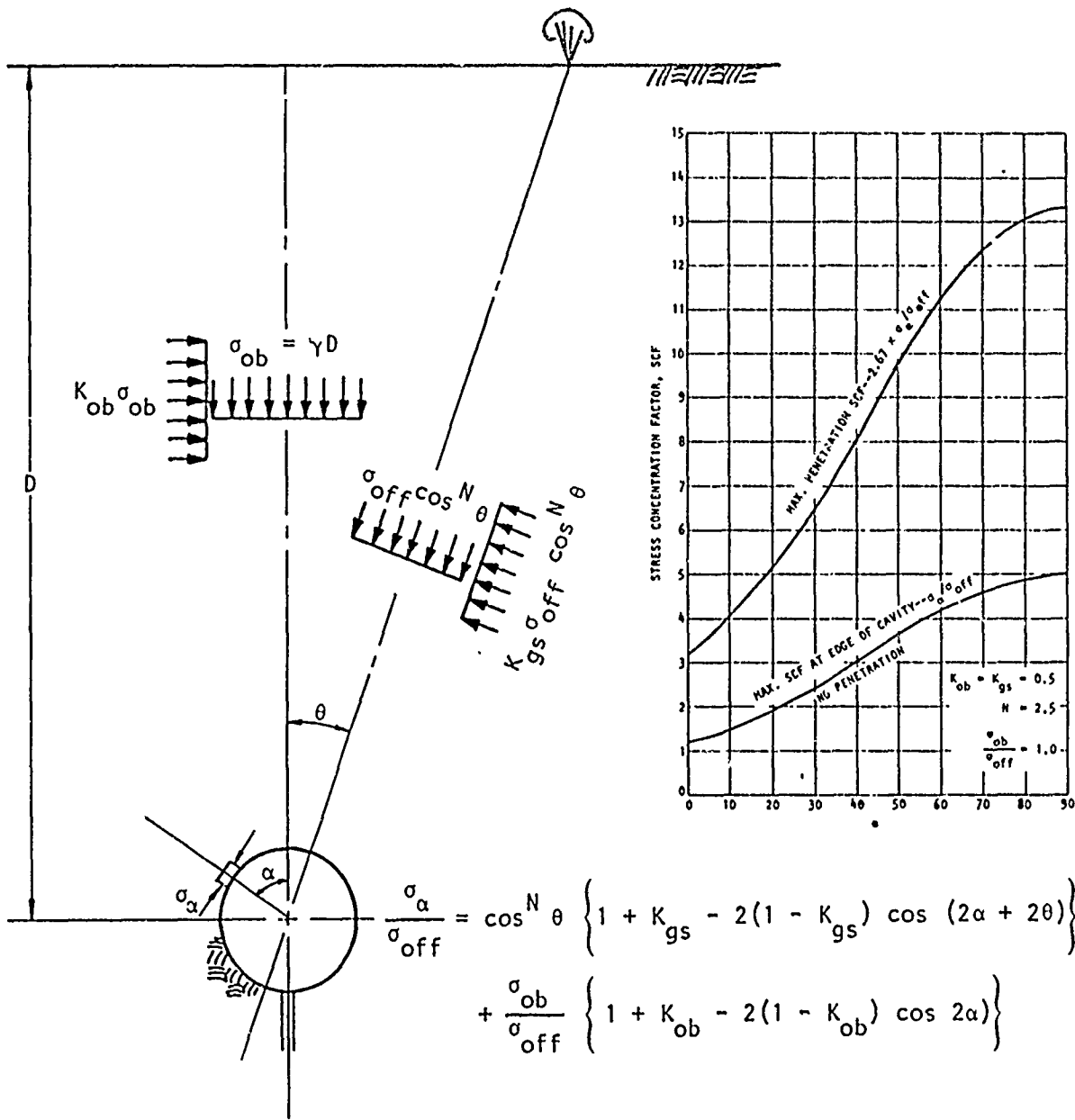
FIGURE 3-2. ELASTOSTATIC STRESS CONCENTRATION FACTORS FOR PENETRATION OF HORIZONTAL CYLINDRICAL CAVITY
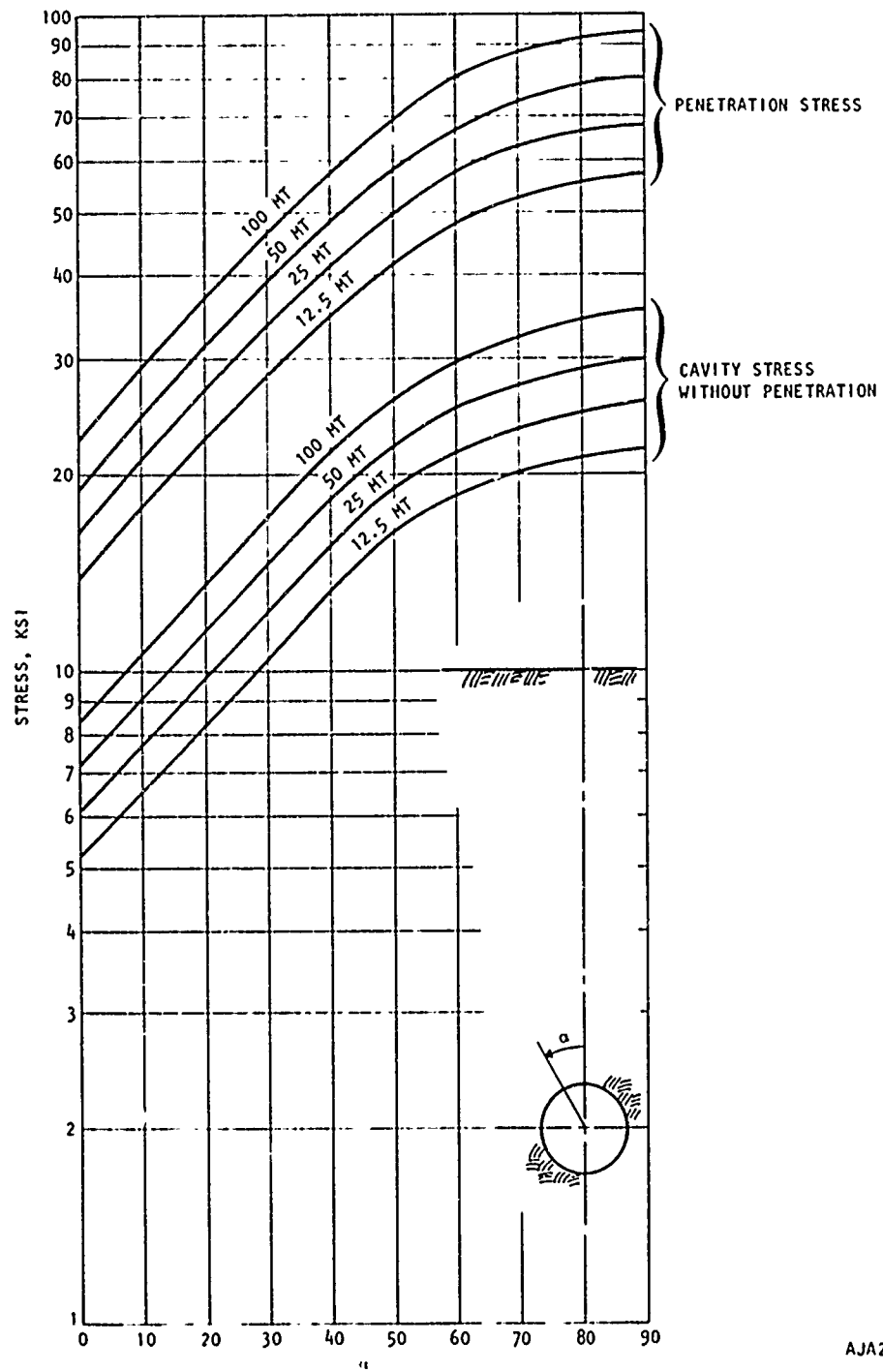
FIGURE 3-3.   CAVITY AND PENETRATION MAXIMUM STRESSES

46
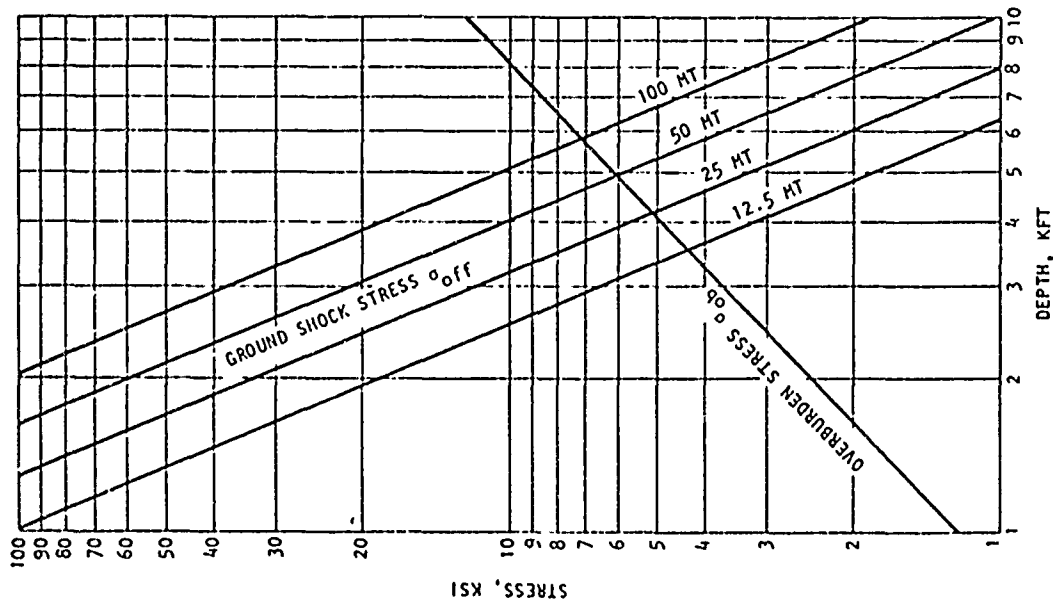
$$\epsilon_{off} = 0.0015 \left(\frac{W}{1 \text{ MT}}\right)^{5/6} \left(\frac{1000 \text{ FT}}{D}\right)^{5/2} \left(\frac{165 \text{ PCF}}{\gamma}\right)^{5/6} \left(\frac{18,000 \text{ FPS}}{C}\right)^{5/3}$$ (REFERENCE 9)

$$\sigma_{off} = \epsilon_{off} E$$

$$\sigma_{ob} = \gamma D$$

γ = 175 PCF

C = 15,400 FPS $\}$ (REFERENCE 10)

E = 6.6 × 10⁶ PSI

AJA2853

FIGURE 3-4. GROUND SHOCK AND OVERBURDEN STRESSES VERSUS DEPTH

47
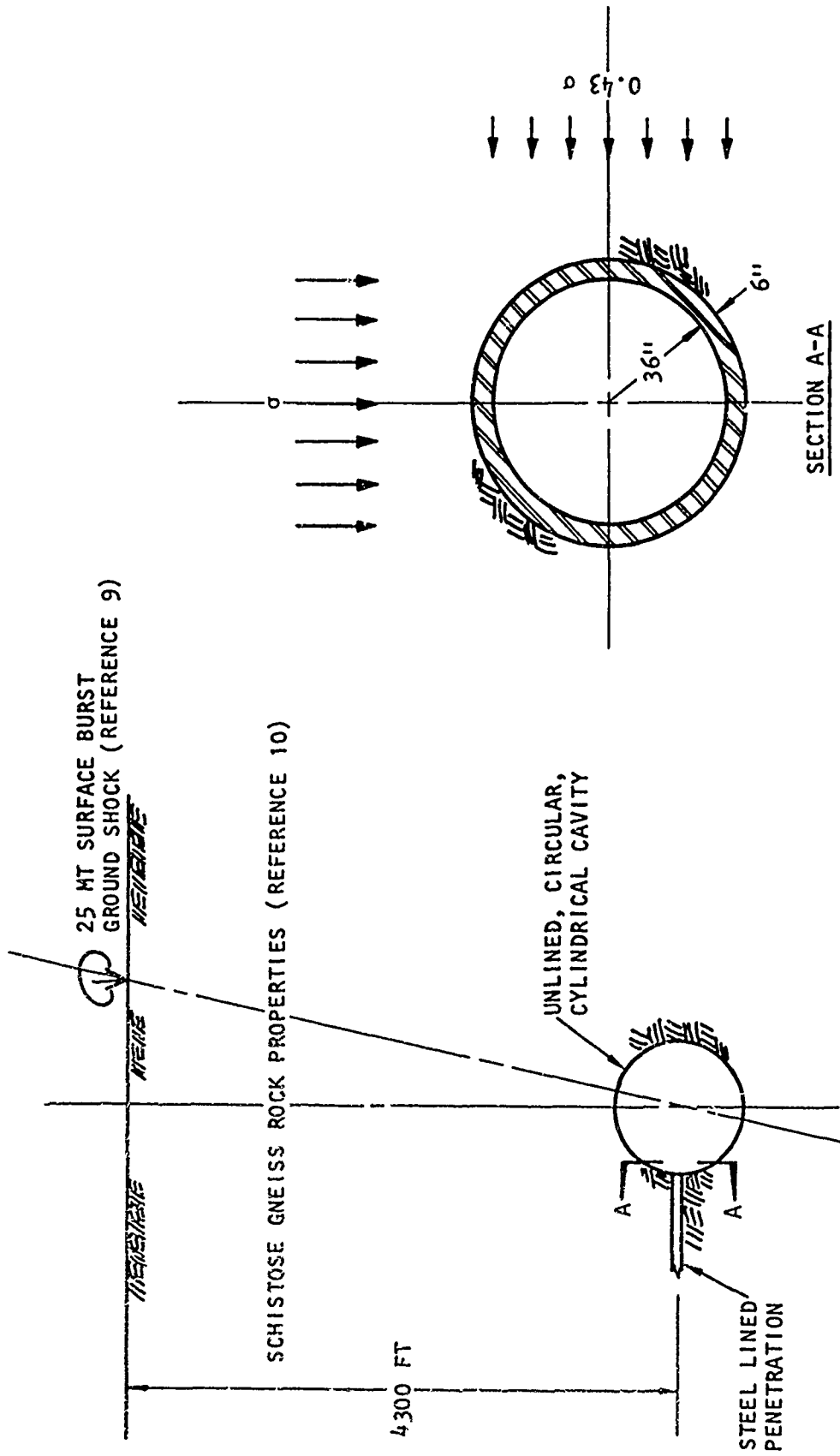
FIGURE 3-5. PENETRATION PROBLEM CONFIGURATION

STEEL LINER
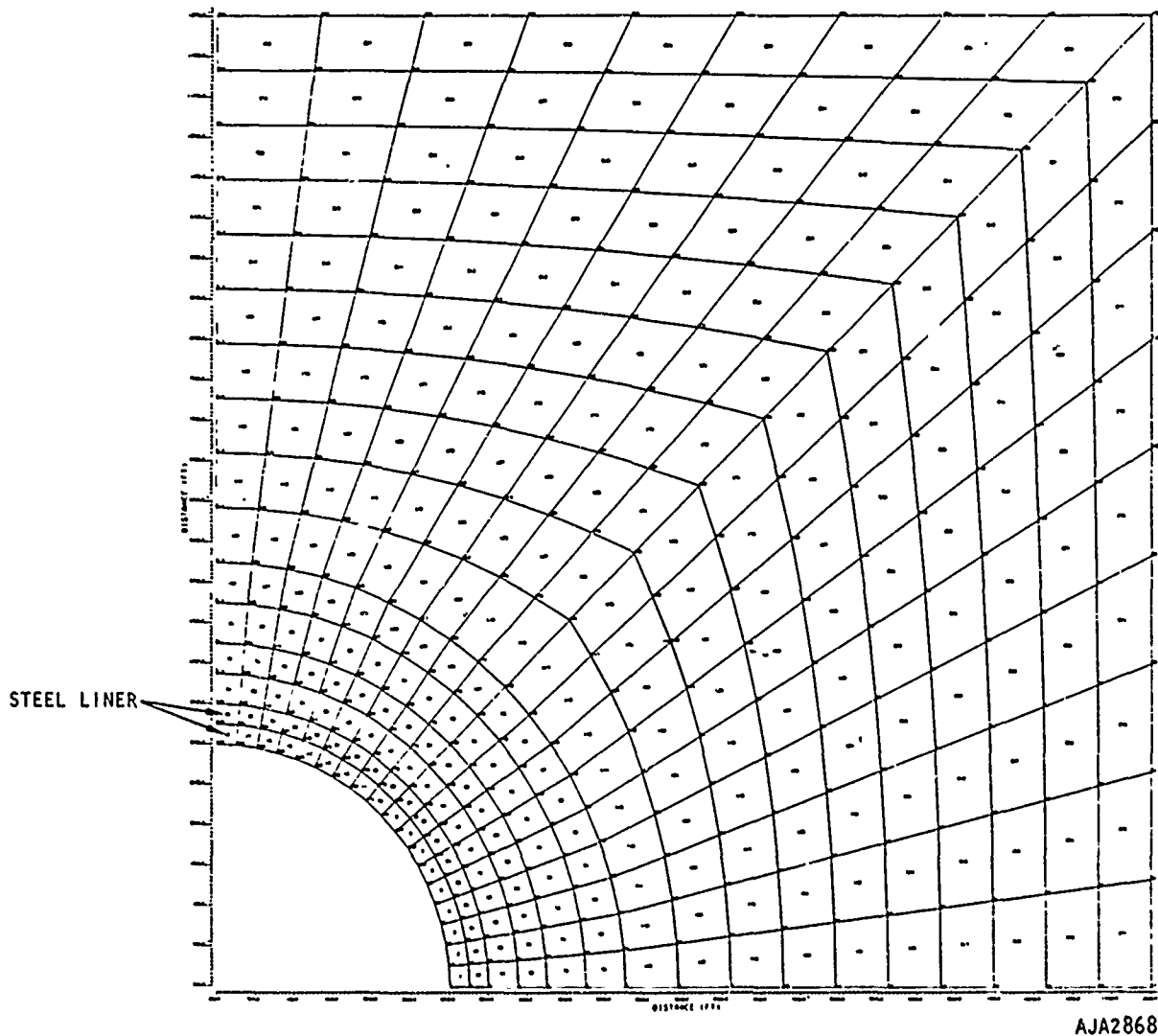
FIGURE 3-6. FINITE ELEMENT MESH OF PENETRATION
(SEE FIGURE 3-1)(b))

AJA2868

49

$$\sqrt{J_2'} = \alpha_2 J_1 + C_2$$

$$\sqrt{J_2'}$$

$$\sqrt{J_2'} = \alpha_1 J_1 + C_1$$

$$\sqrt{J_2'}$$

$$J_1'$$

$$J_1 \qquad (J_1 < 0)$$
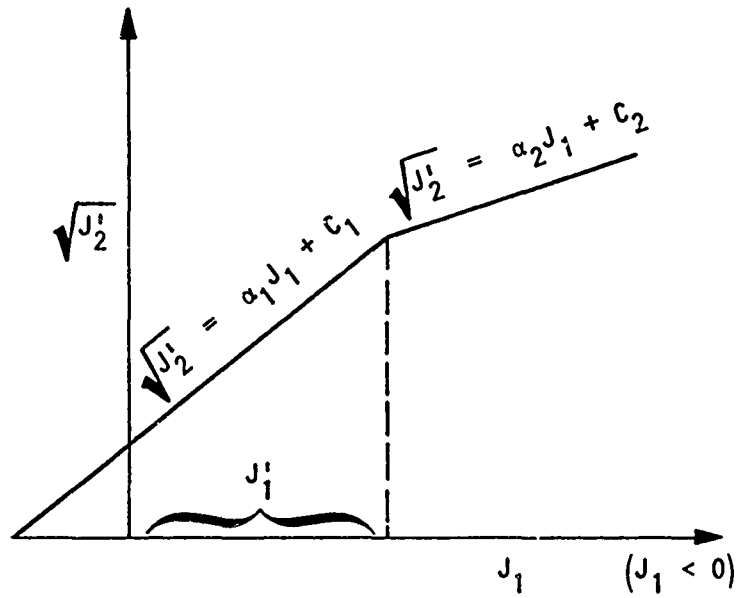
Where

$$J_1 = \sigma_{11} + \sigma_{22} + \sigma_{33}$$

$$J_2' = \left\{ \frac{1}{6} \left[\left(\sigma_{11} - \sigma_{22} \right)^2 + \left(\sigma_{33} - \sigma_{22} \right)^2 + \left(\sigma_{33} - \sigma_{11} \right)^2 \right] \right\}^{1/2}$$

$$J_1' = -34,600 \text{ PSI}$$

$$\alpha_1 = 0.39$$

$$\alpha_2 = 0.205$$

$$C_1 = -2000 \text{ PSI}$$

$$C_2 = -8400 \text{ PSI}$$

FIGURE 3-7.   YIELD CRITERION FOR ROCK MATERIAL

50
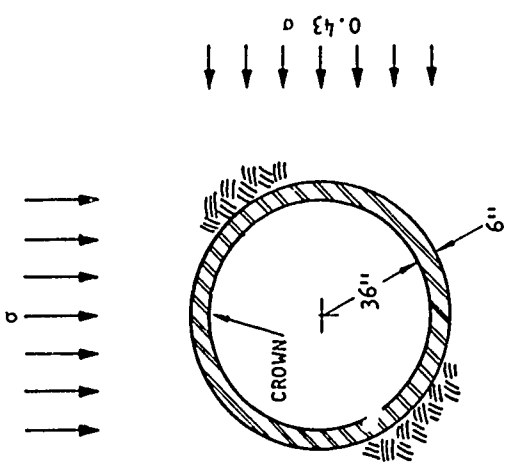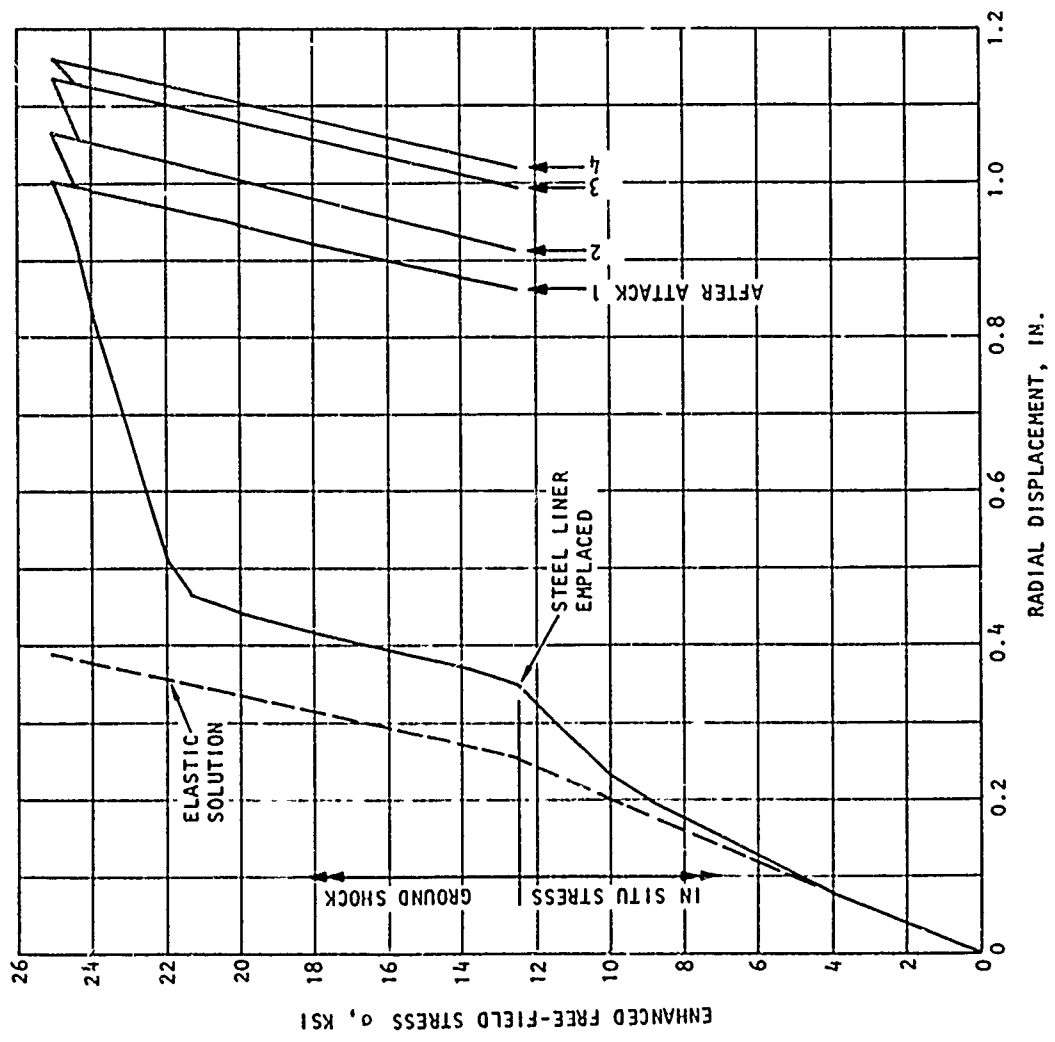
FIGURE 3-8. RADIAL DISPLACEMENT OF PENETRATION CROWN

AJA2864

51
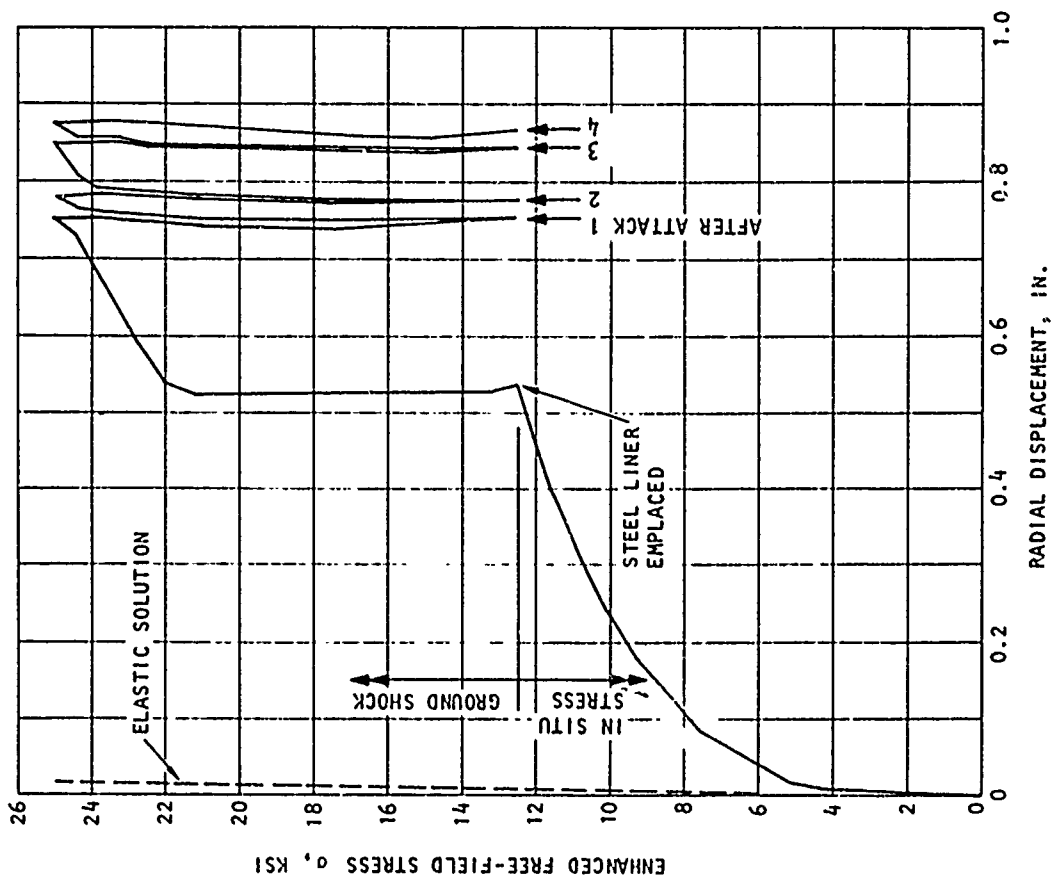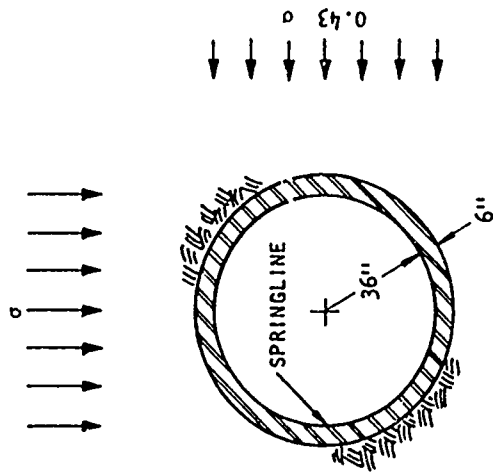
FIGURE 3-9. RADIAL DISPLACEMENT OF PENETRATION SPRINGLINE

AJA2865

52
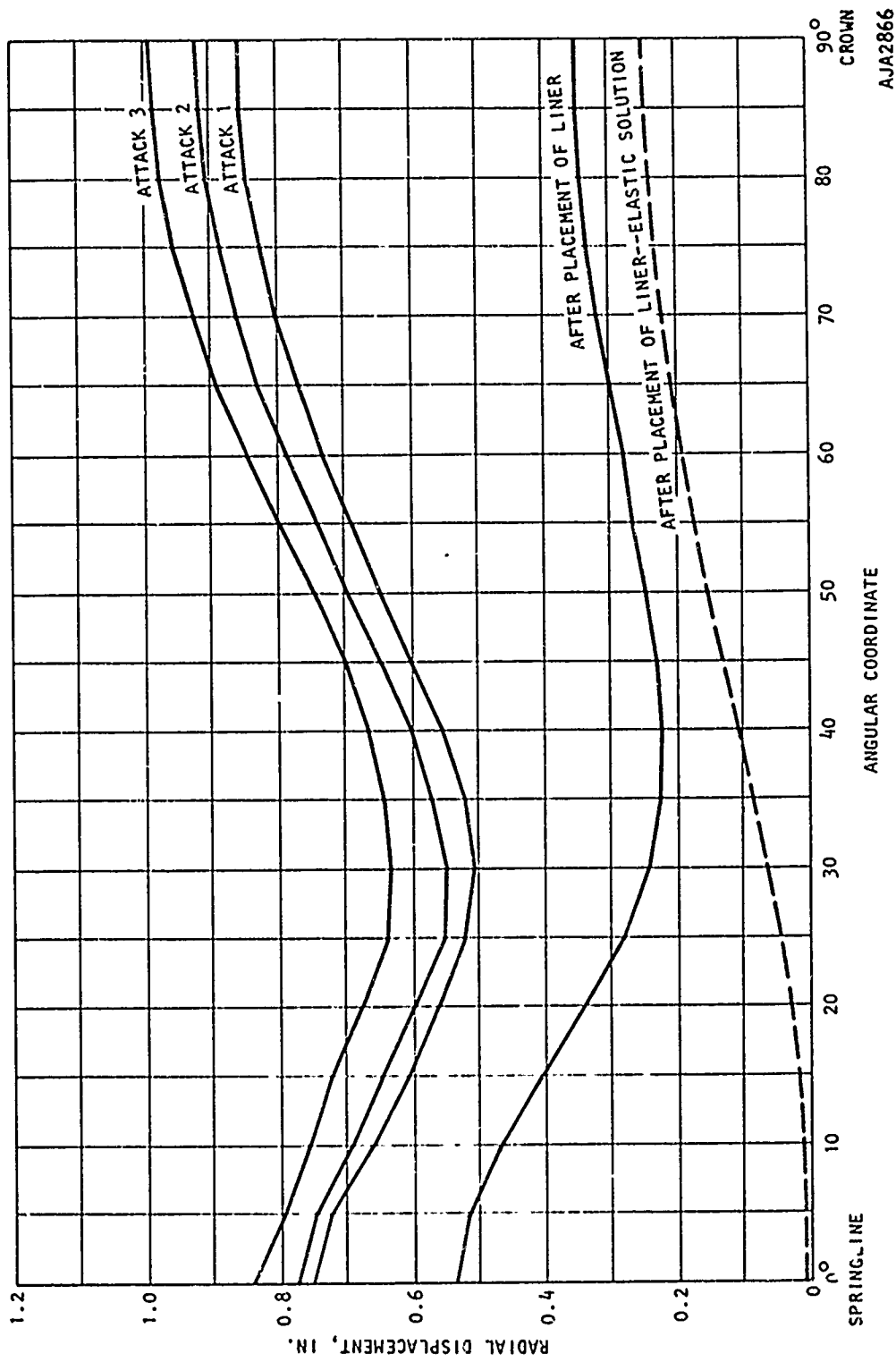
FIGURE 3-10. RESIDUAL RADIAL DISPLACEMENTS OF PENETRATION LINER

53
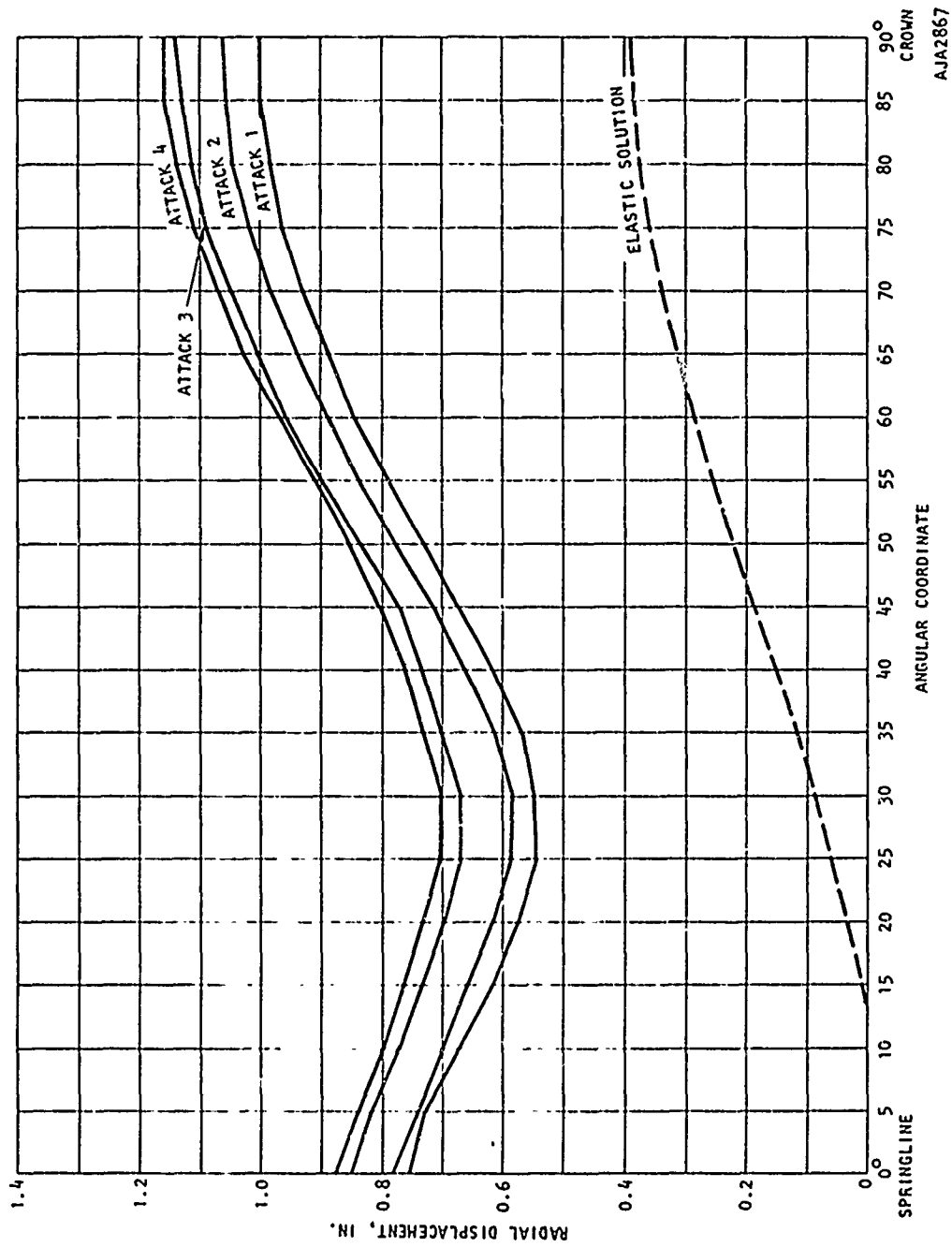
FIGURE 3-11. PEAK TRANSIENT RADIAL DISPLACEMENTS OF PENETRATION LINER

54

NOTE: LINER STIFFNESS ADDED BETWEEN THESE TWO STEPS

(b) FIRST STEP OF GROUND SHOCK LOADING—
FIRST ATTACK

(a) LAST STEP OF OVERBURDEN LOADING

FIGURE 3-12. GROWTH OF INELASTIC RESPONSE IN VICINITY OF THE PENETRATION

55
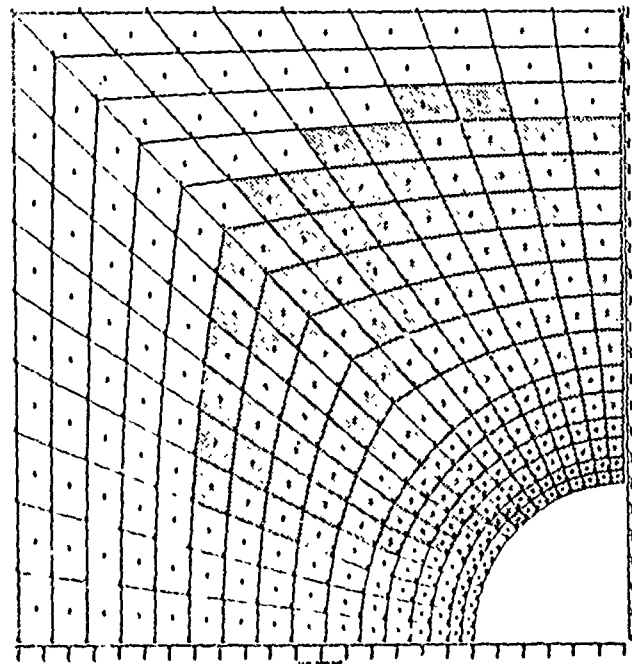
(d) LAST STEP OF GROUND SHOCK UNLOADING--
    FIRST ATTACK

(c) LAST STEP OF GROUND SHOCK LOADING--
    FIRST ATTACK

FIGURE 3-12. (CONTINUED)

56
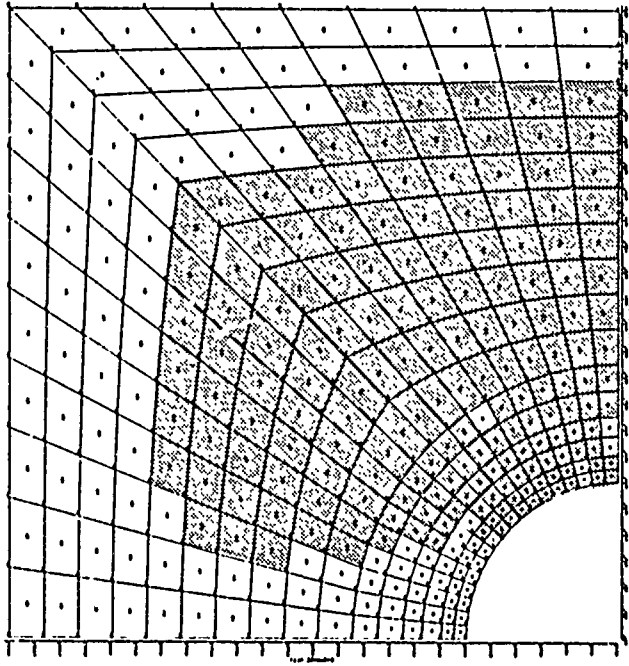
(f) LAST STEP OF GROUND SHOCK LOADING--
THIRD ATTACK
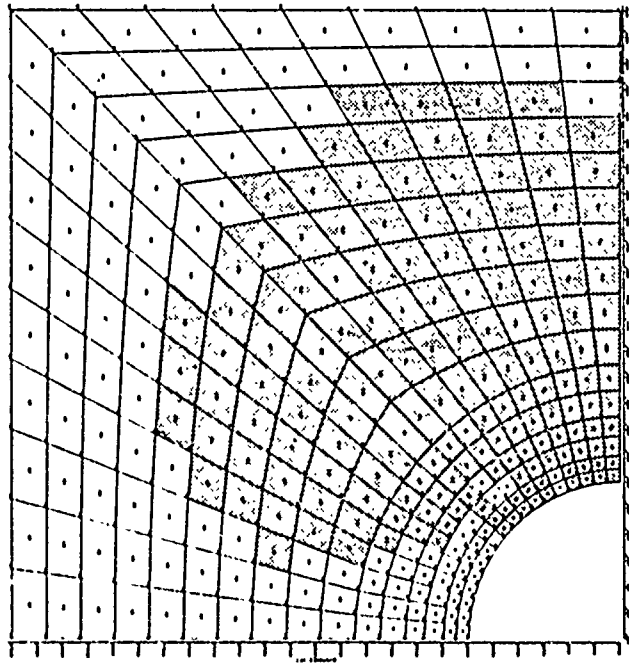
(e) LAST STEP OF GROUND SHOCK LOADING--
SECOND ATTACK

FIGURE 3-12. (CONTINUED)

57
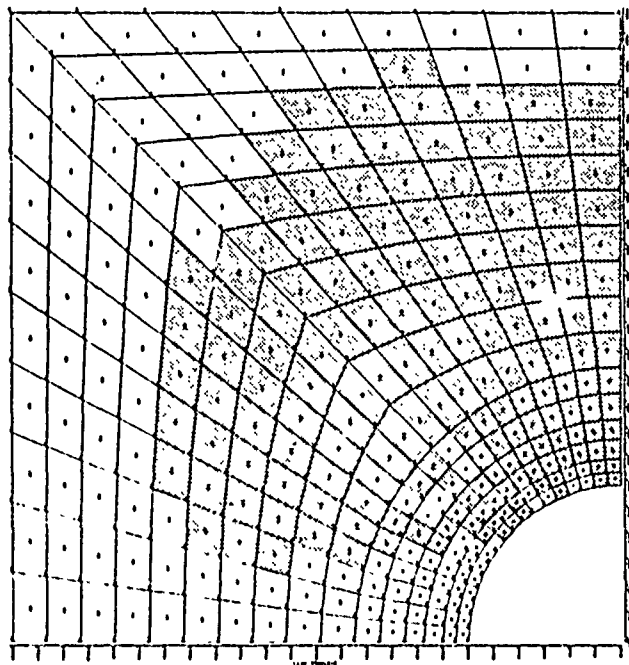
(g) LAST STEP OF GROUND SHOCK LOADING--
FOURTH ATTACK

FIGURE 3-12. (CONTINUED)

SECTION 4

CONCLUSIONS AND RECOMMENDATIONS

4.1 MECHANICAL FAILURE OF A CAVITY UNDER DYNAMIC LOADING

The following conclusions are worthy of restating: the survival of a cavity sited in well-fractured rock under dynamic loading is linearly dependent upon (1) the increment of free-field ground shock acceleration occurring over a period of two cavity engulfment times and (2) the magnitude of the cavity radius.

The investigation presented represents a first attempt at establishing design requirements for reinforcement which functions to prevent mechanical failure of a cavity under dynamic loading. Validation and assessment of the reliability of the design requirements will come from both laboratory and field testing and from more rigorous analytical investigations. Although a number of the assumptions made during the course of this investigation require more careful assessment, it is felt that there is sufficient validity underlying the investigation to warrant interim adoption of the derived design requirements.

4.2 MATERIAL FAILURE OF CAVITY PENETRATIONS

The following conclusions are drawn from the study of material failure of cavity penetrations:

a. Steel-lined penetrations can be adequately and cost-effectively designed to withstand repeated attack with large yield weapons, *provided that there is no significant deterioration in rock strength with each attack.*

b. The analysis technique used here, the INSTEP Code, or an equivalent technique, can be used effectively by today's designer, *provided material property parameters are available.*

The following recommendations are made:

a. The scope of laboratory test programs for determination of material property parameters for rock materials should be expanded to include routine determination of the effect of repeated loading.

b. In order to gain further understanding of material failure of cavity penetrations and its implications in design, calculations of the nature performed in this study should be continued and expanded in scope to include:

1. Consideration of other rock materials

2. Consideration of various liner thicknesses, including the unlined case for comparative purposes

3. Consideration of other burial depths and other in situ stress conditions

4. Additional loading cycles

5. Study of the effect of load increment and computational mesh definition on solution accuracy

6. Simulation of the deterioration of strength of the rock under repeated load cycles

c. A calculational program similar to that conducted here should be initiated to study the performance of lined (backpacked), horizontal, cylindrical cavities of circular and elliptical cross section under multiple attack, where mechanical failure is assumed to be precluded.

REFERENCES

1. Distefano, C. J., et al., *Experiments in Rock Bolting, Project Officers Report--Project 3.7, Operation Flint Lock, Shot Pile Driver (U)*, POR-4515 (WT-4015), (AD 504523), Omaha District, Corps of Engineers, September 19, 1969 (SECRET).

2. Distefano, C. J., et al., *Response of Tunnel Liners, Project Officers Report--Project 3.1, Operation Flint Lock, Shot Pile Driver (U)*, POR-4010 (WT-4010), Omaha District, Corps of Engineers, November 23, 1970 (SECRET).

3. Agbabian-Jacobsen Associates, *Hardened Facilities Design and Verification Test Study (U)*, SAMSO-TR-70-427, prepared for Space and Missile Systems Organization, November 1970 (SECRET).

4. Witt, E. F., and W. N. Butler, *Cable Vulnerability Studies, Project Officers Report--Project 3.8, Operation Flint Lock, Shot Pile Driver (U)*, POR-4016 (WT-4016), Bell Telephone Laboratories, Inc., December 31, 1969.

5. Bagge, C. F., and J. W. Workman, *Free-Field Ground Motion for Beneficial Facility Siting, Volume 4--Medium-Structure Interaction (U)*, SAMSO-TR-70-88, Joint Venture of Applied Theory, Inc., and Agbabian-Jacobsen Associates, June 1970 (SECRET).

6. *Design of Structures to Resist Nuclear Weapons Effects*, ASCE Manual No. 42, 1964 Edition.

7. Timoshenko, S., *Vibration Problems in Engineering*, Third Edition, Van Nostrand, 1955.

8. Flügge, W., *Stresses in Shells*, Springer-Verlag, 1962.

9. Newmark, N. M., et al., *Ditto Tab Test Planning (U)*, SAMSO-TR-68-288, Nathan M. Newmark Consulting Engineering Services, October 1969 (SECRET).

10. Army Corps of Engineers, Missouri River Division Laboratory, *Tests for Strength Characteristics of a Schistose Gneiss*, First Interim Report, MRD Laboratory No. 64/126, May 1965.

APPENDIX A

MATERIAL PROPERTY PARAMETERS
FOR PENETRATION CALCULATION

The sole source of material property data for the gneiss that is represented in the present penetration calculation is Reference A-1. This reference provides quantitative data on the yield criterion and bulk and shear moduli, and it provides a qualitative indication that dilatancy accompanies inelastic deformation.

A.1 BULK MODULUS

Although Reference A-1 shows no results of hydrostatic loading and unloading/reloading, information on the bulk modulus can be obtained from the nominally elastic range of behavior in triaxial compression tests. An ensemble of such data is plotted in Figure A-1 in the form of mean stress and volumetric strain. Each individual experiment has a range in which the inelastic shear deformation is negligible, and in that range the P/μ relation is about linear. In the absence of other data, a constant bulk modulus for the gneiss of

$$B = 5.5 \times 10^6 \text{ psi} \qquad (A-1)$$

is indicated.

For the steel liner, $B = 1.97 \times 10^7$ psi.

A.2 SHEAR MODULUS

The shear modulus G is obtained from data on Poisson's ratio, ν, and from the bulk modulus. An average value of Poisson's ratio for the gneiss of

$$\nu = 0.30 \qquad (A-2)$$

is a reasonable approximation for a number of triaxial compression experiments reported in Reference A-1. Assuming the material to have an elastic isotropic range, the shear modulus is

$$G = B \frac{3(1-2\nu)}{2(1+\nu)} = 2.54 \times 10^6 \text{ psi} \qquad (A-3)$$

For the steel liner, $G = 1.185 \times 10^7$ psi.

A.3 YIELD CRITERION

Data on maximum combined stress is put in the form indicated by the idealized yield criterion in Figure A-2. The data shown in Figure A-3 appear to fall into four main groups. The solid lines, which are labeled f_1 and f_2 to indicate that they are the yield criteria for the present calculations, mainly represent dry specimens that are either intact at the beginning of the experiment or that did not fracture along joint planes. The dashed lines represent specimens that were wet or prefractured or both. The highest reasonable yield criteria was selected for the present calculations. This implies that progressive deterioration of strength due to repeated loading is unaccounted for here. The yield criteria for the rock are as follows, where J_1' as defined in Figure A-2 is -34,600 psi.

$$J_1 > -34,600 \text{ psi}$$

$$f = f_1 = \sqrt{J_2'} + 0.39 \, J_1 - 2000. \text{ psi} \leq 0 \qquad \text{(A-4)}$$

$$J_1 \leq -34,600 \text{ psi}$$

$$f = f_2 = \sqrt{J_2'} + 0.205 \, J_1 - 8400. \text{ psi} \leq 0 \qquad \text{(A-5)}$$

The yield criterion for the steel is

$$f = \sqrt{J_2'} - 29000. \text{ psi} \leq 0 \qquad \text{(A-6)}$$

A.4 REFERENCES

A-1. *Tests for Strength Characteristics of a Schistose Gneiss*, First
      Interim Report, MRD Laboratory No. 64/126, Corps of Engineers,
      U. S. Army, Missouri River Division Laboratory, Omaha, May 1965.

DILITATION, 10^{-6} IN./IN.

P, KSI

AJA2845

$K = 5.5 \times 10^{6}$, PSI

σ_3

9-DRB-2	1 KSI
8-DRB-2	3 KSI
2-DRB-3	3 KSI
7-DRB-2	10 KSI
4-DRB-3	10 KSI
3-DRB-3	10 KSI
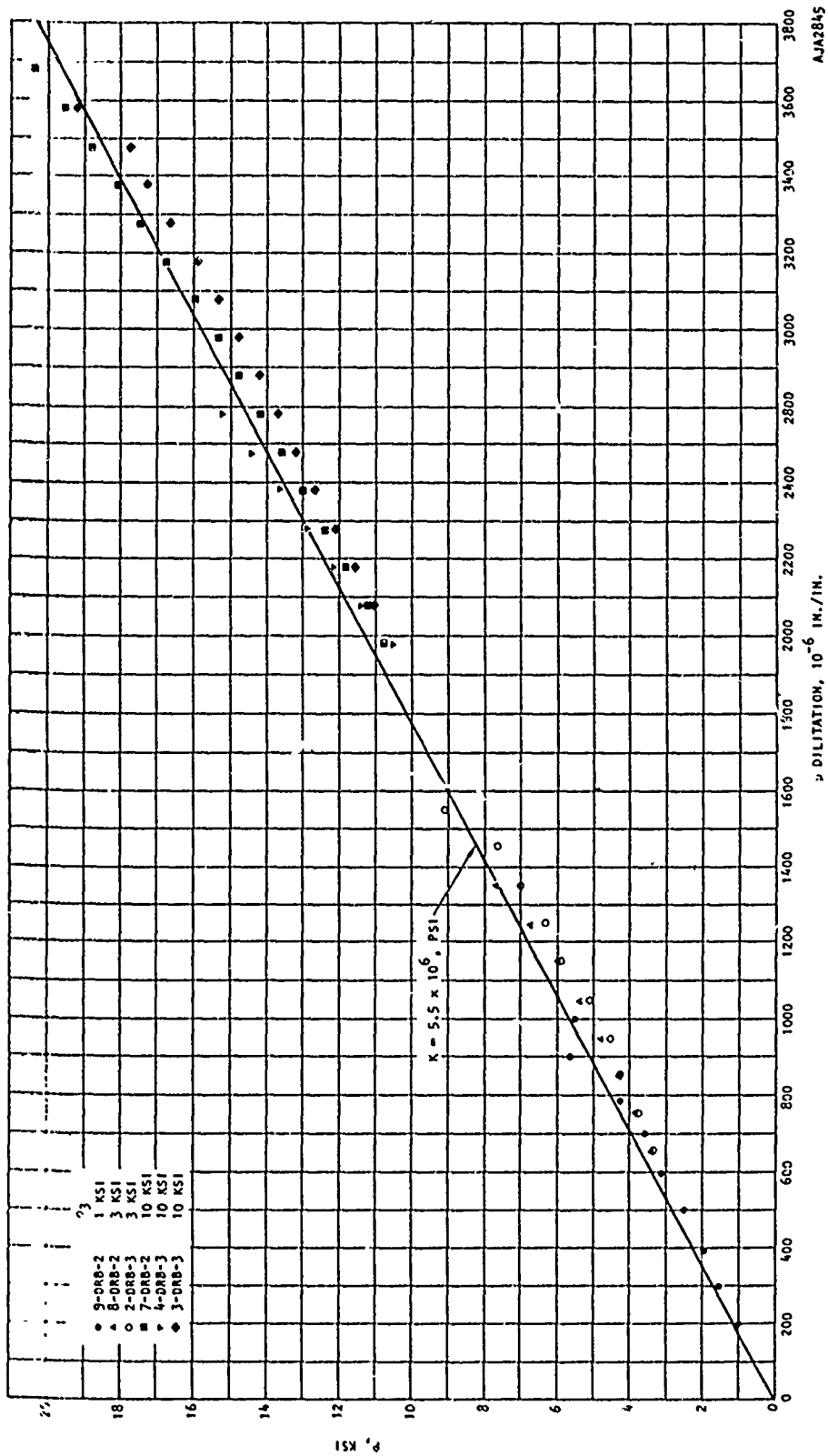
FIGURE A-1. BULK MODULUS USED FOR PENETRATION CALCULATION
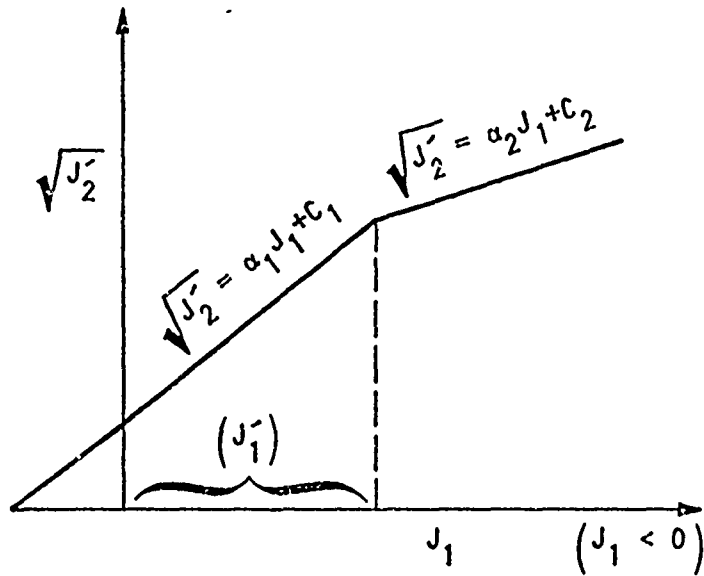
Where

$$J_1 = \sigma_{11} + \sigma_{22} + \sigma_{33}$$

$$J_2' = \left\{ \frac{1}{6} \left[\left(\sigma_{11} - \sigma_{22} \right)^2 + \left(\sigma_{33} - \sigma_{22} \right)^2 + \left(\sigma_{33} - \sigma_{11} \right)^2 \right] \right\}^{1/2}$$

FIGURE A-2. DEFINITION OF YIELD COEFFICIENTS

66
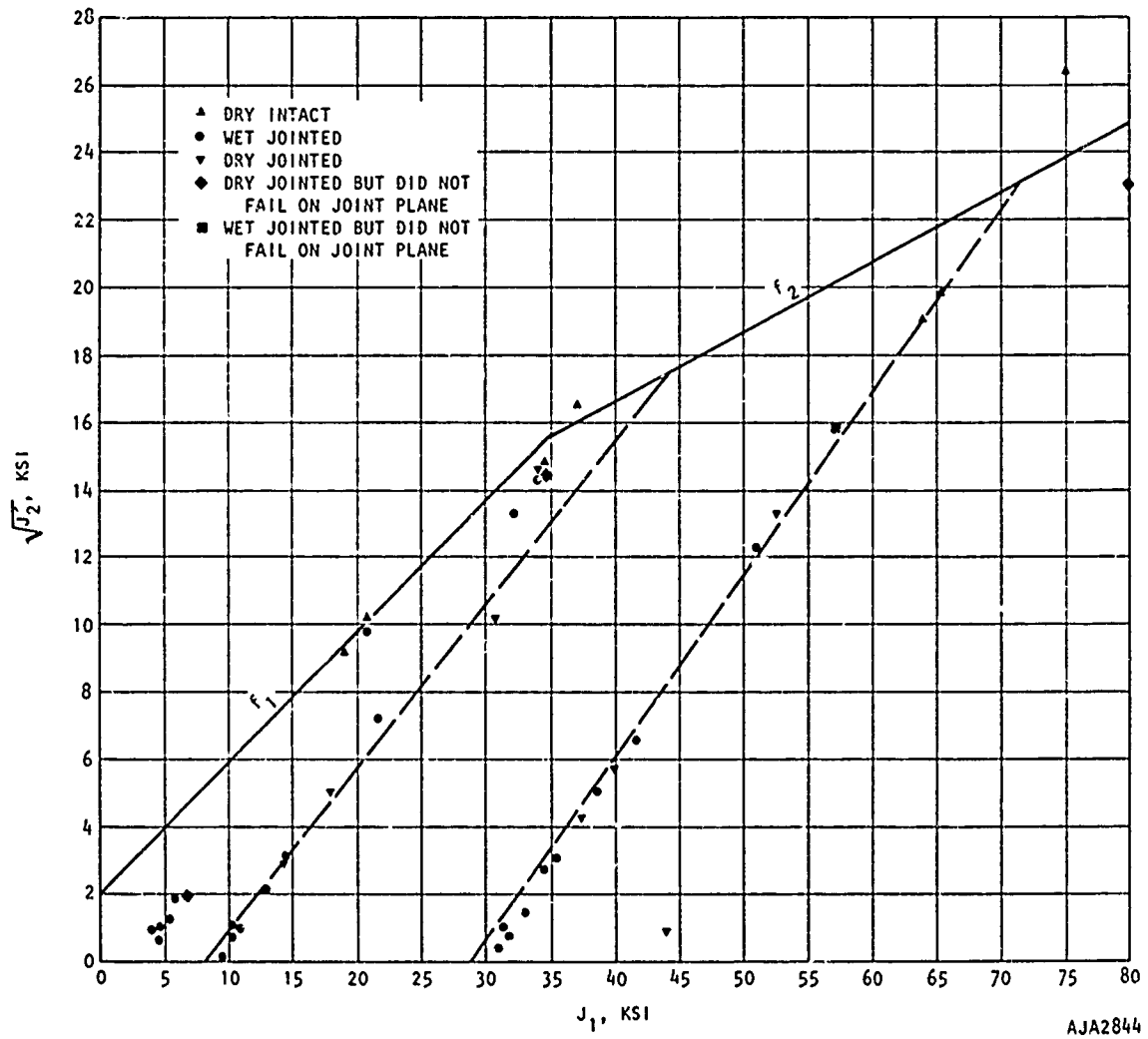
FIGURE A-3. YIELD CRITERIA USED FOR PENETRATION CALCULATION

APPENDIX B

GROWTH OF INELASTIC RESPONSE IN THE VICINITY OF A
CAVITY PENETRATION THROUGH FIRST GROUND SHOCK APPLICATION
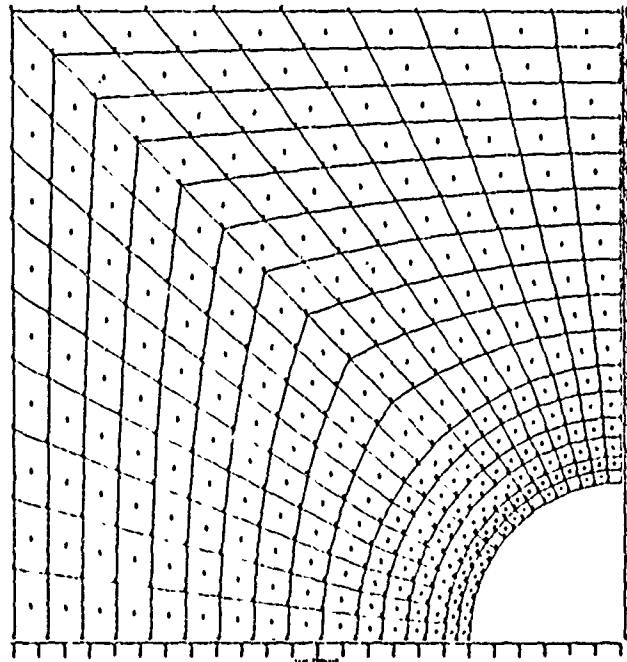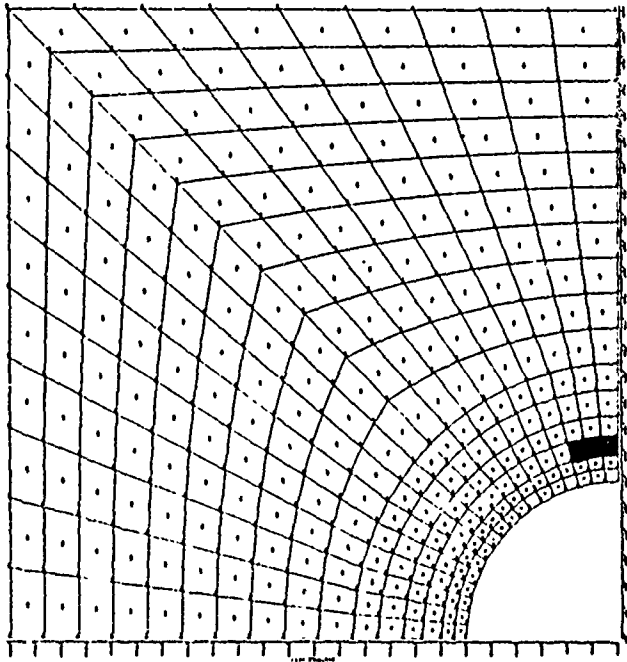
PLASTIC INCREMENT DURING CURRENT AND PREVIOUS STEP

PLASTIC INCREMENT DURING CURRENT STEP

(a) LOAD STEP 1--3600 PSI

(b) LOAD STEP 2--4400 PSI

FIGURE B-1. GROWTH OF INELASTIC RESPONSE IN THE VICINITY OF A CAVITY
PENETRATION--THROUGH FIRST GROUND SHOCK LOADING
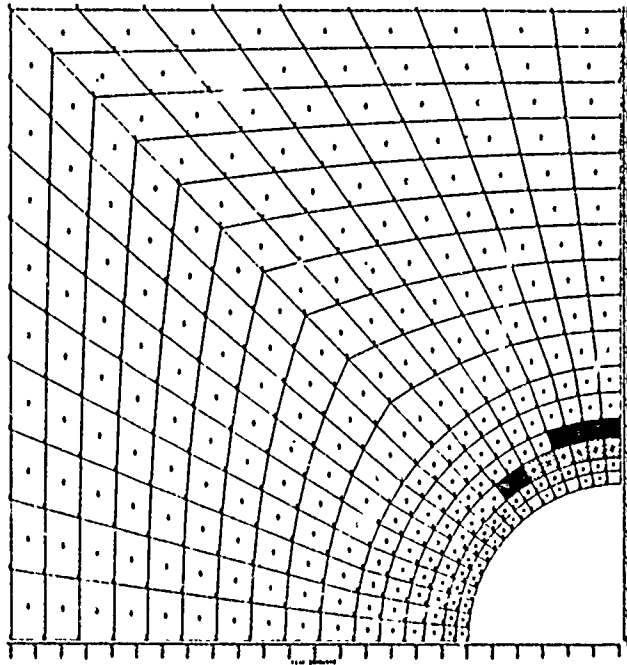
PLASTIC INCREMENT DURING CURRENT AND PREVIOUS STEP

PLASTIC INCREMENT DURING CURRENT STEP

(c) LOAD STEP 3--5200 PSI   (d) LOAD STEP 4--6000 PSI

FIGURE B-1.   (CONTINUED)

70

PLASTIC INCREMENT DURING CURRENT AND PREVIOUS STEP
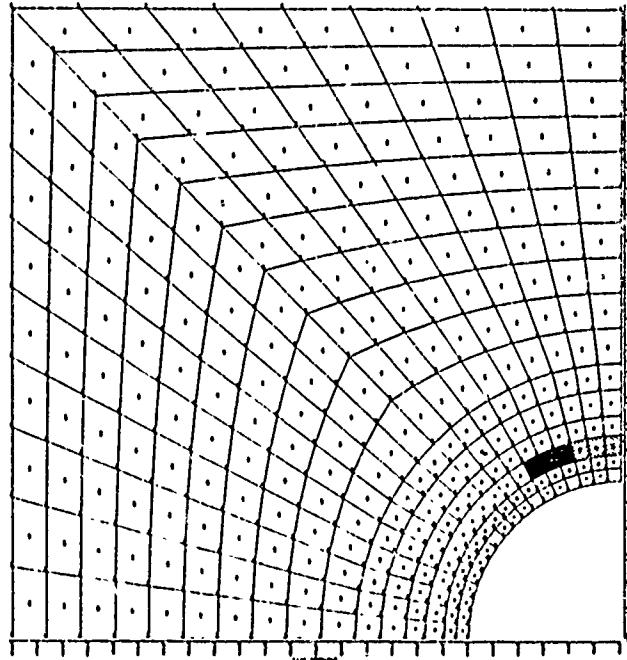
PLASTIC INCREMENT DURING CURRENT STEP
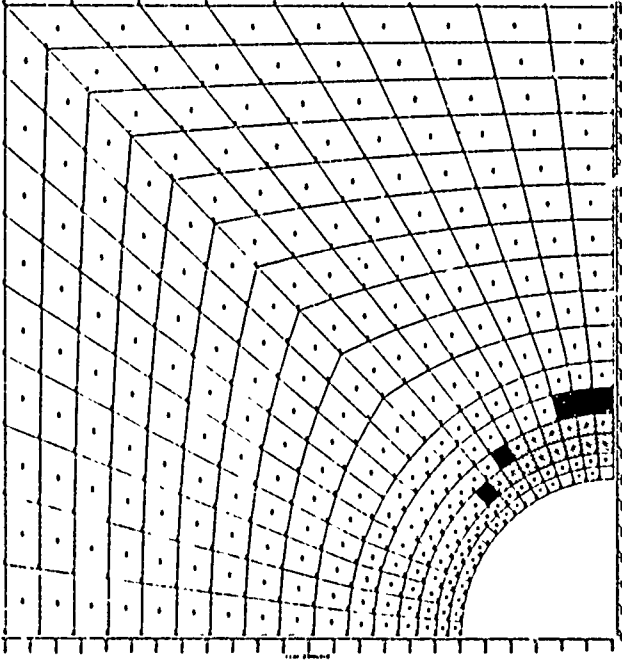
(e) LOAD STEP 5--6800 PSI
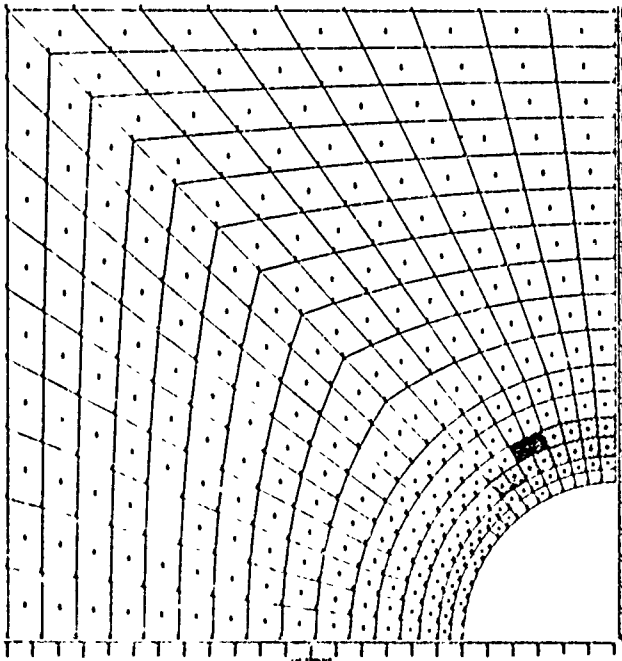
(f) LOAD STEP 6--7600 PSI

FIGURE 3-1. (CONTINUED)

71

PLASTIC INCREMENT DURING CURRENT AND PREVIOUS STEP
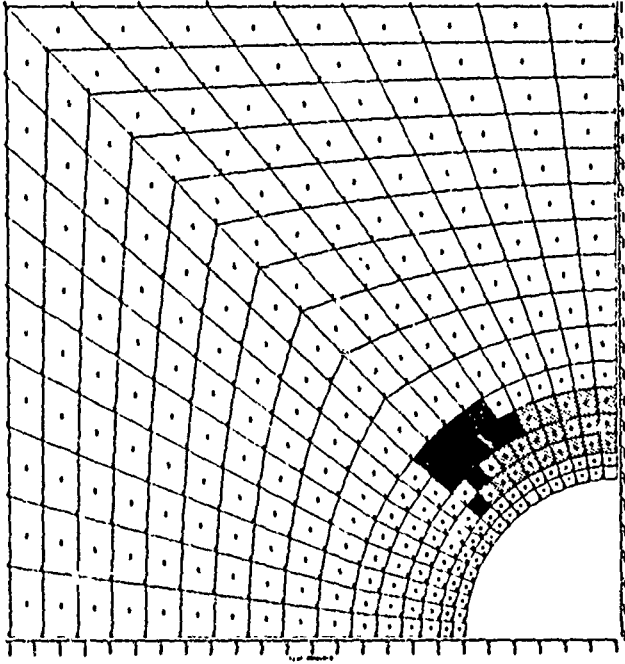
PLASTIC INCREMENT DURING CURRENT STEP

(g) LOAD STEP 7--8400 PSI

(h) LOAD STEP 8--9200 PSI

FIGURE B-1. (CONTINUED)

PLASTIC INCREMENT DURING CURRENT AND PREVIOUS STEP

PLASTIC INCREMENT DURING CURRENT STEP
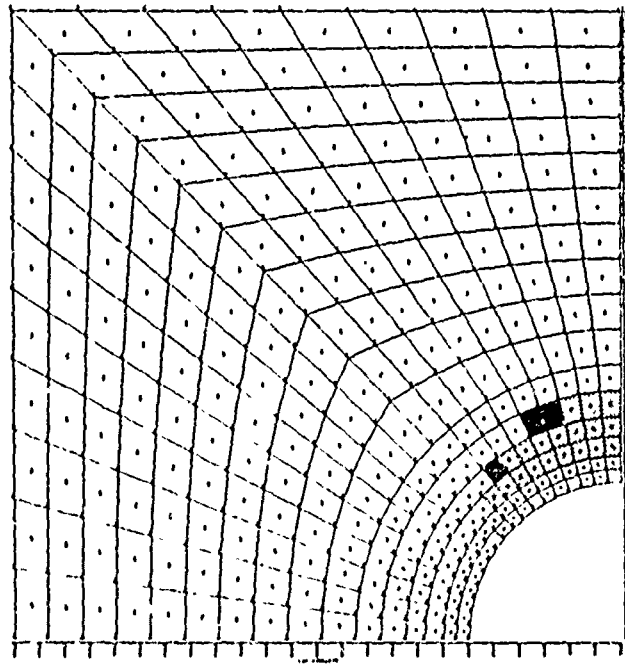
(i) LOAD STEP 9--10000 PSI

(j) LOAD STEP 10--10800 PSI

FIGURE B-1. (CONTINUED)

73

PLASTIC INCREMENT DURING CURRENT AND PREVIOUS STEP

PLASTIC INCREMENT DURING CURRENT STEP

(k) LOAD STEP 11--11600 PSI
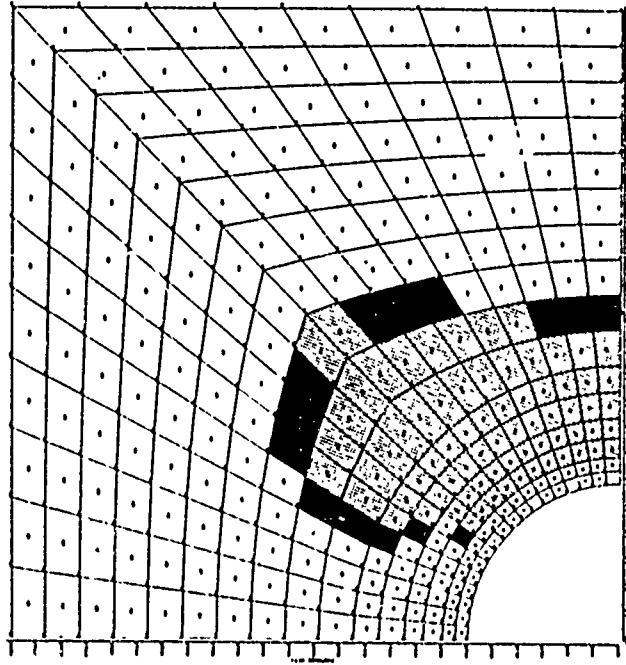
(l) LOAD STEP 12--12500 PSI
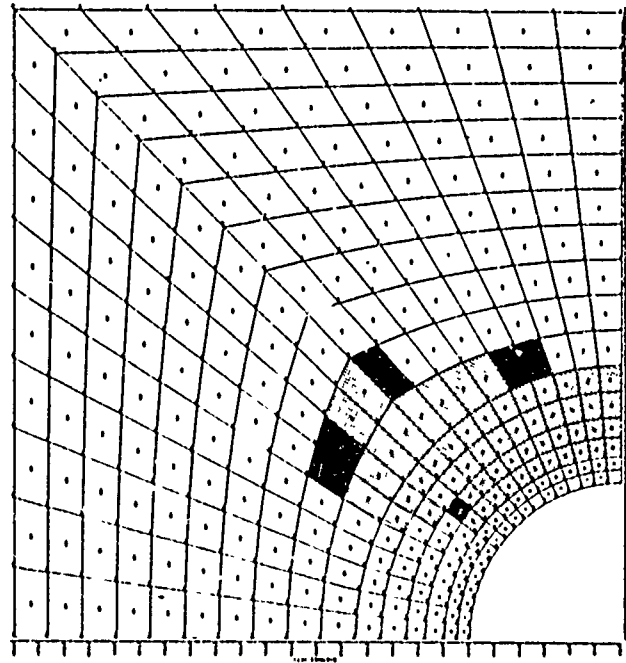
FIGURE B-1. (CONTINUED)

74

NOTE: LINER STIFFNESS ADDED BETWEEN LOAD STEPS 12 AND 13
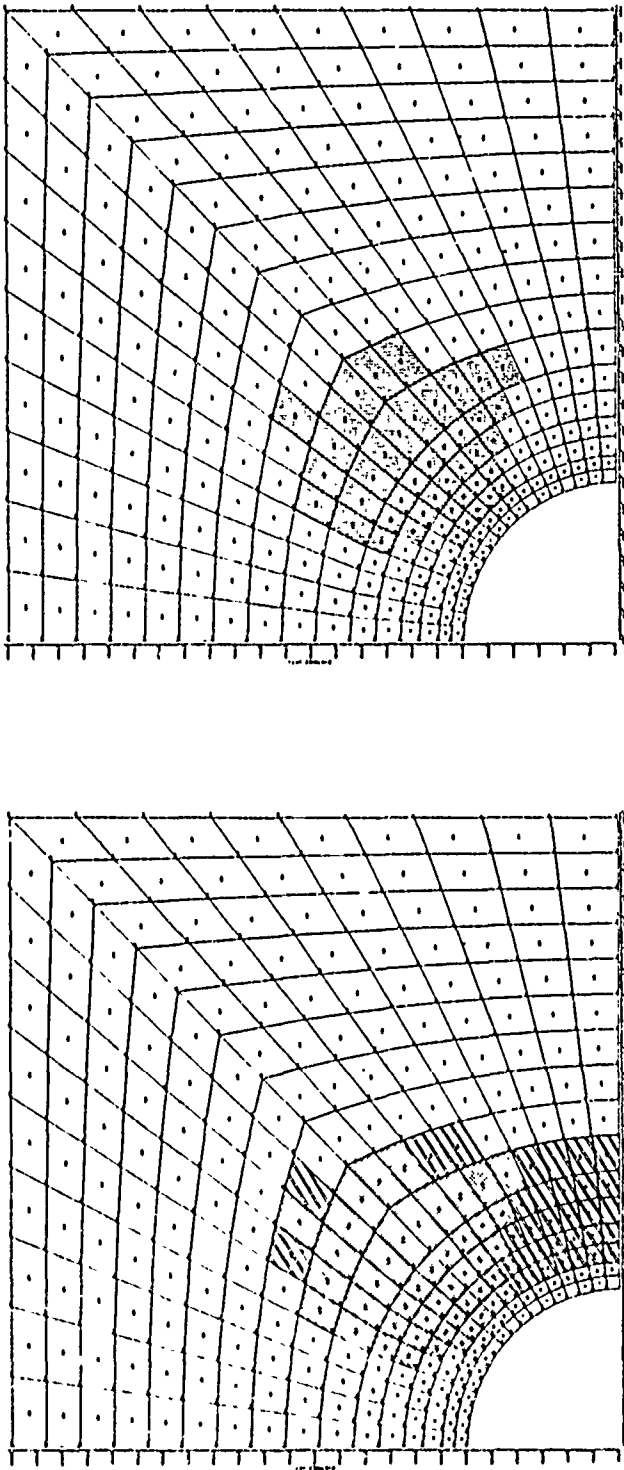
PLASTIC INCREMENT DURING CURRENT AND PREVIOUS STEP

ELASTIC UNLOADING FROM PLASTIC STATE DURING CURRENT STEP

(m) LOAD STEP 13--13200 PSI

(n) LOAD STEP 14--14000 PSI

FIGURE B-1. (CONTINUED)

PLASTIC INCREMENT DURING CURRENT AND PREVIOUS STEP

PLASTIC INCREMENT DURING CURRENT STEP
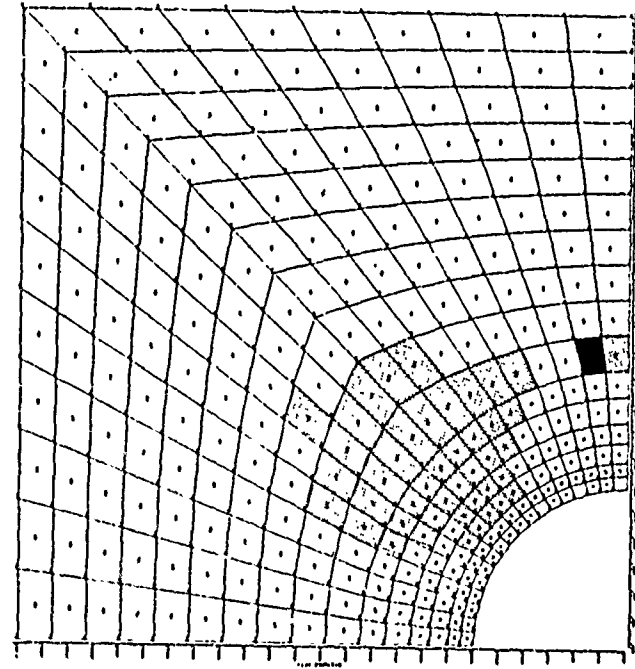
(o) LOAD STEP 15--14800 PSI
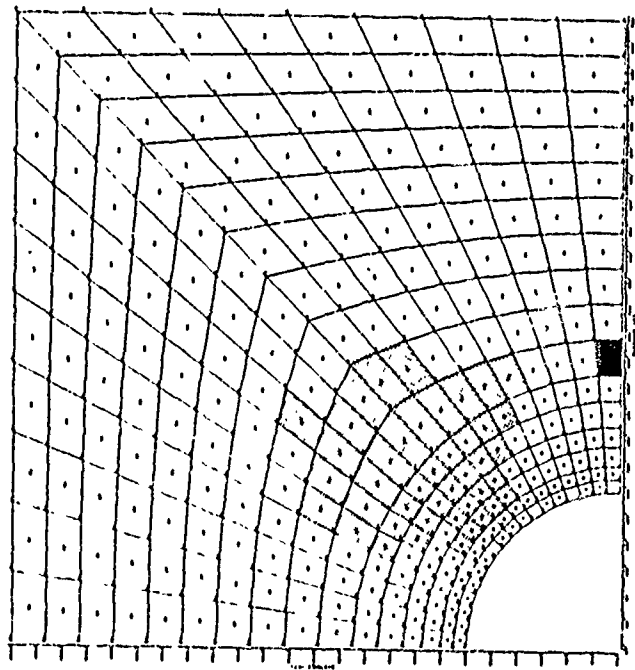
(p) LOAD STEP 16--15600 PSI

FIGURE B-1. (CONTINUED)

PLASTIC INCREMENT DURING CURRENT AND PREVIOUS STEP

PLASTIC INCREMENT DURING CURRENT STEP
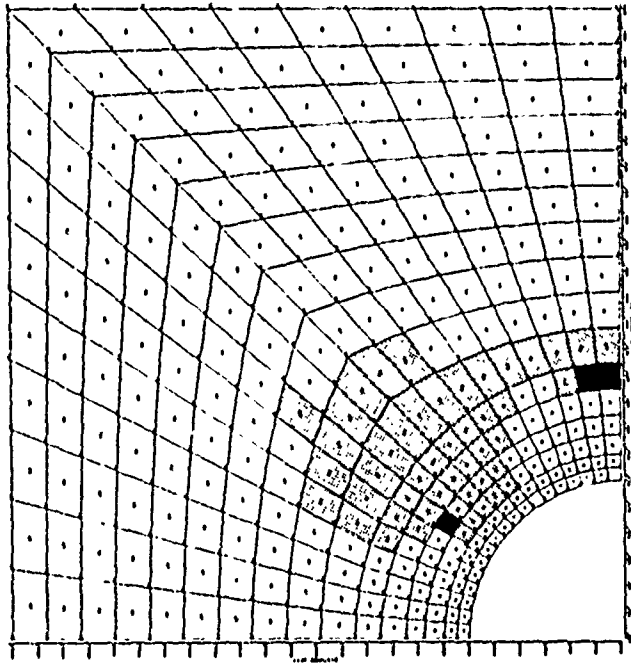
(q) LOAD STEP 17--16400 PSI   (r) LOAD STEP 18--17200 PSI
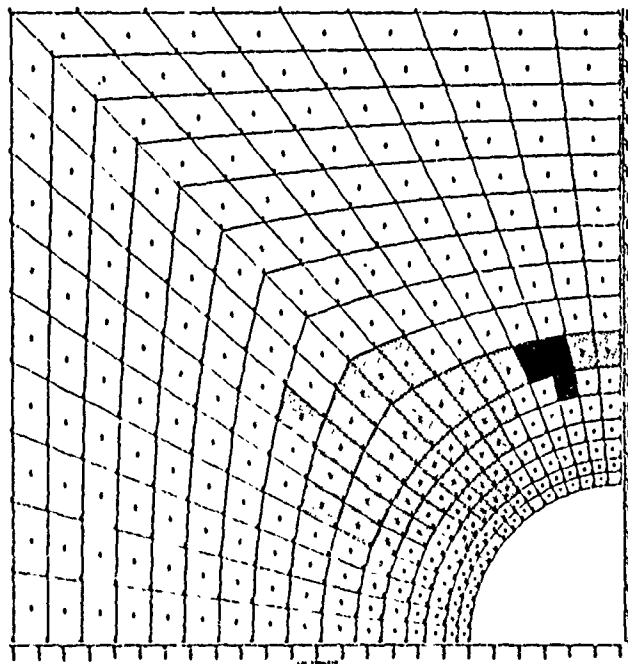
FIGURE B-1.   (CONTINUED)

77

PLASTIC INCREMENT DURING CURRENT AND PREVIOUS STEP

PLASTIC INCREMENT DURING CURRENT STEP

(s) LOAD STEP 19--18000 PSI

(t) LOAD STEP 20--18800 PSI

FIGURE B-1. (CONTINUED)

78
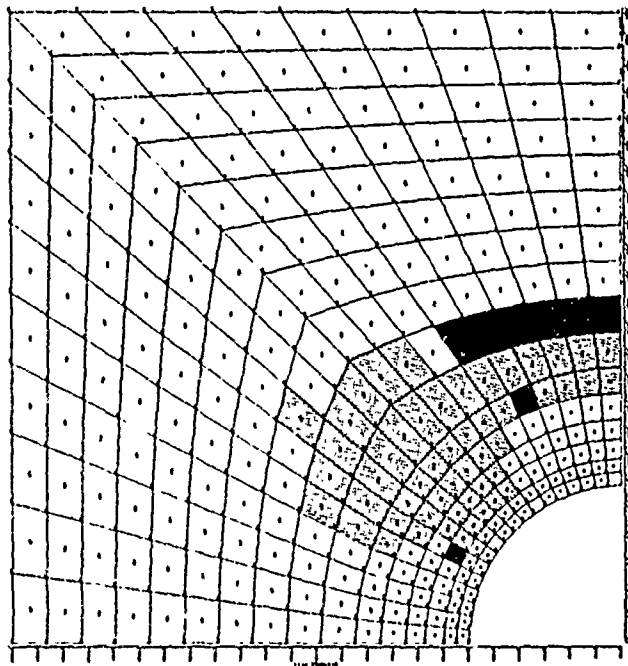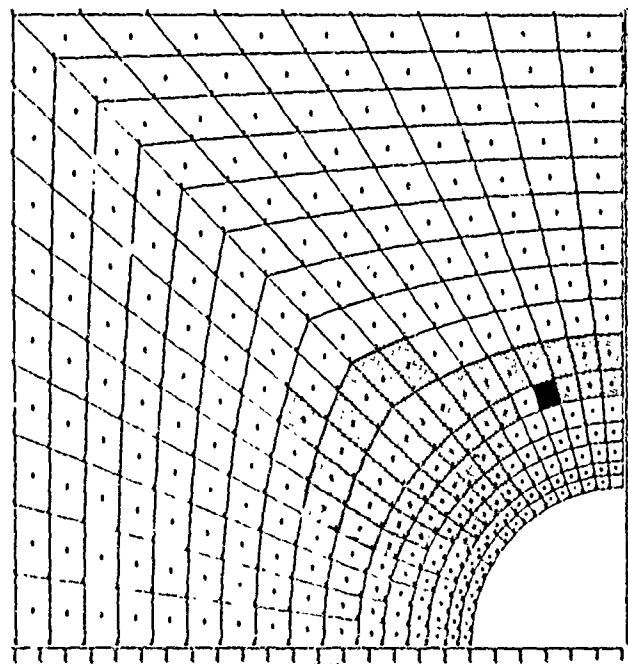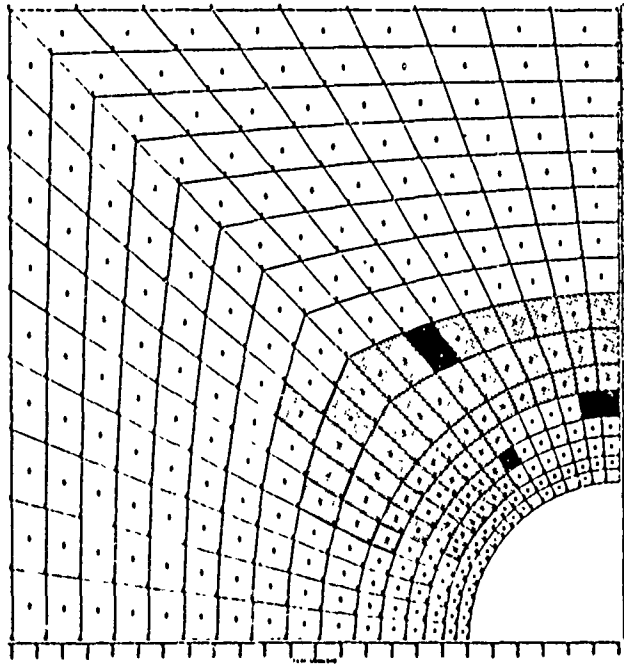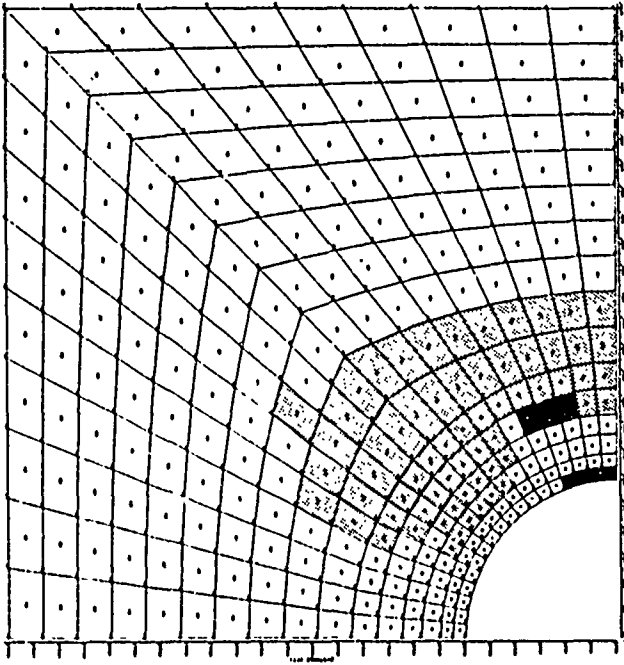
PLASTIC INCREMENT DURING CURRENT AND PREVIOUS STEP

PLASTIC INCREMENT DURING CURRENT STEP

(u) LOAD STEP 21--19600 PSI

(v) LOAD STEP 22--20400 PSI

FIGURE B-1. (CONTINUED)
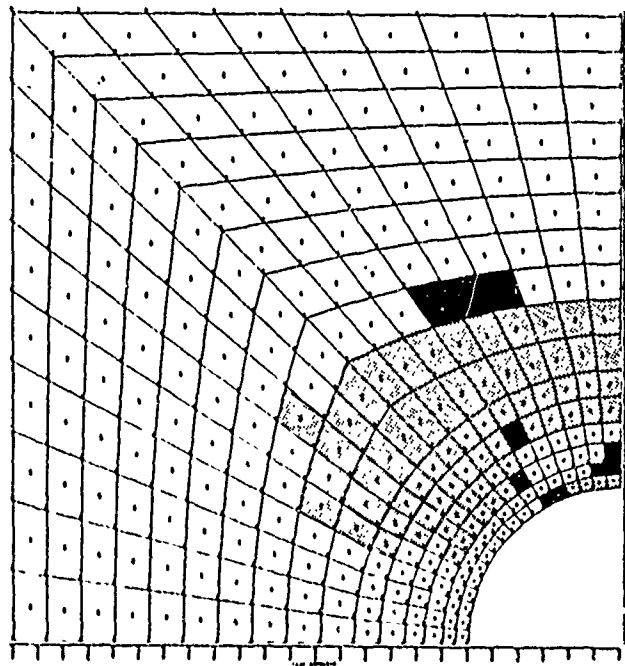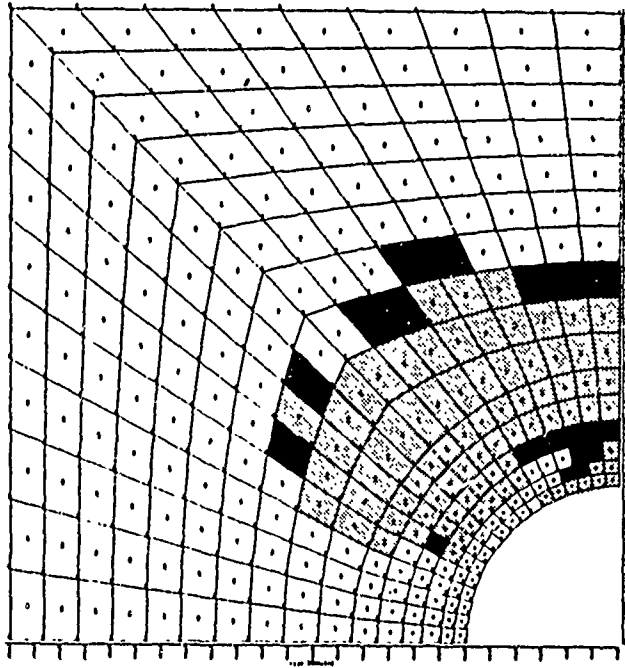
79

PLASTIC INCREMENT DURING CURRENT AND PREVIOUS STEP

PLASTIC INCREMENT DURING CURRENT STEP

(w) LOAD STEP 23--21200 PSI

(x) LOAD STEP 24--22000 PSI

FIGURE B-1, (CONTINUED)
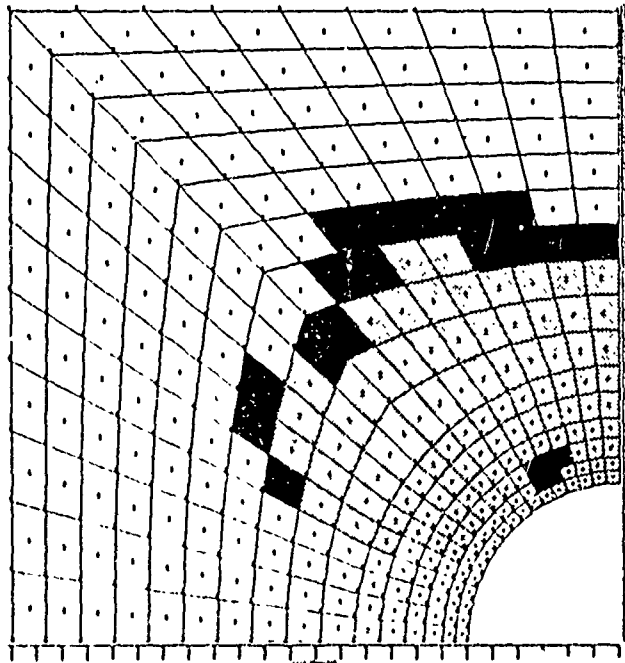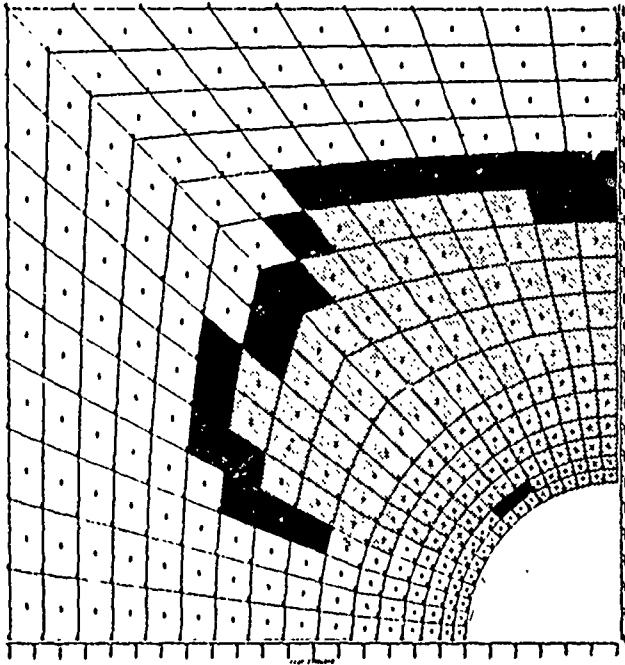
80

PLASTIC INCREMENT DURING CURRENT AND PREVIOUS STEP

PLASTIC INCREMENT DURING CURRENT STEP

(y) LOAD STEP 25--22800 PSI

(z) LOAD STEP 26--23600 PSI

FIGURE B-1. (CONTINUED)
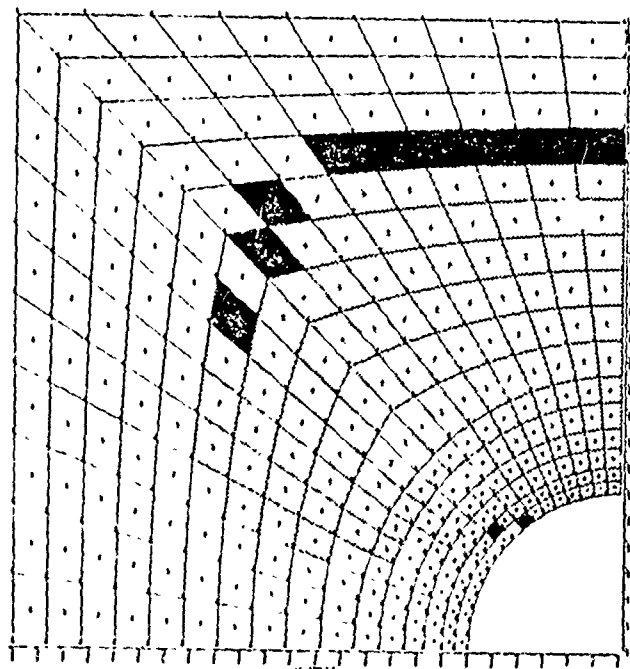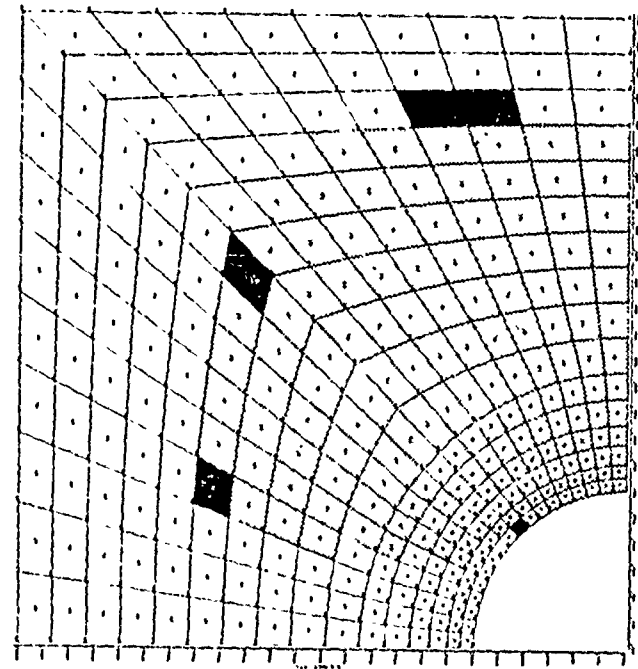
81

PLASTIC INCREMENT DURING CURRENT AND PREVIOUS STEP

PLASTIC INCREMENT DURING CURRENT STEP

(aa) LOAD STEP 27--24400 PSI

(bb) LOAD STEP 28--25000 PSI

FIGURE B-1. (CONTINUED)

82

APPENDIX C

INSTEP CODE

The calculations of material failure of a penetration were performed using a static, two-dimensional nonlinear finite element computer program called INSTEP. Features of the code include the following:

a.   Use of constrained quadrilateral finite element for plane stress or plane strain

b.   Use of midpoint rule of integration for incremental loading

c.   Acceptance of nonlinear material property representations incorporating general yield criterion, flow rule, and bulk and shear moduli

d.   Allowance for elements to be added or subtracted or material properties of designated elements to be changed as prescribed by the user

C.1 CONSTRAINED QUADRILATERAL ELEMENT

The type of element used (Reference C-1) is a quadrilateral composed of two triangular elements. Within each triangular element, Figure C-1, the assumed displacement field forces a compatible linear variation of displacements along sides 1-2, 2-3, 3-4, and 4-1. The displacements along line 1-5-3 vary parabolically; compatibility is maintained since each of these points is forced to have the same displacement as the corresponding points of the second triangle. Each of the five nodal points has two degrees of freedom, making a total of ten for the quadrilateral element and leading to a 10 x 10 element stiffness matrix. The unknown displacements associated with point 5 are then expressed in terms of those at points 1 through 4 and eliminated from the system. The remaining 8 x 8 element stiffness matrices are combined by direct stiffness procedures to form the global stiffness matrix [K]. The program also includes constant-strain triangles and bar elements. These may be attached to the corner points of the quadrilaterals or to each other.

QUADRILATERAL ELEMENT   TWO LINEAR STRAIN TRIANGLES
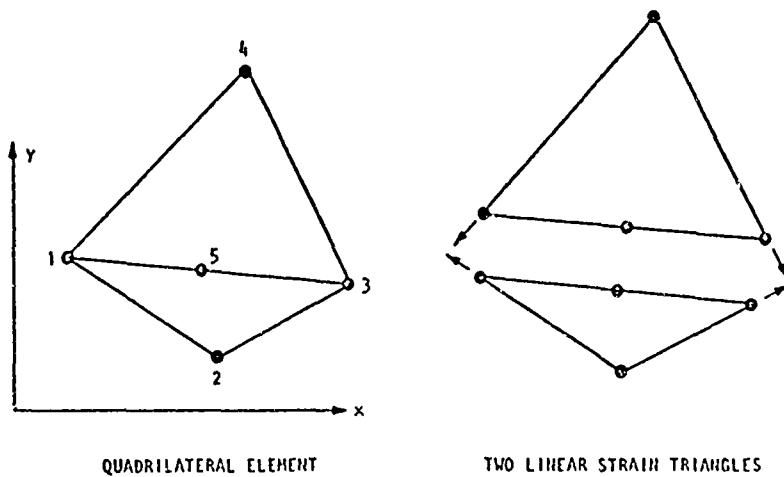
AJA1863

FIGURE C-1. LINEAR STRAIN QUADRILATERAL ELEMENT (WILSON, REFERENCE C-1)

C.2 STEP-BY-STEP INTEGRATION

The constrained quadrilateral elements are assembled in the global stiffness matrix, [K], by the direct stiffness method. The incremental equations of equilibrium,

$$[K] \{du\} = \{dP\} \qquad (C-1)$$

where

$\{du\}, \{dP\}$ = Incremental displacement and load vectors, respectively

are then solved for the incremental displacements by a step-by-step integration procedure called the "midpoint rule of integration for incremental loading" (References C-2 and C-3).

Each step of the solution consists of two passes. During the first pass, the solution corresponding to B (Figure C-2) is obtained from the solution A (the end of a previous step) by using the stiffness matrix K_A. During the second pass, the accepted solution C is obtained from A using the stiffness matrix corresponding to the solution M, which is the midpoint solution of A and B, i.e.,

$$u_M = \frac{u_A + u_B}{2} \qquad (C-2)$$

84
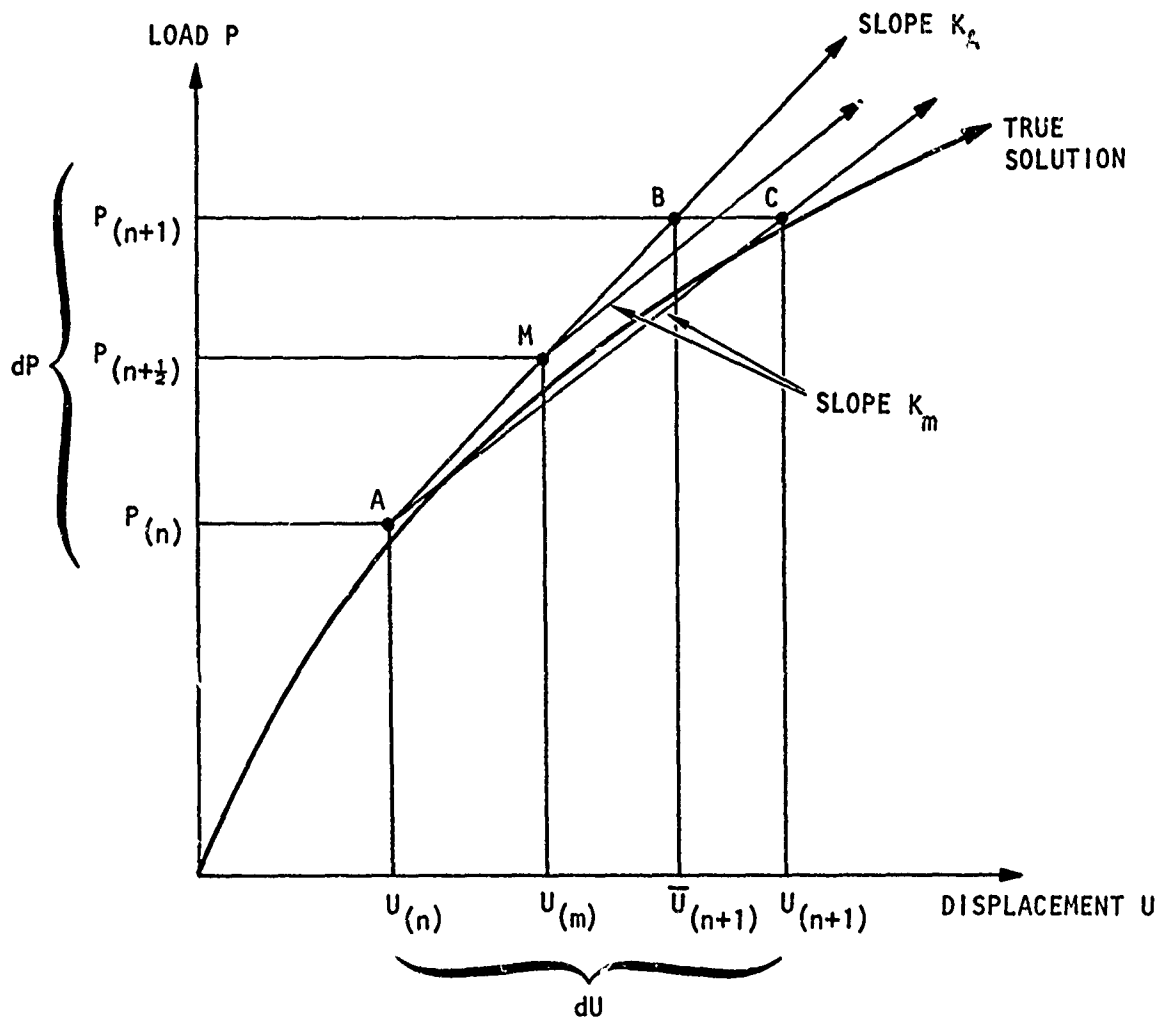
FIGURE C-2. MIDPOINT RULE OF INTEGRATION
(REFERENCE C-2)

85

C.3 MATHEMATICAL MODEL OF MATERIAL PROPERTIES

The mathematical model of material behavior used in the present work has the following basic features. A more complete description of the general model is given in Reference C-4.

a. Bulk modulus (B) may be a function of the excess compression $\mu = \rho/\rho_0 - 1$, where ρ = current density, and ρ_0 = initial density.

b. Shear modulus (G) may be a function of the current state of stress.

(In the present study B and G are assumed to be constant.)

c. The yield criterion may be a function of the first stress invariant (J_1) and of the second invariant of stress deviator (J_2') (Reference C-5).

d. Work-hardening or strain-hardening rules prescribing how the yield criterion may vary as a function of plastic work or plastic strain may be used.

(In the present study, hardening is assumed to be zero, and the initial yield criterion is a permanent property of the material (Reference C-5).

e. A variety of flow rules prescribing how changes in plastic strain are related to changes in stress when the yield criterion is satisfied may be adopted.

(The plastic potential flow rule (Reference C-6) is used in the present study.)

This mathematical model must be expressed as a matrix of coefficients [C] relating stress increments $\{d\sigma\}$ to strain increments $\{d\varepsilon\}$.

$$\{d\sigma\} = [C] \{d\varepsilon\} \tag{C-3}$$

The yield criterion for an isotropic material whose properties are insensitive to temperature and strain may be expressed in terms of the stress invariants

$$f(J_1, J_2, J_3) = 0 \tag{C-4}$$

where J_1, J_2, J_3 = invariants of the stress tensor. Equation C-4 represents the yield criterion for an ideally plastic material since the criterion is a permanent property of the material and does not change with loading history.

At the beginning of each load step, Hooke's law is tentatively assumed to be valid as follows:

$$d\sigma_{ij} = \lambda(de_{kk})(\delta_{ij}) + 2G(de_{ij}) \qquad \text{(C-5)}$$

where

$d\sigma_{ij}$ = Stress increment tensor

de_{ij}^e = Elastic strain increment tensor

λ = Lame's parameter = $B - \dfrac{2}{3}G$

B, G = Bulk modulus, shear modulus

δ_{ij} = Kronecker delta (= 1 if $i = j$, = 0 if $i \neq j$)

Equation C-5 can readily be put in the form of Equation C-3. If the state of stress

$$\left(\sigma_{ij}\right)_{new} = \left(\sigma_{ij}\right)_{old} + d\sigma_{ij} \qquad \text{(C-6)}$$

does not satify the yield criterion, i.e., if

$$f < 0 \qquad \text{(C-7)}$$

Equation C-5 correctly gives the stress increment. If the new state of stress, considered as a trial state, exceeds the yield criterion,

$$f \geq 0 \qquad \text{(C-8)}$$

An explanation of Equations C-7 and C-8 is given in Reference C-7, Page 140.

[C] in Equation C-3 is given by the following matrix.

$$
C = \begin{bmatrix}
\lambda + 2G - \dfrac{\lambda F + 2Gf_r}{\lambda F^2 + 2Gx} & \lambda - \dfrac{(\lambda F + 2Gf_z)(\lambda F + 2Gf_r)}{\lambda F^2 + 2Gx} & \lambda - \dfrac{(\lambda F + 2Gf_\theta)(\lambda F + 2Gf_r)}{\lambda F^2 + 2Gx} & -2Gf_{rz}\dfrac{\lambda F + 2Gf_r}{\lambda F^2 + 2Gx} \\[4mm]
 & \lambda + 2G - \dfrac{(\lambda F + 2Gf_z)^2}{\lambda F^2 + 2Gx} & \lambda - \dfrac{(\lambda F + 2Gf_z)(\lambda F + 2Gf_\theta)}{\lambda F^2 + 2Gx} & -2Gf_{rz}\dfrac{\lambda F + 2Gf_z}{\lambda F^2 + 2Gx} \\[4mm]
\text{Symmetrical} & & \lambda + 2G - \dfrac{(\lambda F + 2Gf_\theta)^2}{\lambda F^2 + 2Gx} & -2Gf_{rz}\dfrac{\lambda F + 2Gf_\theta}{\lambda F^2 + 2Gx} \\[4mm]
 & & & G - \dfrac{4G^2 f}{LF^2 + 2Gx}
\end{bmatrix}
$$

(C-9)

where

$$ F = f_x + f_y + f_z $$

$$ x = f_x^2 + f_y^2 + f_z^2 + 2f_{xy}^2 $$

f_x, etc. = Derivatives of the yield function f with respect to stress components (plastic potential flow rule). Subscripts x, y, and z indicate differentiation with respect to x, y, and z components of stress while subscript xy indicates differentiation with respect to shear stress.

The [C] matrix, Equation C-9, for a plastic material and its elastic equivalent, must be modified for plane stress calculations. The technique used in the present study in all cases is to form the [C] matrix as if a plane strain matrix were needed and then to perform the revision indicated in Equation C-10.

88

The revised [C] for plane stress is:

$$[C] = \text{(revised for plane stress)} = \begin{bmatrix} c_{11} - \dfrac{c_{13}c_{31}}{c_{33}} & c_{12} - \dfrac{c_{13}c_{32}}{c_{33}} & 0 & c_{14} - \dfrac{c_{13}c_{34}}{c_{33}} \\[2em] & c_{22} - \dfrac{c_{23}c_{32}}{c_{33}} & 0 & c_{24} - \dfrac{c_{23}c_{34}}{c_{33}} \\[2em] \text{SYM} & & 0 & 0 \\[2em] & & & c_{44} - \dfrac{c_{43}c_{34}}{c_{33}} \end{bmatrix} \qquad (C\text{-}10)$$

C.4 INSTALLING LINER

The technique of installing the liner in a cavity subjected to overburden loads in the computer is as follows. The finite element mesh is initially constructed to include elements corresponding to the steel liner as well as to the rock. During the phase when overburden loads are being applied, the elements corresponding to the liner are assigned properties to simulate the stiffness of air. As a result, the stress distribution in the rock is very nearly the same as around an unlined cavity. When the last increment of overburden load has been applied (in this case, the second pass of load step No. 12), the computer automatically changes the properties of the liner elements from air to steel. At this stage there is no stress in the steel liner, as would be the actual case following installation and before ground shock loading. During ground shock loading, stress develops in the steel liner and in the rock just as for any lined cavity.

C.5 REFERENCES

C-1. Wilson, E. L., *A Computer Program for the Dynamic Stress Analysis of Underground Structures*, Contract No. DACA 39-67-C-0020, University of California, Berkeley, January 1969.

C-2. Felippa, C. A., *Refined Finite Element Analysis of Linear and Nonlinear Two-Dimensional Structures*, Structural Engineering Laboratory Report No. 66-22, University of California, Berkeley, 1966.

C-3. Adham, S. A., and J. A. Malthan, *The Finite Element Method for Investigating Edge Effects in the High-Explosive Simulation Technique (HEST), Project HEST Test V*, Technical Report No. AFSWC-TR-68-26, Kirtland Air Force Base, New Mexico, pp. 124-125, 1969.

C-4. Isenberg, J., et al., *Spherical Waves in Inelastic Materials*, DASA 2404, Defense Atomic Support Agency, March 1970.

C-5. Hill, R., *The Mathematical Theory of Plasticity*, Clarendon Press, 1950.

C-6. Drucker, D. C., and W. Prager, "Soil Mechanics and Plastic Analysis or Limit Design," *Applied Mathematics*, Vol. 10, No. 2, July 1952, pp. 57-165.

C-7. Fung, Y. C., *Foundations of Solid Mechanics*, Prentice-Hall International Series in Dynamics, Englewood Cliffs, New Jersey, 1965.

DISTRIBUTION LIST

	No. of Copies
(Number of Copies of Report Shown in Parentheses)	Form 1473

Chief of Research and Development; Department of the Army;
ATTN: CRDNCB, CRDSTI (1), CRDPES, CRDES (1); Washington,
D. C. 20310 2

Chief of Engineers; Department of the Army; ATTN: CER (1),
ENGAS-I (2), ENGAS-IL (1), ENGBR (1), ENGCE (1), ENGCW-E (2),
ENGCW-EC (1), ENGCW-ED (1), ENGCW-EG (1), ENGCW-ES (1),
ENGCW-RR (1), ENGCW-Z (1), ENGMC-D (1), ENGMC-DE, ENGMC-E (1),
ENGMC-EA (1), ENGMC-ED (1), ENGMC-EP (1), ENGMC-ER (1),
ENGMC-M (1), ENGMC-S (1), ENGME-E (1), ENGME-EF (1), ENGME-ER
(1), ENGME-ET (1), ENGME-RD (2), ENGME-S (1), ENGML (1),
ENGSA (1) 1

Division Engineers, U. S. Army Engineer Divisions

Huntsville	(2)	North Pacific	(2)
Lower Mississippi Valley	(2)	Ohio River	(2)
Missouri River	(2)	South Atlantic	(2)
New England	(2)	South Pacific	(2)
North Atlantic (Resume only)		Southwestern	(2)

(1)

Directors, U. S. Army Engineer Division Laboratories

Missouri River	(2)	Ohio River	(2)
New England	(2)	South Atlantic	(1)
North Atlantic	(2)	South Pacific	(1)
North Pacific	(2)	Southwestern	(2)

District Engineers, U. S. Army Engineer Districts

Alaska	(2)	New Orleans	(2)
Albuquerque	(2)	New York	(2)
Baltimore	(2)	Norfolk	(2)
Buffalo	(2)	Omaha	(2)
Charleston	(2)	Philadelphia	(2)
Chicago	(2)	Pittsburgh	(1)
Detroit	(2)	Portland	(2)
Fort Worth	(2)	Rock Island	(2)
Galveston	(2)	Sacramento	1
Huntington	(2)	St. Louis	(2)
Jacksonville	(2)	St. Paul	(2)
Kansas City	(2)	San Francisco	(2)
Little Rock	(2)	Savannah	(2)
Los Angeles	(2)	Seattle	(2)
Louisville	(2)	Tulsa	(2)
Memphis	(2)	Vicksburg	(2)
Mobile	(2)	Walla Walla	(2)
Nashville	(2)	Wilmington	1

(Number of Copies of Report Shown in Parentheses)	No. of Copies Form 1473

President; Mississippi River Commission; CE; P. O. Box 80; Vicksburg, Mississippi 39180 (1)

Research Center Library; U. S. Army Engineer Waterways Experiment Station; P. O. Box 631; Vicksburg, Mississippi 39180 (10)

U. S. Army Cold Regions; Research and Engineering Laboratory; (USA CRREL); Hanover, N. H. 03755 (1)

U. S. Army Engineer School Library; Thayer Hall (Bldg. 270); Fort Belvoir, Virginia 22060   1

Ballistic Research Laboratories; ATTN: AMXRD-BD; Aberdeen Proving Ground, Maryland 21005   1

Coastal Engineering Research Center; ATTN: Library; 5201 Little Falls Rd. N. W.; Washington, D. C. 20016   1

U. S. Army Engineer Nuclear Cratering Group; Lawrence Radiation Laboratory; P. O. Box 808; Livermore, California 94550   1

DEPARTMENT OF THE AIR FORCE

Research and Applications Br.; ATTN: AF/Preer; Directorate of Civil Eng.; HQ USAF; Pentagon; Washington, D. C. 20030   1

Office of Director of Defense Research and Engineering; ATTN: Director Strategic Weapons; Room 3E129; Pentagon, Washington, D. C. 20301   1

Headquarters, SAMSO (AFSC); ATTN: MNHFI-Luedeking (1), XRTBN; Norton AFB, California 92409   1

SAMSO/DEE; ATTN. William A. Platt; AF Unit Post Office; Los Angeles, California 90045   1

DEPARTMENT OF THE NAVY

Naval Civil Engineering Laboratory; ATTN: Technical Library L31; Port Hueneme, California 93041 (1)

Naval Facilities Engineering Command; Navy Department; ATTN: William J. Bobisch, Chief Engineer; Washington, D. C. 20390   1

(Number of Copies of Report Shown in Parentheses)	No. of Copies Form 1473

OTHER DOD AGENCIES

Advanced Research Projects Agency; ATTN: Nuclear
Monitoring Research Office; 1400 Wilson Blvd.;
Arlington, Virginia 22209   1

Director; Defense Nuclear Agency; Washington,
D. C. 20304 (1)

Test Command; ATTN: TCDT-E; Sandia Base, New
Mexico 87115   1

Administrator; Defense Documentation Center; Cameron
Station; (12), Building 5; Alexandria, Virginia 22314

Director of Defense Research and Engineering; ATTN:
Assistant Director Nuclear Programs; Assistant Director
Strategic Weapons; Technical Library; Washington, D. C.
20301   3

OTHER GOVERNMENT AGENCIES

U. S. Bureau of Mines; ATTN: Leonard Obert, Science
Adviser-Mining Research; Building 20, Denver Federal
Center; Denver, Colorado 80225 (1)

U. S. Bureau of Mines; ATTN: J. R. McWilliams, Division
of Mining Systems; Washington, D. C. 20240 (5)

U. S. Bureau of Reclamation; ATTN: M. H. Logan, Chief,
Geology and Geotechnology Branch; Bldg. 67, Denver
Federal Center; Denver, Colorado 80225 (1)

U. S. Bureau of Reclamation; ATTN: D. L. Misterek,
Code 1512; Bldg. 56, Denver Federal Center, Denver,
Colorado 80225 (1); Mr. G. B. Wallace (1)

U. S. Department of Commerce; NOAA - National Ocean
Survey Lake Survey Center; 630 Federal Bldg. & U. S.
Courthouse; Detroit, Michigan 48226 (2)

California Dept. Water Resources; ATTN: L. B. James,
Chief Geologist; P. O. Box 388; Sacramento, California
95802 (1)

California Dept. Water Resources; ATTN: J. A. Wineland,
Chief, Design Branch, Div. of Design & Construction;
P. O. Box 388, Sacramento, California 95802 (1)

OTHER GOVERNMENT AGENCIES (Cont'd)

Federal Highway Administration; 400 Seventh Street,
S.W.; Washington, D. C. 20591 (1)

Federal Highway Administration; Office of Research;
ATTN: W. J. Halstead, Chief, Materials Division;
Washington, D. C. 20591 (1)

Highway Research Board; ATTN: Librarian; 2101
Constitution Avenue N.W.; Washington, D.C. 20418 (1)

U. S. Geological Survey; ATTN: H. W. Olsen, Engineering
Geology Branch; 345 Middlefield Road; Menlo Park,
California 94025 (1)

U. S. Geological Survey; ATTN: E. C. Robertson; Acorn
Bldg.; 8001 Newell St.; Silver Spring, Maryland 20910
(1)

Tennessee Valley Authority; ATTN: R. B. Connelly,
Manager's Office, Engineering Design and Construction;
700 Union Bldg.; Knoxville, Tenn. 37902 (2)

Tennessee Valley Authority; ATTN: J. H. Coulson;
300 Arnstein Bldg.; Knoxville, Tennessee 37902 (1)

FOREIGN OFFICE

Chief of Engineers; Department of the Army;
ATTN: ENGME-AS; Washington, D. C. 20314   1

FOR FORWARDING TO:

AWRE; Foulness Island; Southend-on-Sea; Essex, England   1

Canadian Forces Liaison Officer (Engr); USAMERDL,
Fort Belvoir, Va. 22060 for: Dr. N. B. Hutcheon;
Canadian Joint Staff; Department of Transport; Div. of
Bldg. Research, National C Research Council of Canada;
Ottawa; Construction Engineer; Air Service Branch;
Ottawa, Ontario, Canada   5

Nova Scotia Technical College; ATTN: Dr. G. G. Meyerhof,
Dept. of Civil Engineering; Halifax, N.S., Canada   1

(Number of Copies of Report Shown in Parentheses)

UNIVERSITY

University of California; ATTN: R. E. Goodman,
Assoc. Prof., Dept. of Civil Engineering; 475 Davis
Hall; Berkeley, California 94720 (1)

University of California; ATTN: Lawrence Radiation
Laboratory Technical Information Dept. L-3; P. O.
Box 808; Livermore, California 94550 (1)

University of California; Los Alamos Scientific
Laboratory; ATTN: Report Librarian; P. O. Box 1663;
Los Alamos, N. Mex. 87544   1

Colorado School of Mines; ATTN: John J. Reed, Dept.
of Mining Engineering; Golden, Colorado 80401 (1)

Cornell University; ATTN: G. A. Kiersch, Chairman;
Dept. of Geological Sciences; 125 McGraw Hall,
Ithaca, N.Y. 14850 (1)

Colorado State University; Foothills Engineering
Research Station; ATTN: Prof. K. S. Lane; Ft. Collins,
Colorado 80521 (1)

Cornell University; ATTN: Dr. D. A. Sangrey, Assoc.
Prof., Dept. of Geotechnical Engineering; School of
Civil and Environmental Engineering; Ithaca, New York
14850 (1)

Florida State University; ATTN: E. G. Henneke; School
of Engineering Science, Tallahassee, Florida 32306   1

Harvard University; ATTN: Prof. A. Casagrande; Pierce
Hall; Cambridge, Mass. 02138   1

University of Illinois; ATTN: E. J. Cording; 2221 CE
Bldg., Urbana, Illinois 61801 (1); R. B. Peck;
2230 CE Bldg. (1)

University of Illinois; Dept. of Civil Engineering;
ATTN: Dr. D. U. Deere (1); Dr. N. M. Newmark (1);
Prof. A. J. Hendron, Jr. (1); Metz Reference Room,
B106 C. E. Bldg.; Urbana, Illinois 61801 (1)

University of Illinois; Department of Geology; ATTN:
Dr. F. A. Donath; Urbana, Illinois 61801 (1)

(Number of Copies of Report Shown in Parentheses)

UNIVERSITY (Cont'd)

Iowa State University; ATTN: L. V. A. Sendlein,
Department of Earth Science; Ames, Iowa 50010 (1)

Louisiana State University; ATTN: Dr. O. A. Nance,
Consultant to RAND and DASA; P. O. Box 16006-LSU;
Baton Rouge, Ia. 70803   1

Massachusetts Institute of Technology; ATTN: R. C.
Hirschfeld, Room 1-330 (1); Asst. Prof. H. H.
Einstein, Room 1-380 (1); Prof. W. F. Brace, Room
54-720 (1); Cambridge, Mass. 02139

University of Minnesota; ATTN: Prof. C. Fairhurst;
Dept. of Civil and Mineral Engineering; Minneapolis,
Minnesota 55455 (1)

University of Missouri at Rolla; ATTN: Dr. N. B.
Aughenbaugh, Chairman; Dept. Mining, Petr., & Geol.
Engrg. (1); Dr. G. B. Clark; Director, Rock Mechanics
& Explosives Research Center (1); Rolla, Missouri 65401

University of New Mexico; Eric H. Wang Civil Engineering
Research Facility; ATTN: Dr. E. Zwoyer; Dr. G. E.
Triandafilidis; Mr. P. A. Abbott; Mr. D. E. Calhoun;
P. O. Box 188, University Station, Albuquerque, New
Mexico 87106   4

City College of New York; Dept. of Civil Engineering;
ATTN: Prof. C. A. Miller; New York, N. Y. 10031   1

Pennsylvania State University; Dept. of Architectural
Engineering; ATTN: J. S. Futrick, Admin. Aide;
101 Engineering "A" Bldg., University Park, Pa.
16802 (1)

Pennsylvania State University; ATTN: R. Stefanko,
Assistant Dean, Earth & Mineral Sciences Continuing
Education; 110 Mineral Sciences Building; University
Park, Pa. 16801 (1)

Purdue University; School of Civil Engineering;
ATTN: Prof. Wm. R. Judd; Lafayette, Indiana 49707
(1)

South Dakota School of Mines & Technology; Department
of Mining Engineering; ATTN: Dr. E. Hoskins (1);
Prof. E. H. Oshier (1); Rapid City, South Dakota 57701

UNIVERSITY (Cont'd)

University of Texas At Austin; Dept. of Petr. Engineering;
ATTN: Dr. K. E. Gray; Austin, Texas 78712 (1)

Texas A & M University; Center for Tectonophysics;
ATTN: Dr. Melvin Friedman (1); Prof. J. Handin,
Director (1); College Station, Texas 77843

Texas A & M University; College of Geosciences; Center
for Tectonophysics; College Station, Texas 77843 (1)

Utah State University; Engineering Experiment Station;
ATTN: Dr. R. K. Watkins, Associate Director; Logan,
Utah 84321   1

Virginia Polytechnic Institute; Mining Engineering
Department; ATTN: Lawrence Adler (1); Dr. C. Haycocks
(1); Blacksburg, Va. 24060

INDUSTRY

The Aerospace Corporation; P. O. Box 5866; San
Bernardino, California 92408; ATTN: S. B. Batdorf,
B2/2020; M. Watson; W. Pfefferle (1)   2

Analytic Services, Inc.; ATTN: Geo. Hesselbacher;
5613 Leesburg Pike; Falls Church, Va. 22041   1

Applied Theory, Inc.; ATTN: Dr. J. Trulio; 1010 Westwood
Blvd., Los Angeles, California 90024   1

AVCO Systems Division; Research Library; 201 Lowell
Street, Wilmington, Mass. 01887   1

Battelle Memorial Institute; ATTN: Dr. R. W. Klingensmith;
505 King Avenue; Columbus, Ohio 43201   1

Bell Telephone Laboratories; ATTN: G. F. Weissmann,
Room 1A-105A; Mountain Avenue, Murray Hill, N. J. 07974   1

Bell Telephone Laboratories; ATTN: R. W. Mayo;
Whippany Road, Whippany, N. J. 07981   1

Boeing Company - MASD Library; ATTN: 23-99 R. E. Shipp
for L. E. Fleishman; P. O. Box 3955; Seattle, Washington
98124   1

(Number of Copies of Report Shown in Parentheses)	No. of Copies Form 1473

INDUSTRY (Cont'd)

Boeing Company - ATTN: J. A. Blaylock, 2-5410, 8C-41;
K. Levien, Orgn. 2-5511 M/S 89-70; Mr. H. G. Leistner,
Aerospace Group, Research Division, M/S 89-70; P.O. Box
3999, Seattle, Washington 98124 3

Boeing Company; ATTN: Technical Library; P. O. Box
3999; Seattle, Washington 98124 1

Engineering Societies Library; ATTN: Howard Gordon;
345 East 47th Street, New York, N. Y. 10017 (1)

General American Research Division; ATTN: Dr. L. B.
Holmes; 7449 N. Natchez Avenue; Niles, Illinois 60648 1

LIBRARY, General Electric Company Space & RESD Divs.,
ATTN: Mr. L. Chasen, Manager; P. O. Box 8555;
Philadelphia, Pennsylvania 19101 1

General Electric TEMPO; ATTN: DASIAC; P. O. Drawer QQ,
Santa Barbara, California 93102 1

General Motors Technical Center; Manufacturing
Development /33/; ATTN: W. M. Isbell; Warren,
Michigan 48090 1

Gulf Radiation Technology; ATTN: H. R. Kratz;
P. O. Box 608; San Diego, California 92112 1

IIT Research Institute; 10 West 35th Street;
ATTN: Document Library (1); Dr. K. E. McKee
(1); Chicago, Illinois 60616

Lockheed Missiles & Space Company, ATTN: Dr. R. E.
Meyerott/C. C. Old; P. O. Box 504; Sunnyvale,
California 94088 2

J. L. Merritt, Consulting and Special Engineering
Services, Inc. (1); P. O. Drawer 1206; Redlands,
California 92373

Mueser, Rutledge, Wentworth & Johnston; ATTN: P. C.
Rutledge; 415 Madison Avenue, New York, N.Y. 10017 1

NOAA Environmental Research Laboratories; ATTN:
Dr. J. S. Rinehart; Boulder, Colorado 80302 1

(Number of Copies of Report Shown in Parentheses)	No. of Copies Form 1473

INDUSTRY (Cont'd)

The RAND Corporation; ATTN: Dr. H. L. Brode; Dr. C. C. Mow; 1700 Main Street, Santa Monica, California 90406 — 2

Research Analysis Corporation; ATTN: Documents Library; Route 123; McLean, Virginia 22101 — 1

Sandia Laboratories; ATTN: M. L. Merritt, Dept. 9150; W. R. Perret, Division 9111; P. O. Box 5800, Albuquerque, N. M. 87115 — 2

Test Command, ATTN: TCDT-E; Sandia Base, New Mexico 87115 — 1

Shannon & Wilson, Inc.; ATTN: Dr. R. P. Miller; 1105 N. 38th Street, Seattle, Washington 98103 (1); S. D. Wilson (1)

Southwest Research Institute; ATTN: R. C. DeHart; 8500 Culebra Road; San Antonio, Texas 78228 — 1

Systems, Science & Software; ATTN: Document Control; P. O. Box 1620; La Jolla, California 92037 — 1

TRW Systems (R1/1138); ATTN: Norman Lipner; 1 Space Park; Redondo Beach, California 90278 — 1

TRW Systems Group; ATTN: F. A. Pieper; P. O. Box 1310, San Bernardino, California 92402 — 1

Paul Weidlinger, Consulting Engineer; 110 East 59th Street, ATTN: Dr. M. L. Baron; New York, N. Y. 10022 — 1

Woodward-Clyde & Associates; ATTN: A. T. Harrigan, Librarian; P. O. Box 24075; Oakland, California 94623 (1)

Woodward-Clyde & Associates; ATTN: R. L. McNeill; 758 N. Batavia; Orange, California 92668 (1)

Woodward-Clyde & Associates, Inc.; ATTN: Dennis Leary; 31 Orton Road; West Caldwell, New Jersey 07012 (1)

Woodward-Lundgren & Associates; ATTN: C-Y Chang; P. O. Box 24075; Oakland, California 94623 (1)